Isotope labelling and interaction studies of the *Vibrio cholerae* colonization factor GbpA

Abelone Tislevoll

Master Thesis in Biochemistry

60 credits

Department of Chemistry
Faculty of Mathematics and Natural Sciences

UNIVERSITY OF OSLO

06/21

2021

Isotope labelling and interaction studies of the *Vibrio cholerae* colonization factor GbpA

Abelone Tislevoll

http://www.duo.uio.no/

Trykk: Reprosentralen, Universitetet i Oslo

Acknowledgements

I would like to express my gratitude to my main supervisor, Ute Krengel[1]. Thank you for providing me with such an interesting project and for giving me great feedback and ideas along the way. I appreciate that you were always updated on my project and always available for a discussion. I am very grateful for the opportunity to have worked in your group and I appreciate that you took the time and initiative to arrange social outgoings. You create a positive, including working environment that I know we all appreciate and value. Being a member of your group has been a very positive experience and I have learned so much.

I would like to thank my co-supervisor Henrik V. Sørensen[2], for introducing me to this project and for everything you taught me since the very first day. Thank you for taking the time to answer and discuss my many questions throughout this project. I would also like to thank my co-supervisor Per-Eugen Kristiansen[3] for helping me with NMR and CD experiments. You were always available for discussing ideas and answering my question, and you always had a solution to any challenges I encountered along the way. Thanks to Daniel[4] for all your help with the LPS experiments. A big thank you to Gabriele[5] for all your advice and for helping me in the lab whenever needed. For all other members of the group, it has been a pleasure getting to know you and I am very grateful for having worked with all of you.

A big thanks to my family for the great support and for always believing in me. I would like to thank all my friends, especially Ingvild and Gaute, for staying by my side through the difficult times of this pandemic. Thank you to Helene, for reading through my thesis and giving me feedback. Last but not least, I would like to thank my boyfriend Henrik, for the endless support and encouragement.

UiO, June 2021

Abelone Tislevoll

[1] Professor, Department of Chemistry, University of Oslo, Norway
[2] M. Sc., Department of Chemistry, University of Oslo, Norway
[3] Senior Engineer, Department of Biosciences, University of Oslo, Norway
[4] Researcher, Department of Biosciences, University of Oslo, Norway
[5] Senior Engineer, Department of Chemistry, University of Oslo, Norway

Sammendrag

Kolera er en infeksjonssykdom som forårsakes av bakterien *Vibrio cholerae.* Det antas at rundt 100 000 dør årlig av sykdommen og den rammer hovedsakelig utviklingsland der tilgangen på rent vann er begrenset. *V. cholerae* koloniserer tynntarmen til mennesker, i tillegg til alger og kitinoverflater på blant annet krepsdyr og dyreplankton. Bakterien skiller blant annet ut proteinet GbpA, som fester seg til disse overflatene og hjelper bakterien i koloniseringsprosessen. GbpA er et multifunksjonelt protein som består av fire ulike domener. Det første domenet er et enzym som bryter ned kitin, og kan i tillegg binde muciner, glykoproteiner i tarmsystemet. Det fjerde domenet kan interagere med kitin, men ikke med mucin. I tillegg har det blitt vist at domene 2 og 3 interagerer med celleoverflaten til bakterien, og det antas derfor at GbpA danner en slags bro mellom bakterien og overflatene den koloniserer. Strukturen til de tre første domenene er allerede løst ved hjelp av røntgenkrystallografi, men det finnes foreløpig ingen høyoppløst struktur av domene 4. Mekanismen GbpA benytter i koloniseringsprosessen til *V. cholerae* er ikke kjent.

I løpet av dette prosjektet utviklet vi protokoller for å produsere og isotopmerke GbpA ved hjelp av ekspresjonssystemet Vmax, som er nært beslektet med *V. cholerae*. Vår hypotese var at GbpA skilles ut av Vmax cellene på samme måte som når det produseres naturlig av *V. cholerae*. Foreløpig finnes det veldig lite litteratur på isotopmerking med Vmax, og det finnes ingen litteratur på deuterering. I denne sammenheng etablerte vi en effektiv protokoll for ^{15}N-merking av GbpA, som gav svært høyt utbytte. Videre utviklet vi en protokoll for deuterering av GbpA, som også førte til en betraktelig forbedring i utbyttet. I tillegg brukte vi NMR spektroskopi til å undersøke interaksjonene til GbpA. Vi hadde en hypotese om at GbpA interagerer med LPS, som er molekyler på celleoverflaten til bakterier. LPS ble isolert fra *V. cholerae* celler ved hjelp av en metode som innebærer ekstraksjon med fenol. Vi undersøkte dermed interaksjonen mellom GbpA og LPS ved ^{15}N-TROSY NMR titreringen og kom frem til at de ikke interagerer eller at det foregår en svak interaksjon. Vi testet så interaksjonen til GbpA med *V. cholerae* celler og med forskjellige kitinsubstrater. Disse eksperimentene viste seg å være utfordrende, spesielt når vi brukte kitin. Etter flere forsøk, greide vi ikke å detektere bindingen av GbpA til kitin ved denne metoden. Videre vurderte vi NMR som en passende metode for strukturbestemmelse av domene 4 og utviklet en protokoll for produksjon i minimalt medium. Sekundærstrukturen til domene 4 ble også undersøkt med CD spektroskopi, noe som tydet på en høy andel β-struktur og ustrukturerte områder. Denne masteroppgaven legger grunnlaget for fremtidige interaksjonsstudier og strukturbestemmelse av GbpA.

Abstract

Cholera is a potentially fatal disease caused by ingestion of food and water contaminated with the bacterium *Vibrio cholerae*. The disease is estimated to cause 100 000 deaths every year and represents an ongoing threat in developing countries with limited access to clean water. *V. cholerae* colonizes the human gastrointestinal tract as well as chitinous surfaces in the environment. Colonization of *V. cholerae* involves a secreted adhesin known as the *N*-acetyl glucosamine-binding protein A (GbpA), a four-domain multifunctional protein. The N-terminal domain of GbpA is a lytic polysaccharide monooxygenase, an enzyme that catalyses the cleavage of polysaccharides such as chitin. This domain can additionally interact with mucins, glycoproteins present in the human intestine. Furthermore, GbpA possesses a C-terminal chitin-binding domain and two domains believed to mediate attachment of GbpA to the cell surface of *V. cholerae.* The crystal structure of the first three domains of GbpA is already known, however, a high-resolution structure of domain 4 has not been reported. Moreover, it is not clear how GbpA mediates bacterial attachment to its substrates.

In this thesis, we established high-yield production and isotope labelling protocols for GbpA using Vmax, an alternative expression system related to *V. cholerae*. We hypothesized that GbpA would be subjected to the same secretion pathway as when expressed in *V. cholerae*, which could result in higher yields and a more functionally relevant protein. Currently, the literature on isotope labelling in Vmax is sparse, and there is no literature regarding deuteration. Here, we established a high-yield, efficient production protocol for ^{15}N-labelled GbpA. Furthermore, we developed a deuteration protocol for GbpA, which resulted in a drastic improvement in expression yields, while significantly reducing the time of deuteration. Furthermore, we used NMR spectroscopy to investigate the interactions of GbpA. We hypothesised that domains 2 and 3 of GbpA might interact with lipopolysaccharide (LPS) on the cell surface of *V. cholerae*. LPS was isolated from *V. cholerae* cells using the phenol-water extraction method and the interaction was evaluated by ^{15}N-TROSY NMR titration experiments. The results indicated that GbpA cannot bind to LPS, or that the interaction is weak. Furthermore, interactions of GbpA with *V. cholerae* cells and chitin substrates were probed. These experiments proved to be challenging, particularly for chitin. Although several approaches were attempted, we could not detect the binding of GbpA to chitin. We further evaluated NMR as a suitable technique for structure characterisation of domain 4 and devised a production protocol in minimal medium. The secondary structure of domain 4 was investigated by CD spectroscopy, which indicated a high degree of β-structure and unstructured regions. These results provide a framework for future interaction studies and structure characterisation of GbpA.

Abbreviations

AA	Auxiliary activity
AEX	Anion-exchange chromatography
C-terminus	Carboxyl-terminus
CAZy	Carbohydrate
CbpD	Chitin binding protein D
CD	Circular dichroism
CT	Cholera toxin
D-GbpA	Deuterated GbpA
Da	Dalton
DNase	Deoxyribonuclease
DTT	Dithiothreitol
E. coli	*Escherichia coli*
EDTA	Ethylenediamine-tetraacetate
FL-GbpA	Full-length GbpA
g	Gravitational force
GbpA	*N*-acetylglycosamine binding protein A
GbpA-D1	GbpA domain 1
GbpA-D2	GbpA domain 2
GbpA-D3	GbpA domain 3
GbpA-D4	GbpA domain 4
GH	Glycosyl hydrolase
GlcNAc	*N*-acetylglucosamine
GlcNAc-5	Pentaacetyl-chitopentaose
GST	Glutathione S-transferase
hLTB	*E. coli* heat-labile enterotoxin
HSQC	Heteronuclear single quantum correlation spectroscopy
I	Spin quantum number
IBV	Department of Biosciences, University of Oslo
K_a	Association constant
K_d	Dissociation constant
kDa	Kilodalton
IM	Inner membrane
IPTG	Isopropyl β-d-1 thiogalactopyranoside
LB	Lysogeny broth
LPMO	Lytic polysaccharide monooxygenase
LPS	Lipopolysaccharide
mAU	Milli-absorbance unit
MDa	Megadalton
MHz	Megahertz
MQ-H_2O	Milli-Q filtered and ion-exchanged water
MW	Molecular weight
MWCO	Molecular-weight cut-off

^{15}N-GbpA	^{15}N-labelled GbpA
N-terminus	Amino-terminus
NMR	Nuclear magnetic resonance
O-PS	O-polysaccharide chain
OD600	Optical density at 600 nm
OM	Outer membrane
PAGE	Polyacrylamide gel electrophoreses
PCR	Polymerase chain reaction
PDB	Protein data bank
pI	Isoelectric point
PMSF	Phenylmethylsulphonyl fluoride
ppm	Parts per million
rpm	Revolutions per minute
SAXS	Small angle X-ray scattering
SDS-PAGE	Sodium dodecyl sulphate-polyacrylamide gel electrophoreses
SEC	Size-exclusion chromatography
TB	Terrific broth
TCP	Toxin-coregulated pilus
Tris	Tris(hydroxymethyl)aminomethane
TROSY	Transverse relaxation-optimized spectroscopy
UV	Ultraviolet
V. cholerae	*Vibrio cholerae*
V. natriegens	*Vibrio natriegens*
WHO	World Health Organization

Table of contents

1 Introduction

1.1 Cholera

Cholera is an acute diarrheal disease affecting developing countries with poor sanitation and inadequate access to clean water. The Gram-negative bacterium *Vibrio cholerae* is the causative agent of the disease, which is transmitted through contaminated water and food. Upon ingestion of pathogenic *V. cholerae*, colonization of the small intestine takes place, causing symptoms to appear after 12-72 hours [1]. Typical symptoms are vomiting and diarrhoea, which may cause severe dehydration and death. Infected humans excrete the bacterium back into the environment, and the disease is spread through ingestion of contaminated water and food. It was estimated in 2015 that cholera causes 95 000 deaths worldwide every year [2]. However, this estimate comes with a high uncertainty, as the majority of cases are not reported [3]. The global impact of the disease is therefore largely unknown. Furthermore, an increasing number of cases is expected in the future as a result of climate change [4]. There are two serogroups of *V. cholerae* responsible for the recent cholera outbreaks, O1 and O139 [5]. The O1 serogroup, which has caused all recent cholera pandemics, can be subdivided into two biotypes; El Tor and Classical [5]. Although there are treatment options available, prevention of cholera remains a challenge in areas with poor infrastructure, where access to clean drinking water and food is lacking [6]. Destruction of water and sanitation infrastructure due to e.g. natural disasters may lead to outbreaks of cholera, which was the case after the earthquake in Haiti in 2010 [7, 8] that lead to a massive outbreak of cholera [9]. The vaccines currently available are not suited for populations in endemic countries as they are high cost and require cold-chain circulation [10]. Three WHO pre-qualified oral cholera vaccines are currently available; Dukoral, Shanchol and Euvichol, which all require a double dose for full protection and can only provide short-term protection [11]. Consequently, new treatment options need to be developed to overcome current and future cholera outbreaks.

1.2 The membrane of Gram-negative bacteria

V. cholerae is a Gram-negative, comma-shaped bacterium with a single polar flagellum and pili located on the cell surface. It was first discovered as a bacterium in 1854 by Filippo Pacini, and was identified

as the cause of cholera by Robert Koch in 1884 [12]. Most bacteria can be broadly divided into two classes: Gram-positive and Gram-negative, according to the structure of their cell envelope. The Gram-negative cell envelope consists of three principle layers: the inner membrane (IM), the peptidoglycan (PG) cell wall, and the outer membrane (OM). The IM is a phospholipid bilayer and surrounds the cytoplasm. The PG cell wall is located in the periplasmic space, which is the region between the IM and the OM. It is composed of sugars and amino acids arranged in a mesh-like structure, and its main function is to provide the bacterial envelope with mechanical strength. The OM separates the bacterium from the environment. In contrast to the IM, the OM is highly asymmetrical, consisting of phospholipids in the inner leaflet and lipopolysaccharides (LPS) in the outer leaflet [13].

1.2.1 Lipopolysaccharide

LPS are large glycolipids important for the structural and functional integrity of Gram-negative bacteria. Besides serving as a physical barrier for protection against environmental factors, LPS contributes to bacterial pathogenicity upon encounter with the host immune system. Although the structure of LPS varies between different species of bacteria, they all conform to a general common architecture characterized by three distinct regions; lipid A, the polysaccharide (PS) core and the O-polysaccharide (O-PS) chain (Figure 1) [14]. The lipid A component anchors LPS to the OM and gives rise to the endotoxin activity of LPS [15]. Typically, lipid A is composed of a phosphorylated *N*-acetyl glucosamine (GlcNAc) dimer attached to 6 or 7 saturated fatty acids (Figure 1) [16]. The inner polysaccharide core is composed of the unusual sugars 3-deoxy-D-manno-octulosonic acid (Kdo) and L-glycero-D-manno heptose (heptulose), while the outer core contains more common hexose sugars like glucose and galactose (Figure 1) [14]. The O-PS chain is the outer, hydrophilic part of LPS and consists of repeating oligosaccharide subunits (Figure 1). Major variations occur in the O-PS chain with respect to e.g. sugars, sequence, and substitution [14]. The O-PS chain is also known as the O-antigen, since it triggers host immune responses highly specific to the O-PS chain [14]. Structural variations in the O-PS chain occur between strains and even within strains of Gram-negative bacteria [17]. All characterized serogroups of *V. cholerae* have differences in O-PS composition, which is the basis for classification into serogroups [18]. *V. cholerae* LPS performs several important biological processes related to endotoxin activity [19, 20], intestinal adherence [21] and colonization [22, 23]. In one study, the O-PS chain of LPS was found to play a major role in adhesion of *V. cholerae* to intestinal mucus in vitro [21]. Moreover, several studies have shown that LPS mutations significantly decreases the efficiency of intestinal adherence [22, 23]. Gram-negative bacteria, including *V. cholerae,* are known to release membrane vesicles from the bacterial surface containing LPS, glycerophospholipids and

outer membrane proteins [24, 25]. Experiments conducted on Gram-negative bacteria suggest that membrane vesicles are involved in bacteria-bacteria and bacteria-host interactions such as toxin delivery [26]–[28]. Although *V. cholerae* LPS is essential for proper bacterial function, the specific roles of LPS related to intestinal adherence and colonization are not fully understood.

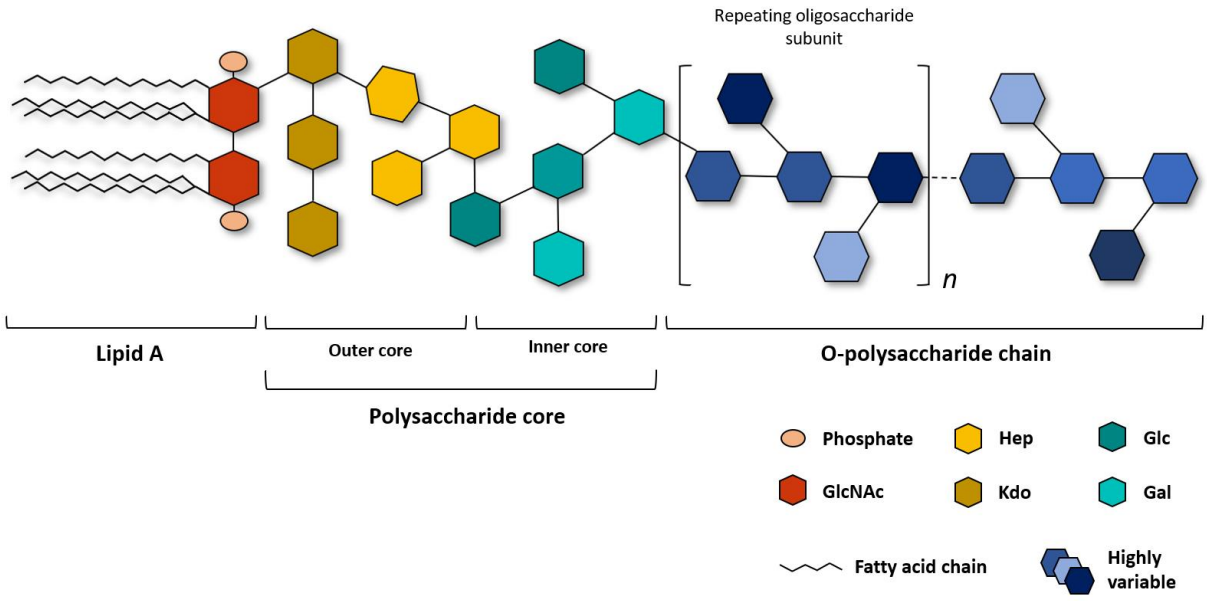

Figure 1. The general structure of Gram-negative LPS. The lipid A component is embedded in the membrane, while the PS core and the O-PS chain extend from the bacterial surface. The O-PS chain is highly variable and consists of a wide variety of sugars and substitutions. This figure was created using Microsoft PowerPoint and was inspired by Erridge et al. 2002 [14].

1.3 *Vibrio cholerae* colonization

V. cholerae is a natural part of aquatic ecosystems, with the ability to survive in diverse aquatic environments including lakes, rivers, brackish water and the ocean [29]. The ability to form biofilms on both biotic and abiotic surfaces is an important factor contributing to the environmental persistence of the bacterium [30]. A common substrate for biofilm formation is chitin, an abundant polymer found in the exoskeleton of marine crustaceans [31]. Besides serving as a surface for colonization, chitin is utilized by *V. cholerae* as a source of carbon and nitrogen [32]. It has been suggested that the ability of *V. cholerae* to colonize surfaces promotes survival in the environment, by providing a source of nutrients as well protection against environmental factors [33]. Furthermore, patient stools have been

shown to contain biofilm-like aggregates, suggesting that biofilm formation also plays a role in the transmission of cholera between hosts [34]. The monomer of chitin, GlcNAc, is also present in mucins, which represent the major component of the mucus layer covering the epithelial surface of the human intestine [35]. The mucus layer serves as a protective barrier against invasion by many pathogenic microorganisms [36]. In order to colonize the small intestine and deliver cholera toxin (CT), *V. cholerae* must penetrate the mucus layer [37].

1.4 Virulence factors of *Vibrio cholerae*

Pathogens produce virulence factors to enhance their ability to cause disease in the host. A wide range of molecules fall into the category of virulence factors, including secreted molecules like toxins and enzymes as well as cell surface structures like LPS [38]. Virulence factors employ various mechanism to promote pathogenicity, such as host colonization, counteracting host immune responses and acquiring nutrients from the environment [39]. Most bacterial pathogens promote attachment to host tissue surfaces by a mediated interaction involving microbial adhesins [40]. The initial adherence of *V. cholerae* to the intestine has been shown to involve a coordinated interaction between the colonization factor *N*-acetylglucosamine binding protein A (GbpA) and GlcNAc sugars of intestinal mucin [41]. Toxicogenic strains of *V. cholerae* produce a number of virulence factors, where CT and toxin-coregulated pilus (TCP) are essential for pathogenesis [42]. CT is a multimeric protein complex responsible for the characteristic symptoms of cholera infection and is secreted by *V. cholerae* upon colonization of the small intestine [43]. Expression of CT and TCP is coregulated by the regulatory protein ToxR, demonstrating that cholera pathogenesis is dependent on the synergistic effect of several virulence factors [44].

1.4.1 The cholera toxin

CT is classified as an AB_5 toxin, which are virulence factors utilized by several major pathogens [45]. The first high-quality three-dimensional structure of CT was solved in 2004 [46], which was an important contribution to our current understanding of the toxin. The catalytic subunit of AB_5 toxins is known as the A-subunit, which elicits the toxic effect in the host [45]. The B-subunit forms a pentameric pore that binds to specific glycan receptors on the target cell surface [45]. The two subunits are linked by an α-helix from the A-subunit extending into the B-subunit pore, forming the holotoxin [45]. CT

shares an 80 % sequence homology with the *Escherichia coli* heat-labile enterotoxin (hLTB) [47], and the two toxins assume a similar structure [48]. Although there are only minor differences in their receptor binding specificity and catalytic activity, the infection caused by hLTB is less severe [49]. The Kuehn group demonstrated in 2002 that hLTB is secreted extracellularly and associates with the cell surface through binding to LPS [50]. Furthermore, in 2003, is was shown that the Kdo component of the inner core (Figure 1) is required for binding of hLTB and CT to *E. coli* LPS [51]. *V. cholerae* LPS did not bind to hLTB or CT, as the Kdo component is phosphorylated, which may explain the different outcomes of the diseases [51].

1.5 Chitin and chitinases

Chitin is a linear polymer of β1-4 linked GlcNAc units (Figure 2). After cellulose, chitin is the second most abundant biopolymer in nature and can be found in insects, crustaceans and in the exoskeleton of marine invertebrates. There are three types of crystalline structures of chitin found in nature; α, β and γ [52], which are all insoluble in aqueous and most organic solvents. Many organisms produce chitinases, which are glycosyl hydrolases (GHs) that degrade chitin into chito-oligosaccharides [53]. According to their amino acid sequence, GHs are classified into different families in the Carbohydrate-Active enZYme database (CAZy), where chitinases constitute families 18, 19 and 20 [54]. Some bacteria, including *V. cholerae,* produce chitinases to utilize chitin as a nutrient source [53].

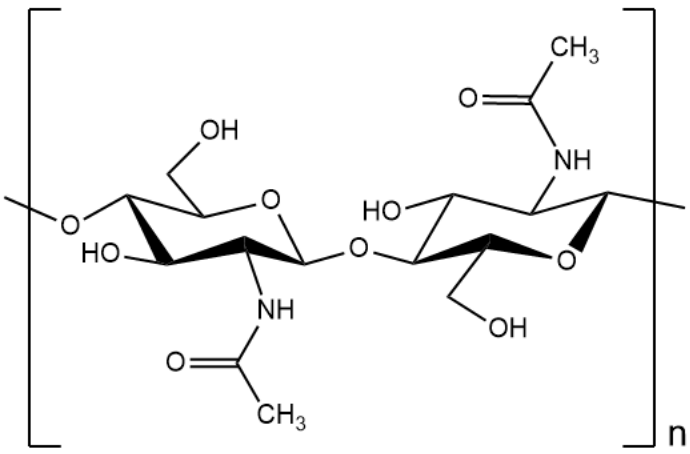

Figure 2. The chemical structure of chitin, showing two β1-4 linked *N*-acetylglucosamine units that form a long chain polymer. This figure was created using ChemDraw.

1.6 Lytic polysaccharide monooxygenases

In 2010, a group of metalloenzymes known as lytic polysaccharide monooxygenases (LPMOs) was discovered by Vaaje-Kolstad et al. [55]. LPMOs catalyse the oxidative cleavage of 1,4-linked glycosidic bonds in crystalline polysaccharides like chitin and cellulose, facilitating further degradation of polysaccharides by hydrolytic enzymes [56, 57]. Although glycosyl hydrolases also degrade chitin, the activity on crystalline substrates is less efficient than soluble carbohydrate chains [58]. The surface-exposed active site of LPMOs consists of a copper ion coordinated by two histidine residues, which are conserved across all families of LPMOs [59], and a tyrosine, present in most LPMOs (Figure 3). Moreover, LPMOs share common structural features despite low sequence identity between different family members [59]. The catalytic domain adopts a characteristic pyramidal shape consisting of a distorted β-sandwich [59]. LPMOs are classified in the CAZy database as auxiliary activities (AA) [60]. Currently, LPMOs are categorized into seven AA families based on their sequence [61]: AA9, AA10, AA11, AA13, AA14, AA15 and AA16 [62]. LPMOs can exist in multi-modular forms, often in combination with carbohydrate-binding modules (CBMs) or chitinases [63]. Cellulose and chitin-oxidizing bacterial LPMOs, classified as AA10 LPMOs, were previously known as chitin-binding proteins and as CBM33 members [64]. The active site is located on a flat, substrate-binding surface, where interactions with the substrate occur through polar interactions [65].

Genes encoding LPMOs have been identified in many pathogenic organisms, and certain LPMOs are known to act as virulence factors [66]–[69]. Recently, the *Pseudomonas aeruginosa* LPMO chitin-binding protein D (CbpD) was shown to promote immune evasion by enhancing survival of the bacterium in human blood [70]. Because LPMOs resembling CbpD are found in other pathogens, it is suggested that these may have similar roles in pathogenesis [70].

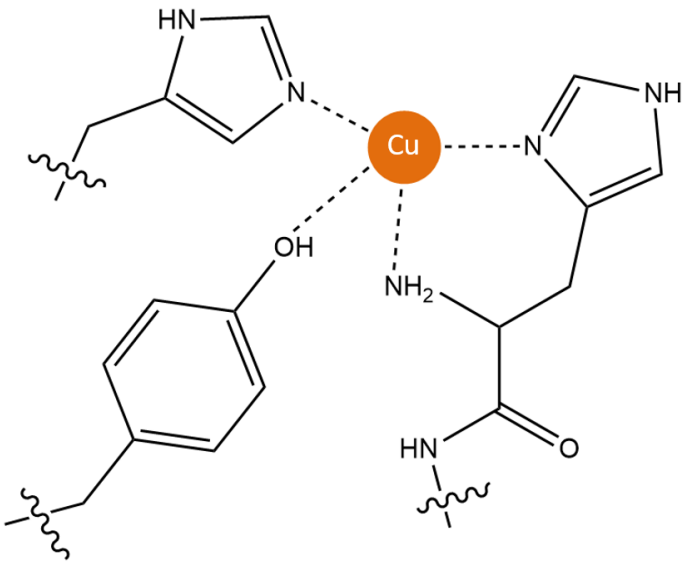

Figure 3. The active site of an LPMO, the histidine brace, showing a copper ion coordinated by two histidine residues and a tyrosine, which is conserved among most LPMOs. However, in some AA10 and AA15 LPMOs, the tyrosine is replaced by a phenylalanine [71]. This figure was created using ChemDraw.

1.7 *N*-acetylglucosamine binding protein A (GbpA)

V. cholerae produces several chitinases and chitin-binding proteins [32]. GbpA is required for efficient colonization of human epithelial cells as well as attachment to the exoskeleton of marine organisms [69]. GbpA consists of four domains and promotes bacterial attachment by interactions with GlcNAc residues present in both mucin and chitin [72]. Binding studies have shown that GbpA interacts with several forms of chitin through its N-terminal (GbpA-D1) and C-terminal domain (GbpA-D4) (Figure 4A), including amorphous forms of chitin as well as chito-oligosaccharides [72]. Additionally, it has been demonstrated that GbpA-D1 interacts with the GlcNAc residues of intestinal mucin [41, 72] (Figure 4A). GbpA and mucin appear to upregulate each other in a cooperative manner, facilitating the process of pathogenesis to host cells [41]. In 2014, GbpA was found to be active on β-chitin nanofibers, revealing that GbpA-D1 has LPMO activity, and was classified into the AA10 family [73].

GbpA is secreted by *V. cholerae* through the extracellular protein secretion system [69]. There are many open questions regarding the mechanism of the mediated attachment of GbpA to its substrates. Wong et al. demonstrated through a binding assay that domains 2 and 3 of GbpA (GbpA-D2, GbpA-D3) interact with the bacterial surface [72]. This suggests that bacterial colonization takes place through an interaction between substrate-adhered GbpA and the *V. cholerae* bacterium, forming a stable interface between the bacterium and the host [72] (Figure 4B). Moreover, it has been proposed that

GbpA is present in a bacterial-surface-associated form as well as a secreted form, promoting a more direct interaction between the bacterium and GlcNAc surfaces [69]. Further insight into the mechanism of GbpA is crucial to understand its role in surface colonization and pathogenesis. It is likely that other pathogens exploit a similar colonization mechanism, since GbpA-like genes are also expressed in other organisms [74, 75].

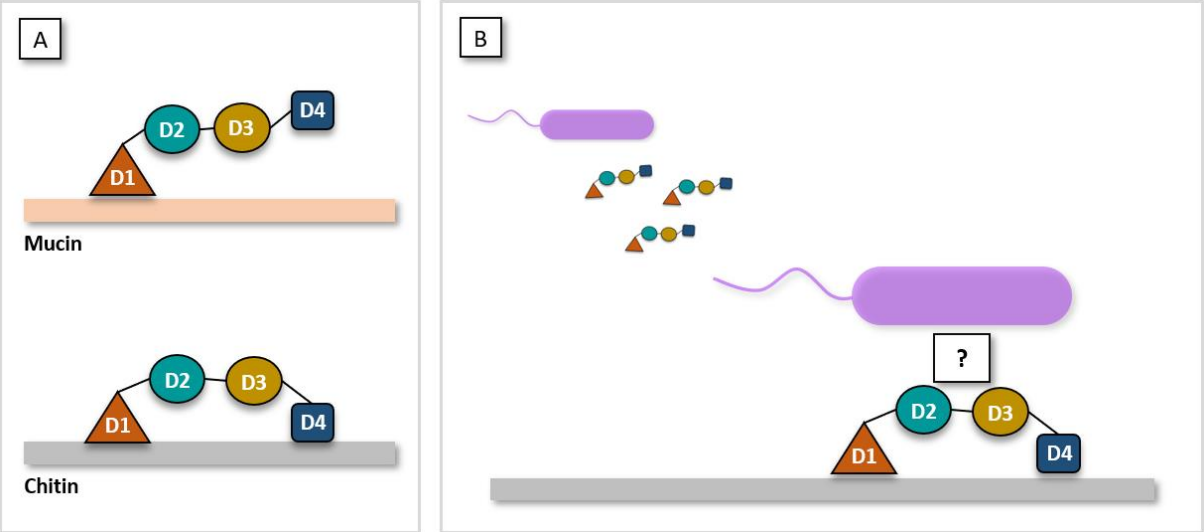

Figure 4. A: The *V. cholerae* colonization factor GbpA interacts with mucin through domain 1 and chitin through domains 1 and 4. **B:** GbpA is secreted by *V. cholerae* and colonization takes place through a coordinated interaction between GbpA and the bacterium. This figure was created using Microsoft PowerPoint.

1.7.1 GbpA structure

The three-dimensional structure of the first three domains of GbpA has been solved by X-ray crystallography [72] (Figure 5A). The N-terminal LPMO domain (GbpA-D1) has a β-sandwich structure consisting of a three-stranded and a four-stranded β-sheet, which includes a loop/helical region between two of the β-strands [72]. Like other members of the LPMO family, GbpA-D1 has a characteristic flat substrate binding surface, with a copper ion binding site [73, 76]. GbpA-D2 and GbpA-D3 has some similarities with other proteins, like the chaperones SFAE [77] and FimC [78], that interact with pili on the bacterial surface [72]. The three-dimensional structure of GbpA-D4 has not yet been reported. GbpA-D4 shares 26 % sequence identity with the chitin binding domain of

chitinase B (SmChiB) from *S. marcescens* [72]. Circular dichroism (CD) experiments on GbpA-D4 indicated a high degree of β-secondary structure, which is also the case for SmChiB [72].

Upon binding to GlcNAc-containing surfaces, GbpA appears to undergo a conformational change (Sørensen et al., unpublished results). However, a three-dimensional structure of GbpA bound to its substrate has so far not been reported. Small angle X-ray scattering (SAXS) studies of FL-GbpA have shown that the protein is an elongated monomer in solution, resembling beads on a string [72] (Figure 5B).

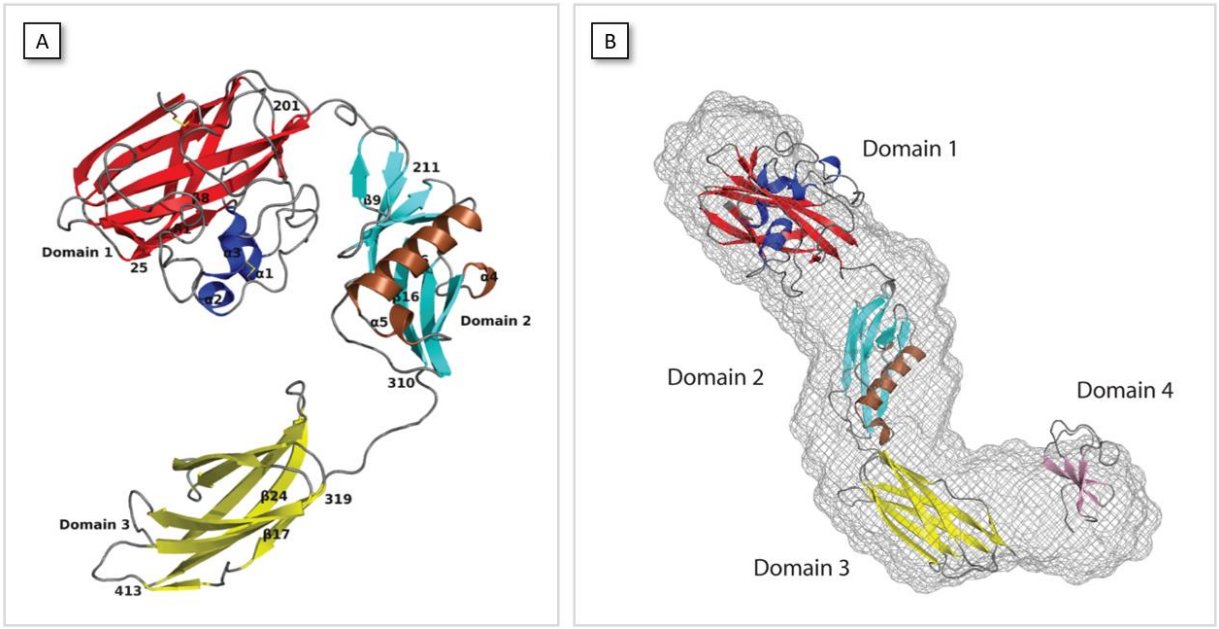

Figure 5. The structure of GbpA. **A:** The X-ray structure of GbpA-D1-3. **B:** A superimposition of the X-ray structure of GbpA-D1-3 and a modelled structure of GbpA-D4 onto the *ab initio* SAXS model of FL-GbpA (Wong et al., 2012 [72]).

1.8 Theoretical background

1.8.1 Nuclear magnetic resonance spectroscopy

Nuclear magnetic resonance (NMR) spectroscopy is a versatile and powerful technique frequently used in fields like chemistry, physics and biology to identify and acquire structural information on a molecule. NMR plays an important role in the characterization of proteins and other biomolecules, and

is used to gain information on protein structure, dynamics and molecular interactions [79]. The technique is based on the interaction of certain atomic nuclei with a static magnetic field. The atomic nuclei of all elements are characterized by a nuclear spin quantum number *I* [80]. Nuclei with $I \neq 0$ possess a magnetic spin and are observable by NMR, such as the proton. Nuclei with an atomic mass and atomic number that are both even, have $I = 0$, and possess no nuclear spin. Thus, the nuclei of elements like carbon-12 and oxygen-16 are not observable by NMR. Nuclei that possess spin have an associated magnetic moment and acts like a small magnet. In the presence of an external magnetic field, spin-½ nuclei like the proton can take on two different spin states and will align either with or against the field, where the energy difference between the two states is proportional to the imposed magnetic field [80] (Figure 6). The spins aligned with the field are of lower energy and are therefore more populated. When a radio pulse at the frequency corresponding to the energy gap between the two spin states is applied, the nuclei aligned with the field are excited to a higher energy state and will oppose the applied field (Figure 6). The frequency of the radio pulse that is absorbed induces resonance and causes a peak to appear in the spectrum at that particular frequency. This frequency is expressed in parts per million (ppm), known as the chemical shift. Nuclei are surrounded by electrons, which gives rise to a small magnetic field opposing the applied field, termed shielding. The applied magnetic field must therefore be increased to achieve resonance in more shielded nuclei. Consequently, nuclei in different environments will resonate at different radiation frequencies and will therefore give rise to different chemical shifts.

Over the past few decades, NMR has been among the primary methods for the three-dimensional structure determination of proteins at atomic resolution [81]. Recent technological advancements and the development of efficient isotope labelling schemes has enabled characterization of increasingly larger proteins [82]. Even though the majority of reported structures are determined by X-ray crystallography, NMR is the only method that can obtain a high-resolution three-dimensional structure in solution. Furthermore, NMR provides access to information on protein dynamics [83] and ligand interactions [84], which is less accessible to other structural biology techniques. Investigating interactions of proteins is not only essential for understanding their function in biological processes, but also for identification of potential novel drugs [85]. NMR is an efficient technique for obtaining information on protein interactions at atomic resolution. Typically, a spectrum of the protein is first acquired, and a series of ligand titrations are performed. The residues involved in direct interaction with the ligand will experience changes in the local electron density, resulting in chemical shift perturbations [86].

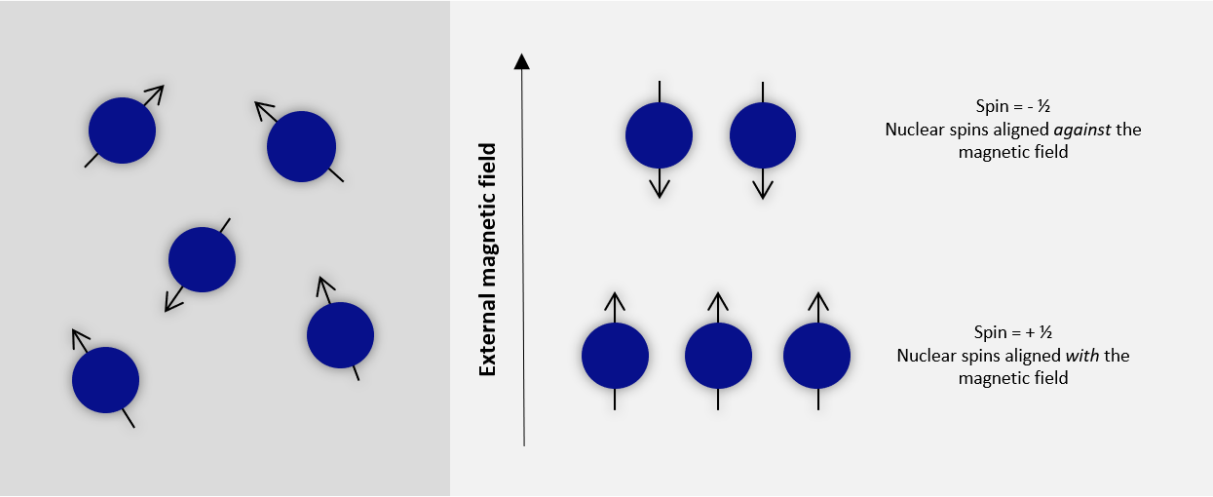

Figure 6. Nuclear spin properties of a nucleus with *I* = 1/2. Spinning nuclei will have random orientations when not exposed to a magnetic field. When an external magnetic field is applied, spins align either with or against the field. This figure was created using Microsoft PowerPoint.

Heteronuclear single quantum correlation spectroscopy (HSQC)

The most frequently used experiment for mapping chemical shift perturbations of proteins is the ^{15}N-heteronuclear single quantum correlation (^{15}N-HSQC) experiment. ^{15}N-HSQC is a two-dimensional NMR experiment that determines the correlation between amide protons and ^{15}N separated by one bond, yielding one peak in the spectrum for each amide group [87]. With the exception of proline, each residue of the protein will produce one peak in the spectrum. The spectrum of a folded protein will usually contain peaks that are well dispersed, such that individual peaks are distinguishable. The ^{15}N-HSQC spectrum is often referred to as the fingerprint of a protein as a unique pattern of signals is produced for each protein. The ^{15}N-HSQC experiment is performed relatively quickly and is usually the first to be performed on ^{15}N-labelled proteins in order to determine if the protein is suitable for structure determination under the given conditions.

Transverse relaxation-optimized spectroscopy (TROSY)

The study of large proteins by solution NMR is complicated by mainly two factors; resonance overlap due to a large number of signals and peak broadening, resulting in poor-quality spectra. Peak broadening is a consequence of the slow tumbling rate of larger molecules, leading to accelerated relaxation and rapid signal decay. This problem can be overcome by the application of transverse relaxation-optimized spectroscopy (TROSY) [88], designed to select for relaxation mechanisms that cancel each other out. TROSY experiments are used to acquire similar information as the HSQC

experiment, but the resolution and sensitivity of large proteins is greatly enhanced. In the past, characterization by NMR was only possible for proteins with a molecular weight below ~30 kDa. Combined with efficient isotope labelling schemes and technical advancement, TROSY has enabled the study of molecules up to 1 MDa [89].

1.8.2 Isotope labelling of proteins

The main isotopes used for protein NMR are ^{1}H, ^{2}H, ^{15}N and ^{13}C, as these nuclei possess spin characteristics required for commonly used biomolecular NMR experiments. Of these, only ^{1}H has a high natural abundance, so proteins often need to be isotope labelled. The most common strategy involves bacterial expression of proteins in minimal medium, providing the bacteria with essential salts and trace elements, in addition to isotope labelled sources of nitrogen and carbon [90]. The isotopes present in the medium are incorporated into the growing polypeptide chain, resulting in the production of uniformly labelled proteins. One of the drawbacks of protein NMR is the requirement for relatively large amounts of protein, due to poor sensitivity. There are numerous established protocols for efficient expression of isotope labelled proteins in *E. coli*. For some proteins, however, low expression yield remains a significant problem. Moreover, isotope labelled sources of nitrogen, carbon and hydrogen are relatively expensive. Isotope labelling is also required for several other techniques for structure and function studies of proteins, such as deuteration for neutron scattering and diffraction techniques [91].

1.8.3 Circular dichroism (CD) spectroscopy

Circular dichroism (CD) is a spectroscopic technique used to determine the secondary structure and folding properties of proteins [92]. Biological molecules like proteins are optically active, meaning that they can rotate plane polarized light. When circularly polarized light is passed through an optically active molecule, circular dichroism occurs due to differential absorption of left-handed and right-handed circularly polarized light [93]. Different structural elements like α-helices and β-strands will generate characteristic CD spectra, which are analysed to predict the types of secondary structure present and their overall contributions [94]. Since the spectra are dependent on the conformation of the protein, CD can also be used to monitor conformational changes as a result of e.g. heat, pH, ligand interactions or mutations [95]. CD is widely used in fields where rapid characterization of proteins is of interest and is often used to provide complementary information to other techniques. Although CD

does not provide residue-specific information, it is considered an excellent alternative in cases where characterization by X-ray crystallography and NMR is not suitable.

1.9 Thesis aim

In this thesis, we aim to gain insight into the colonization mechanism of the *V. cholerae* colonization factor GbpA, by investigating potential interaction partners. We hypothesize that GbpA interacts with LPS on the bacterial surface. ^{15}N-TROSY NMR is a suitable method to test this hypothesis and to furthermore evaluate binding of GbpA to *V. cholerae* cells, β-chitin and pentaacetyl-chitopentaose (GlcNAc-5).

To enable interaction studies by NMR, we will establish an efficient, cost-effective ^{15}N-labelling protocol for GbpA, using the Vmax expression system. Since Vmax is closely related to *V. cholerae*, GbpA expressed in Vmax may further be of higher functional relevance. In collaboration with Henrik V. Sørensen, we will develop a high-yield deuteration protocol of GbpA in Vmax, to enable structural and functional characterization by neutron scattering.

In addition, this thesis aims to provide structural information on the C-terminal chitin-binding domain of GbpA (GbpA-D4) and to lay the groundwork for future structure determination by NMR spectroscopy.

This thesis has four main objectives:

A. **Expression and purification of ^{15}N-labelled FL-GbpA in Vmax:** establish an efficient, cost-effective protocol for expression and purification of ^{15}N-labelled GbpA.
B. **Deuteration of FL-GbpA and GbpA-D1 in Vmax:** establish efficient, cost-effective protocols for deuteration of FL-GbpA and GbpA-D1.
C. **Interaction studies by NMR:** investigate potential interaction partners of GbpA by ^{15}N-TROSY titration experiments.
D. **Structural studies of GbpA-D4:** investigate the secondary structure of GbpA-D4 by CD spectroscopy and develop an ^{15}N-labelling protocol for future structure determination by NMR.

2 Methods

A complete list of chemicals and materials can be found under Appendix A. Buffer compositions and solutions are listed under Appendix B.

2.1 Production of GbpA-D4

E. coli BL21(DE3) Star™ cells transformed with the pGEX6P plasmid encoding the GbpA-D4 gene were kindly provided by Prof. Gustav Vaaje-Kolstad, NMBU. GbpA-D4 was expressed in terrific broth (TB) medium (Appendix B) and in M9* medium (Appendix B). All steps of expression were performed in cultures containing 100 µg/mL ampicillin, incubated in a InforsHT Multitron Standard incubator-shaker at 130 rpm.

TB expression protocol: Cells were inoculated in 100 mL baffled culture flaks containing 20 mL TB medium and were incubated at 37 °C overnight. 10 mL of the overnight culture was then transferred to two 5 L baffled culture flask, each containing 1 L TB medium. When the optical density at 600 nm (OD600) reached 0.8, protein expression was induced by addition of IPTG to a concentration of 1 mM. The induced cultures were incubated for 18 hours at 16 °C.

M9 expression protocol:* Cells were inoculated in four culture tubes containing 3 mL lysogeny broth (LB) media (Appendix B) and were incubated for 8 hours at 37 °C. Growth cultures were then prepared by transferring 2.5 mL from each culture tube to four 250 mL baffled culture flasks containing 25 mL M9* medium. After incubating cultures for 15 hours at 37 °C, 25 mL of each culture was transferred to four 2 L baffled culture flasks containing 225 mL M9* medium, followed by incubation at 37 °C until the OD600 reached 3. Protein expression was induced by addition IPTG to a concentration of 1 mM and the cultures were incubated for 20 hours at 16 °C.

Cytoplasmic lysis protocol: Lysis was carried out by the freeze-thawing method followed by incubation with lysozyme. Cells were harvested by centrifugation at 4000 *g* in a Beckman-Coulter Avanti centrifuge for 30 minutes at 4 °C. The bacterial pellet was stored at -80 °C for 1 hour and thawed overnight at 4 °C, followed by resuspension in lysis buffer (Appendix B) containing 1 µL DNase I, 1 mM PMSF and 1 mg/mL lysozyme. The suspension was incubated under stirring on ice for 1 hour and cell debris was removed by centrifugation at 18 500 *g* for 30 minutes at 4 °C. The supernatant, containing GST-GbpA-D4, was filtered with a 0.45 µm PES membrane bottle-top filter and was stored at 4 °C until purification.

2.2 Production of FL-GbpA and GbpA-D1 with Vmax™ X2 Chemically Competent Cells

Vmax™ X2 is a *Vibrio natriegens* strain developed by SGI-DNA [96]. The expression system is designed and optimized for fast growth rate and high levels of protein expression. Transformation of the pET-26b(+) plasmid encoding the FL-GbpA or GbpA-D1 gene (Appendix C) into Vmax™ X2 chemically competent cells was done according to the *Vmax™ Express transformation protocol* [97].

2.2.1 Transformation of FL-GbpA and GbpA-D1

Vmax™ Express transformation protocol: ~150 ng plasmid DNA was added to cells thawed on ice. Cells were left on ice for 1 h and heat-shocked for 45 seconds at 42 °C, followed by incubation on ice for 90 seconds. 1 mL pre-warmed LB-v2 medium was added, and the cells were incubated at 200 rpm for 2 hours at 30 °C. 200 µL of the cell culture was plated on LB-v2 agar (Appendix B) containing 100 µg/mL kanamycin. The remaining culture (800 µL) was centrifuged at 10 000 *g* for 5 minutes. The pellet was resuspended in 100 µL of the supernatant and plated on LB-v2 agar containing 100 µg/mL kanamycin. Following overnight incubation at 30 °C in a Kelvitron T incubator, a single colony was selected and transferred to a culture tube containing 2 mL LB-v2 medium and 200 µg/mL kanamycin. The culture was incubated for at 200 rpm for 6 hours at 30 °C and glycerol stocks were prepared with 25 % glycerol and stored at -80 °C.

2.2.2 Expression of FL-GbpA and GbpA-D1

Expression protocol: All bacterial cultures contained 200 µg/mL kanamycin and were incubated at 30 °C in a InforsHT Multitron Standard incubator-shaker at 130 rpm. Vmax cells transformed with the plasmid encoding the FL-GbpA or GbpA-D1 gene were inoculated in a culture tube containing 3 mL LB-v2 medium (Appendix B). Cultures were incubated for 16 hours. Subsequently, 1 mL of the culture was transferred to 100 mL LB-v2 medium and was incubated for 2 hours before protein expression was induced by addition of IPTG to a concentration of 1 mM. Induced cultures were incubated for 22 hours.

Isolation of protein from cell cultures: Following expression, cells were harvested by centrifugation at 18 500 *g* for 30 minutes at 4 °C in an Eppendorf table-top centrifuge. The supernatant was filtered with

a 0.45 µm sterile bottle-top filter and dialyzed overnight at 4 °C against 100 mM NaCl, 20 mM Tris-HCl pH 8 (FL-GbpA) or 50 mM NaCl, 20 mM Tris-HCl pH 8 (GbpA-D1) using a volume ratio of 1:20 of sample:buffer. A 10 000 MWCO and 3 500 kDa MWCO SnakeSkin dialysis tubing was used for used for FL-GbpA and GbpA-D1, respectively.

2.3 Isotope labelling with Vmax™ Express

A protocol for Vmax expression of ^{15}N-labelled FL-GbpA (^{15}N-FL-GbpA) was developed. In collaboration with Henrik V. Sørensen[6], protocols for deuteration of FL-GbpA (^{2}H-FL-GbpA) and GbpA-D1 (^{2}H-GbpA-D1) were established. All cultures contained 200 µg/mL kanamycin and were incubated in an InforsHT Multitron Standard incubator-shaker at 130 rpm and 30 °C. After harvesting cells, the proteins were isolated from the culture supernatant as described under Section 2.2.2.

Expression protocol for ^{15}N-FL-GbpA: A pre-culture was prepared by inoculating transformed Vmax cells in a culture tube containing 1 mL LB-v2 medium. Following incubation overnight, the culture was transferred to a 100 mL baffled culture flask containing 20 mL ^{15}N-labelled M9 Max medium (^{15}N-M9 Max) (Appendix B) and was incubated for 6 hours. The culture was then transferred to four 2 L baffled culture flasks containing 245 mL ^{15}N-M9 Max. Protein expression was induced after two hours by addition of IPTG to a concentration of 1 mM. Induced cultures were incubated for 20 hours.

Expression protocol for ^{2}H-FLGbpA and ^{2}H-GbpA-D1: Transformed Vmax cells were inoculated in a culture tube containing 1 mL LB-v2 medium and was incubated for 3 hours. 100 µL of the culture was then transferred to a culture tube containing 1 mL deuterated LB-v2 medium (D-LB-v2) (Appendix B), followed by incubation for 5 hours. Subsequently, the culture was transferred to a 100 mL baffled culture flask containing 10 mL deuterated M9 Max (D-M9 Max) (Appendix B). After incubation for 14 hours, the culture was transferred to a 1 L baffled culture flask containing 90 mL D-M9 Max and was incubated for 3 hours (^{2}H-FL-GbpA) or 7 hours (^{2}H-GbpA-D1) before addition of IPTG to a concentration of 1 mM. Induced cultures were incubated for 22 hours.

[6] M.Sc., Department of Chemistry, University of Oslo, Norway

2.4 Protein purification

GST-GbpA-D4 was purified using glutathione S-transferase (GST) affinity chromatography and size-exclusion chromatography (SEC). FL-GbpA and GbpA-D1 (labelled and unlabelled) were purified by anion exchange chromatography (AEX) and size-exclusion chromatography (SEC). The compositions of the binding buffer and elution buffer used for each protein is described under Appendix B. For SEC purification, the binding buffers for AEX and GST affinity chromatography were used as running buffer.

2.4.1 Glutathione S-transferase (GST) affinity chromatography

GST affinity chromatography protocol: A 1 mL GSTrap HP column was connected to an ÄKTA start FPLC and equilibrated with 10 column volumes (CV) of binding buffer. The filtered cell lysate was loaded unto the column at a flow rate of 0.5 mL/min, followed by a washing step with 20 CV of binding buffer, at a flow rate of 1 mL/min. Bound protein was eluted with 10 CV of elution buffer at a flow rate of 1 mL/min and dialysed overnight against 500 mL cleavage buffer (Appendix B), using a 3 500 MWCO SnakeSkin dialysis tubing.

GST-tag cleavage protocol: PreScission protease was added to a concentration 2 U/µL, followed by incubation for 12 hours at 4 ^{o}C. The sample was then concentrated using a 30 mL Vivaspin with a 3.0 kDa MWCO and was purified by SEC to separate GbpA-D4 from the cleaved GST-tag and the PreScission protease.

2.4.2 Anion-exchange chromatography (AEX)

AEX protocol: All purification steps were performed using a flow rate of 1 mL/min. A 5 mL HiTrap Q XL AEX column was connected to an ÄKTA start FPLC and equilibrated with 5 CV of binding buffer. The protein sample was loaded onto the column, followed by a washing step with 20 CV of binding buffer. Bound protein was eluted over a linear gradient (0-100 %) with 12 CV of elution buffer and fractions of 5 mL under the elution peak were collected and analysed by SDS-PAGE. Fractions containing the target protein were pooled and concentrated using a 30 mL Vivaspin with a 5 000 MWCO (GbpA-D1) or a 10 000 MWCO (FL-GbpA). Concentrated protein samples were stored at 4 ^{o}C until SEC purification.

2.4.3 Size-exclusion chromatography (SEC)

SEC protocol: A Superdex 200 Increase 30/100 GL (FL-GbpA, GbpA-D1) or Superdex 75 Increase 30/100 GL column (GbpA-D4) was connected to an ÄKTA purifier and equilibrated with 3 CV of running buffer. The protein sample was filtered with a modified nylon membrane 0.2 µm centrifugal filter and loaded onto the column at a flow rate of 0.5 mL/min using a 500 µL loop. Fractions of 1 mL under the elution peak were collected and analysed using SDS-PAGE. The fractions containing the target protein were pooled and concentrated using a 30 mL Vivaspin with an appropriate MWCO for each protein. Purified GbpA-D4 samples were stored in 100 µL aliquots at -20 ^{o}C. All other samples were stored at 4 ^{o}C.

2.4.4 Quantification

The protein yield was determined by measuring absorbance at 280 nm with an Amersham Biosciences spectrophotometer using the molar extinction coefficient of the protein, assuming all cysteine residues are reduced (obtained from ProtParam tool, by ExPASy). See Appendix C for the respective molecular weights and extinctions coefficients.

2.4.5 Sodium dodecyl sulphate-polyacrylamide gel electrophoresis (SDS-PAGE)

SDS-PAGE protocol for protein samples: 20 µL of sample was mixed with 7 µL 4X LDS loading buffer and 100 mM DTT and was heated at 70^{o} C for 10 minutes. A Bolt Bis-Tris 4-12 % polyacrylamide gel was assembled into a electrophoreses tank containing 1X MES SDS running buffer. 15 µL of each protein sample was loaded onto the gel, in addition to 10 µL SeeBlue Plus2 pre-stained standard for molecular weight referencing. The electrophoreses tank was connected to an Electrophoreses powersupply-EPS601 and run at 200 V for 30 minutes. The gel was then stained with Coomassie staining solution on a shaker for 2-3 hours and de-stained with MQ-H_2O until an adequate contrast was observed.

SDS-PAGE protocol for cell-containing samples: Culture samples containing an amount of cells corresponding to 1 mL of OD600 = 1 were centrifuged at 10 000 *g* for 10 minutes and the supernatant was discarded. The pellet was resuspended in 500 µL 8 M urea, 167 µL 4x LDS loading buffer and

100 mM DTT. The rest of the preparations followed the same protocol as described under *SDS-PAGE protocol for protein samples.*

SDS-PAGE protocol for cell-containing samples for analysis of soluble/insoluble fractions: Culture samples containing an amount of cells corresponding to 1 mL of OD600 = 1 were centrifuged at 10 000 *g* for 10 minutes and the supernatant was discarded. The pellet was resuspended in 250 µL BugBuster protein extraction reagent and 1 µL DNase I, followed by incubation for 15 minutes at room temperature and centrifugation at 10 000 *g* for 10 minutes. Subsequently, 10 µL of the supernatant was transferred to a separate tube containing 5 µL MQ-H_2O and 5 µL 4x LDS loading buffer (soluble fraction) and the rest of the supernatant was discarded. The pellet was resuspended in 500 µL 8 M urea and 167 µL 4x LDS loading buffer (insoluble fraction). The rest of the preparations followed the same protocol as described under *SDS-PAGE protocol for protein samples.*

2.5 Isolation of *V. cholerae* lipopolysaccharide (LPS) and outer membrane (OM) fraction

LPS and the OM fraction were isolated from *V. cholerae* El Tor ΔCTX cells. See Appendix E for safety statement.

2.5.1 *V. cholerae* LPS

A preculture was prepared by inoculating *V. cholerae* cells in 100 mL LB medium. After incubation overnight at 37 °C, 10 mL of the preculture was transferred to 1 L LB media the culture was incubated overnight at 37 °C. Cells were harvested by centrifugation at 5 000 *g* for 15 minutes at 4 °C and subsequently washed with 10 mM Tris-HCl and 2 mM $MgCl_2$. The cells were lysed using a French press (2 times, 1000 psi) and sonicated twice for 30 seconds at 75 % intensity. DNase I and RNase A was added to a concentration of 200 µg/mL and 50 µg/mL, respectively, and the suspension was incubated overnight at 180 rpm and 37 °C. 5 mL 10 mM Tris-HCl pH 8, 0.1 M EDTA and 2.5 mL 10 mM Tris-HCl pH 8, 2 % SDS was added to 15 mL of the cell suspension, followed by sonication for 40 seconds at 75 % intensity. Cell components like peptidoglycan were removed by centrifugation at 40 000 *g* for 30 minutes at 20 °C and the supernatant was lyophilized overnight. The lyophilized crude extract was dissolved in MQ-H_2O and LPS was precipitated with 2 volumes of precooled 95 % ethanol and 375 mM $MgCl_2$ by storing at -20 °C overnight. Precipitated LPS was then collected by centrifugation at

10 000 *g* for 15 minutes at 4 °C and the pellet was resuspended in MQ-H_2O. To remove proteins, an equal volume of 90 % phenol (w/v) was added and the mixture was heated to 65 °C for 30 minutes, with regular mixing. After cooling, the phase separation was accelerated by centrifugation at 3 000 *g* for 10 minutes and the water phase was collected. The phenol extraction procedure was repeated, and the water phase was treated under air flow until the next morning, followed by dialysis against flowing water for 3 days (3 500 MWCO). The mixture was then lyophilized overnight and dissolved in 10 mM Tris-HCl pH 8, 2 mM $MgCl_2$. DNase I and RNase A was added to a concentration of 10 µg/mL and mixture was incubated for 1 hour at 37 °C. Proteinase K was then added to a concentration of 10 µg/mL and the mixture was further incubated for 3 hours at 56 °C. After centrifugation at 87 000 *g* for 2 hours at 15 °C, the pellet was dissolved in MQ-H_2O, followed by another round of centrifugation. Finally, the pellet was lyophilized overnight and stored at room temperature.

2.5.2 *V. cholerae* OM fraction

V. cholerae cells were cultured as described under section 2.5.1. An amount of cells corresponding to 40 mL at OD600 = 1.0 was harvested by centrifugation at 5 000 *g* for 10 minutes. The pellet was resuspended in 1.5 mL cold 10 mM HEPES pH 7.4 and 10 mM $MgCl_2$ followed by centrifugation at 15 600 *g* for 2 minutes at 4 °C. The pellet was then resuspended in 1.5 mL 10 mM HEPES pH 7.4 and 10 mM $MgCl_2$. Lysozyme was added to a concentration of 0.1 mg/mL 10 µL and 10 µL 1 mg/mL DNAse I was added. The suspension was mixed with glass beads in screwcap tubes and the cells were lysed using a SpeedMill, with 2*3 minutes of shaking. The cell lysate was centrifuged at 13 000 *g* for 1 minute at 4 °C and the supernatant was transferred to a new tube and centrifuged at 15 600 *g* for 15 minutes at 4 °C to pellet membranes. The pellet was then resuspended in 200 µL 10 mM HEPES pH 7.4 and 200 µL 2 % lauryl sacrosine in 10 mM HEPES pH 7.4 followed by incubation at room temperature with intermittent mixing. Outer membranes were pelleted by centrifugation at 15 600 *g* for 30 minutes at 4 °C and the pellet was thoroughly resuspended in 60 µL 10 mM HEPES pH 7.4.

2.6 Interaction studies by NMR

2.6.1 Sample preparations for NMR titrations

***V. cholerae* LPS:**

V. cholerae LPS isolated from *V. cholerae* cells (Section 3.5.1) was dissolved in the NMR buffer (Appendix B) to a concentration of 16.25 mg/mL (0.8 mM, assuming LPS has an average molecular weight of 20 kDa). The sample was vortexed thoroughly and heated at 70 ^{o}C for 10 minutes.

***V. cholerae* cells:**

V. cholerae El Tor ΔCTX cells were inoculated in a culture tube containing 2 mL LB medium and was incubated in a InforsHT Multitron Standard incubator-shaker overnight at 130 rpm and 37 ^{o}C (OD600 = 1.7). Assuming that cell cultures at OD600 = 0.1 corresponds to 10^8 colony forming units (CFU)/mL [72], a cell suspension containing approximately 2 × 10^9 cells were used for the titrations. Cells were harvested by centrifugation at 1 000 *g* in an Eppendorf bench-top centrifuge for 10 minutes and were washed three times with the NMR buffer. The pellet was then resuspended in 2 mL NMR buffer containing 100 µg/mL gentamycin.

β-chitin:

β-chitin nanofibers (Appendix A) were added to 20 mM acetic acid pH 3.2 to a concentration of 10 mg/mL. The suspension was then sonicated at 50-70 % power for 5 times 1 minute with 30 second breaks in between, followed by dialysis against 20 mM sodium acetate pH 5.5 or pH 5.0 (Appendix B).

Pentaacetyl-chitopentaose (GlcNAc-5):

Pentaacetyl-chitopentaose (GlcNAc-5) (Appendix A) was dissolved in the NMR buffer to a concentration of 60 mg/mL (58 mM).

^{15}N-FL-GbpA:

All samples containing ^{15}N-FL-GbpA were dialysed against the NMR buffer and were prepared with 10 % D_2O to establish a lock signal.

2.6.2 ^{15}N-TROSY titration experiments

NMR titration experiments were performed by recording a series of ^{15}N-TROSY spectra at increasing titrant concentrations. All spectra were acquired at 37 °C on a Bruker Ascend 800 MHz spectrometer Avance III HD and were processed using TopSpin 3.5.

Titrations with V. cholerae LPS: A ^{15}N-TROSY spectrum of 370 µM ^{15}N-FL-GbpA was first recorded as a reference. A series of titrations were then performed with LPS, and new ^{15}N-TROSY spectra were recorded after each titration. The concentration of ^{15}N-FL-GbpA and LPS after each titration are listed in Table 1.

Table 1. LPS titration scheme.

Titration step	GbpA conc., µM	LPS conc., µM	[LPS]:[GbpA]
1	357	29	0.08
2	339	68	0.20
3	290	174	0.60
4	254	254	1.00
5	221	327	1.48

Titrations with V. cholerae El Tor cells: A ^{15}N-TROSY spectrum of 290 µM ^{15}N-FL-GbpA was first recorded as a reference. A series of titrations were then performed with a suspension of *V. cholerae* cells, and new ^{15}N-TROSY spectra were recorded after each titration. The concentration of ^{15}N-FL-GbpA and amount of cells after each titration are listed in Table 2.

Table 2. Cell titration scheme.

Titration step	GbpA conc., µM	Amount of cells, CFU	Cells/ng GbpA
1	289	3×10^6	0.37
2	286	1×10^7	1.22
3	281	3×10^7	3.67
4	267	8×10^7	9.80
5	250	1×10^8	12.25
6	232	2×10^8	24.49

Titrations with β-chitin: A ^{15}N-TROSY spectrum of 314 µM ^{15}N-FL-GbpA was first recorded as a reference. A series of titrations were then performed with β-chitin, and new ^{15}N-TROSY spectra were recorded after each titration. The concentration of ^{15}N-FL-GbpA and amount of β-chitin after each titration are listed in Table 3.

Table 3. β-chitin titration scheme.

Titration step	GbpA conc., µM	Amount of β-chitin, mg
1	265	0.3
2	203	0.9
3	182	1.2
4	164	1.5

Titrations with pentaacetyl-chitopentaose (GlcNAc-5): A ^{15}N-TROSY spectrum of 280 µM ^{15}N-FL-GbpA was first recorded as a reference. A series of titrations were then performed with GlcNAc-5, and new ^{15}N-TROSY spectra were recorded after each titration. The concentration of ^{15}N-FL-GbpA and GlcNAc-5 after each titration are listed in Table 4.

Table 4. GlcNAc-5 titration scheme.

Titration step	GbpA conc., mM	GlcNAc-5 conc., mM	[GlcNAc-5]:[GbpA]
1	0.275	0.18	0.65
2	0.270	0.35	1.30
3	0.261	1.37	5.25
4	0.241	3.71	15.39
5	0.226	5.47	24.20
6	0.218	7.60	34.86
7	0.211	9.65	45.73

2.7 Circular dichroism (CD) measurements of GbpA-D4

Purified GbpA-D4 was dialysed overnight against sodium phosphate buffer (Appendix B), using a Pur-A-Lyzer Midi 3 500 MWCO dialysis cassette. A sample of 135.3 µg/mL GbpA-D4 was used for CD spectroscopic analysis. CD spectra were recorded at 20 ^{o}C in a 0.1 cm length quartz cuvette using a Jasco J-810 spectrophotometer. Samples were scanned five times with a scanning rate of 50 nm/min with a bandwidth of 0.5 nm and response time of 1 second over the wavelength range 190-260 nm. Three spectra of GbpA-D4 were collected and the buffer spectrum was subtracted.

3 Results and discussion

3.1 Production of GbpA with Vmax express

One of the aims of this thesis was to establish an efficient, cost-effective isotope labelling scheme for GbpA, to enable binding studies by NMR spectroscopy. Isotope-labelled proteins can be obtained by recombinant expression in minimal medium, which contains essential elements to support growth, without the presence of amino acids. Stable isotopes, such as ^{15}N and ^{13}C, are introduced as the sole source of nitrogen and carbon respectively, allowing these to be incorporated into the polypeptide chain. Vmax™ is a protein expression system derived from *Vibrio natriegens,* a non-pathogenic, marine microorganism [98]. *V. natriegens* is known to have a growth rate in M9 medium twice as high as *E. coli* [97], and expression levels up to four times as high can be obtained [99]. One advantage of the Vmax expression system is that induction is independent of the growth phase and can therefore be performed at a wide range of cell densities (OD600) [97, 98]. This eliminates the need to closely monitor OD600 levels prior to expression, enabling a more convenient and efficient production scheme. Since Vmax is more similar to *V. cholerae* than *E. coli* (Vmax belongs to the *Vibrio* family, like *V. cholerae*), we hoped that expression of GbpA in Vmax would result in higher expression yields. Thus, the Vmax expression system was considered as a promising alternative to improve the production efficiency and costs of isotope labelled GbpA. Additionally, production of proteins in expression systems similar to the host could be of higher functional relevance, as the protein may be subjected to similar folding and post-translational modifications as under native conditions. Biologically relevant interaction partners may also be revealed.

3.1.1 Production of FL-GbpA and GbpA-D1 in LB-v2 medium

In order to evaluate Vmax as an expression system for GbpA, pET-26b(+) plasmids encoding the FL-GbpA and GbpA-D1 genes were transformed into Vmax X2 chemically competent cells and expression trials were performed according to the Vmax expression protocol [98]. Briefly, pre-cultures were diluted 1:100 with LB-v2 medium (Appendix B), and expression was induced after ~2 hours. SDS-PAGE analysis of samples taken before and after induction of protein expression revealed that GbpA is secreted into the growth medium during expression (Figure 7A, 8A). Purification of FL-GbpA and GbpA-D1 was carried out by anion exchange chromatography (AEX) and size-exclusion chromatography (SEC), building on the established protocol for production of GbpA in *E. coli*

(Sørensen et al., unpublished results). After harvesting cells, the supernatant was dialysed against the AEX binding buffer, where a 1:20 volume ratio of GbpA:buffer was found to be sufficient. Buffer exchange was crucial to ensure correct salt concentration and pH to promote binding of GbpA to the column material. Following purification by AEX, the proteins were further purified by SEC (Figure 7B, 8B). To evaluate purity, AEX and SEC fractions were analysed using SDS-PAGE (Figure 7C, 8C).

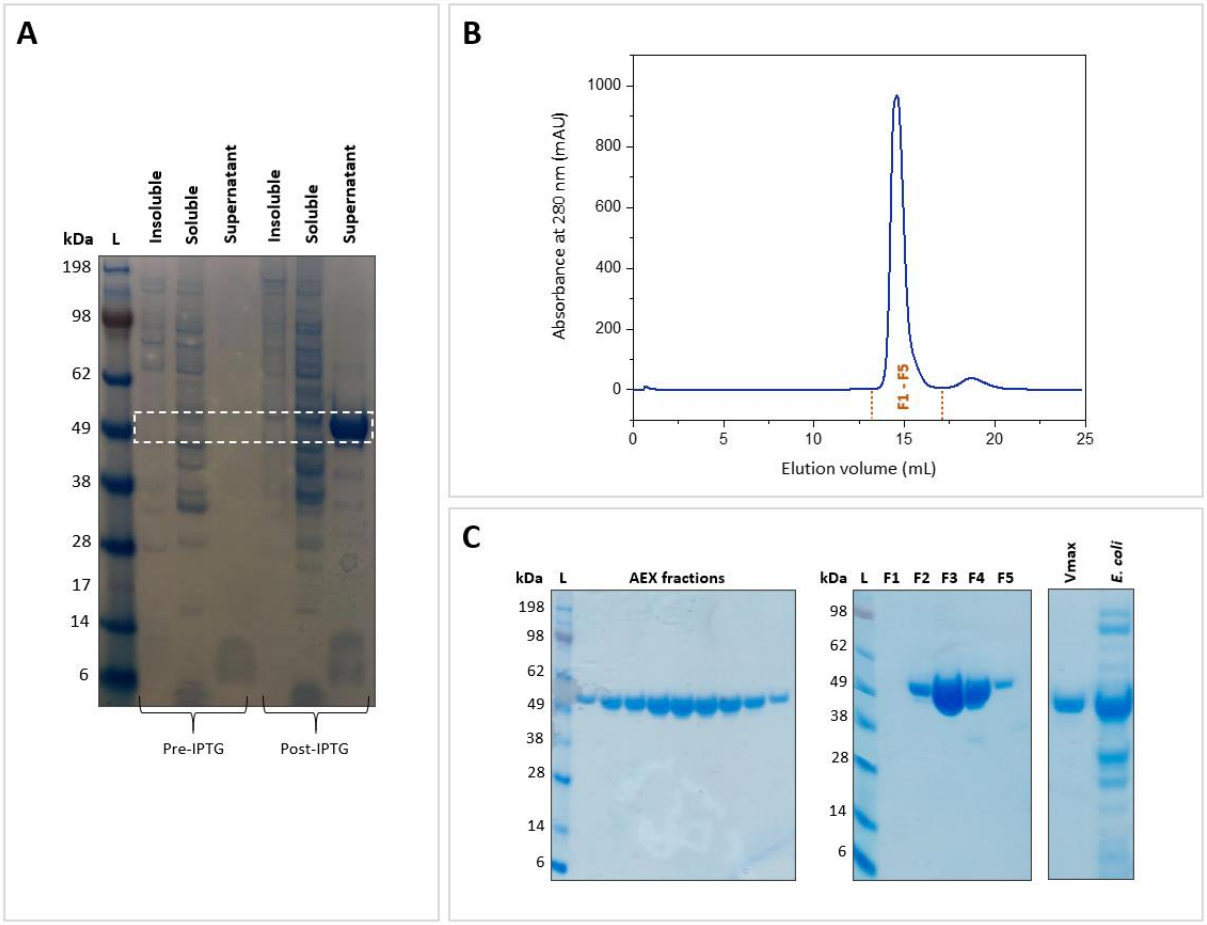

Figure 7. Analysis of Vmax FL-GbpA production. **A:** SDS-PAGE analysis of the soluble/insoluble fraction and supernatant after expression. **B:** SEC chromatogram of FL-GbpA. 5 fractions of 1 mL were collected and analysed by SDS-PAGE. **C:** *Left:* SDS-PAGE analysis of FL-GbpA SEC fractions. *Right:* SDS-PAGE analysis of purified FL-GbpA expressed with Vmax and *E. coli*, demonstrating a major improvement in the purity.

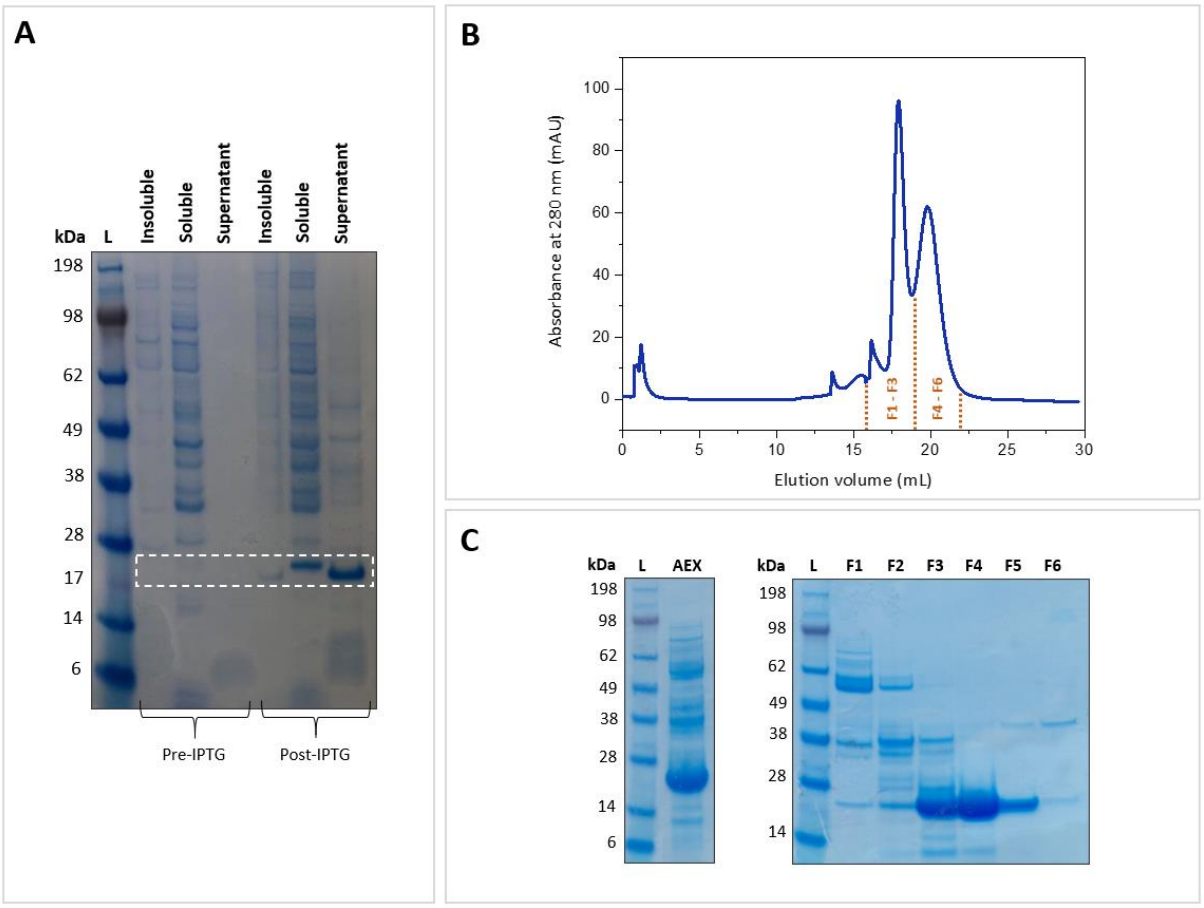

Figure 8. Analysis of Vmax GbpA-D1 production. **A:** SDS-PAGE analysis of the soluble/insoluble fraction and supernatant after expression. **B:** SEC chromatogram of GbpA-D1. 6 fractions of 1 mL were collected and analysed by SDS-PAGE. **C:** *Left:* SDS-PAGE analysis of the pooled AEX fractions. *Right:* SDS-PAGE analysis of GbpA-D1 SEC fractions, showing that fractions F4 and F5, corresponding to the second peak, had higher purity.

When expressed by *V. cholerae,* GbpA is secreted through the type II secretion system, which is present in many Gram-negative bacteria. These results suggest that GbpA is subjected to the same secretion pathway when expressed in Vmax. Interestingly, FL-GbpA appears to be completely secreted during expression (Figure 7A), whereas a fraction of GbpA-D1 was not secreted (Figure 8A). FL-GbpA and GbpA-D1 are produced with the PelB leader sequence, which directs the proteins to the periplasm, where the sequence is cleaved off by a signal peptidase [100]. GbpA-D1 in the soluble fraction had a higher molecular weight than secreted GbpA-D1 (Figure 8A), suggesting that the PelB leader sequence was cleaved off before secretion. Additionally, this indicates that the protein in the soluble fraction remained in the cytosol after being synthetized was not transported to the periplasm. For FL-GbpA expressed in Vmax, the purity after AEX and SEC was very high compared to purified GbpA expressed in *E. coli* BL21(DE3) (Figure 7C). Expression in *E. coli* requires GbpA to be isolated from the periplasmic fraction. Periplasmic lysis is a relatively complicated and time-consuming procedure, and periplasmic contaminants must be separated from the protein during the subsequent purification steps.

Additionally, overproduction may overwhelm the folding machinery, leading to misfolding and aggregation. Here, GbpA is isolated from the culture supernatant, thereby avoiding contaminants from the periplasm and preventing aggregation. Consequently, this allows for higher yields to be obtained. High purity was already achieved after AEX purification (Figure 7C). It may therefore be possible to skip purification by SEC and exchange the buffer by e.g. dialysis, to enable a more efficient purification. The SEC elution profile of GbpA-D1 showed a split peak, indicating that a fraction of the protein elutes in a complex with an impurity, or that the protein dimerizes or aggregates (Figure 8B). The SDS-PAGE analysis corresponding to these fractions (Figure 8C) revealed the presence of several impurities, which may be involved in an interaction with GbpA-D1. However, these interactions are likely not of biological relevance, as these impurities were not observed after purification of FL-GbpA (Figure 7C). In order to improve the purity of GbpA-D1, it might be beneficial to adjust the flow rate or salt gradient during AEX. Alternatively, decreasing the flow rate and increasing the salt concentration during SEC could result in higher purity. Production of FL-GbpA and GbpA-D1 in Vmax resulted in expression yields of 50 mg/L and 25 mg/L, respectively. This was a substantial improvement compared to yields obtained from expression in *E. coli* BL21(DE3) (Table 5).

3.1.2 Expression test of FL-GbpA and GbpA-D1 in M9* medium

To enable titration experiments by ^{15}N-TROSY-HSQC, FL-GbpA needs to be isotope labelled with ^{15}N, which can be obtained by recombinant expression in shaker cultures containing minimal medium with $^{15}NH_4Cl$ as the sole nitrogen source. To evaluate Vmax expression of FL-GbpA and GbpA-D1 in minimal medium, an expression test was conducted using M9* medium (Appendix B), a minimal medium composition developed for expression of GbpA in *E. coli* (Sørensen et al., unpublished results). Vmax expression in M9* was based on the protocol for expression of FL-GbpA and GbpA-D1 in LB-v2 medium (Section 3.1.1) and included an additional step to enable Vmax cells to adapt to growing in M9* medium. A preculture in LB-v2 medium was inoculated in M9* medium. After incubation for 6 hours, the growth culture was diluted 1:100 with M9* before expression was induced after 2 hours. Due to small culture volumes and low cell density at induction, samples were taken after expression only, where the soluble and insoluble fractions as well as the culture supernatant were analysed by SDS-PAGE (Figure 9).

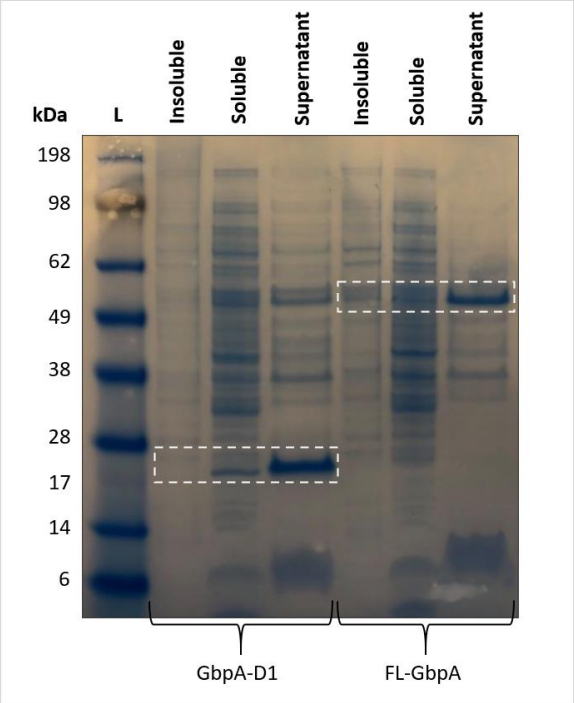

Figure 9. Expression test of GbpA-D1 and FL-GbpA in M9* medium. SDS-PAGE analysis of the insoluble and soluble fractions, as well as the supernatant, showing that GbpA-D1 and FL-GbpA are secreted into the supernatant.

GbpA-D1 expressed well in M9* medium, and a larger fraction of the protein was secreted compared to expression in LB-v2 medium (Figure 8A). A reason for this might be that the folding machinery was less overwhelmed due to slower expression, resulting in more efficient secretion. For FL-GbpA, secretion was very efficient, as no protein was observed in the soluble and insoluble fractions. However, expression yields of FL-GbpA appeared to be lower in M9* compared to LB-v2 medium (Figure 7A).

3.2 High-yield production of ^{15}N-FL-GbpA with Vmax express

Having established that FL-GbpA is successfully expressed and secreted by Vmax in minimal medium, an optimization trial was conducted to determine the optimal conditions for ^{15}N-labelling of FL-GbpA for NMR experiments. Six different ^{15}N-labelled minimal media compositions were tested (Appendix D). First, a minimal medium composition was developed based on reported conditions for Vmax minimal media expression [99] and FL-GbpA minimal medium expression in *E. coli* (Sørensen et al., unpublished results) (Figure 10A). Modifications of this recipe were used in the optimization trial to evaluate how expression levels were affected by increased NaCl concentration, glucose as a carbon source, increased buffer capacity and expression at 30 °C. (Figure 10B). Expression

was carried out as illustrated in Figure 10B and induction was performed 2 hours after inoculation of the expression cultures. The OD600 was measured in the growth culture before inoculation of the expression cultures and at harvest (Figure 10C). Additionally, the pH was measured at harvest (Figure 10C). Samples of 20 µL were taken from the culture supernatant and analysed directly by SDS-PAGE to evaluate the result.

Condition 6 appeared to result in the highest expression yield, where the minimal medium start composition (Figure 10A) was used to evaluate the effect of expression at 30 °C (Figure 10C). For Vmax cells, expression at 30 °C in LB medium is generally recommended [98]. However, expression trials of FKBP-NusA, EYFP-Z2 and TEV-His_6 in M9 medium showed that the optimal expression temperature was 25 °C for all three proteins [99]. Condition 1 had a 1.5 % higher NaCl concentration. Vmax cells grow best in higher osmotic conditions [101], and higher NaCl concentration has been shown to significantly reduce the time of the growth phase [99]. Although the OD600 after induction was the highest for all conditions tested, an increased concentration of NaCl did not appear to increase expression levels (Figure 10C). For conditions 2 and 3, glucose was used as a carbon source (instead of glycerol), at two different concentrations. The SDS-PAGE analysis revealed that there was no protein in the supernatant of these cultures (Figure 10C), which indicates that GbpA was not expressed. It is possible that Vmax uses glucose mainly for cell growth rather than for expression. Another possibility might be that the protein precipitated, as GbpA is less stable at pH < 5.5. The pH in these cultures after expression was 5.5 and 5.4 for conditions 2 and 3, respectively. Finally, the effects of increasing buffer component concentrations (Na_2HPO_4 and KH_2PO_4) with a 3-fold and 6-fold were tested for conditions 4 and 5, respectively (Figure 10C). No evident increase in expression yields was observed. However, increasing the buffer capacity may still be beneficial as condition 6 showed a reduction in pH after expression (Figure 10C). Although it would be interesting to optimize different parameters when expressing at 30 °C, it was evident that expression yields were already very high. Therefore, it was concluded that no further optimization was necessary to scale up expression.

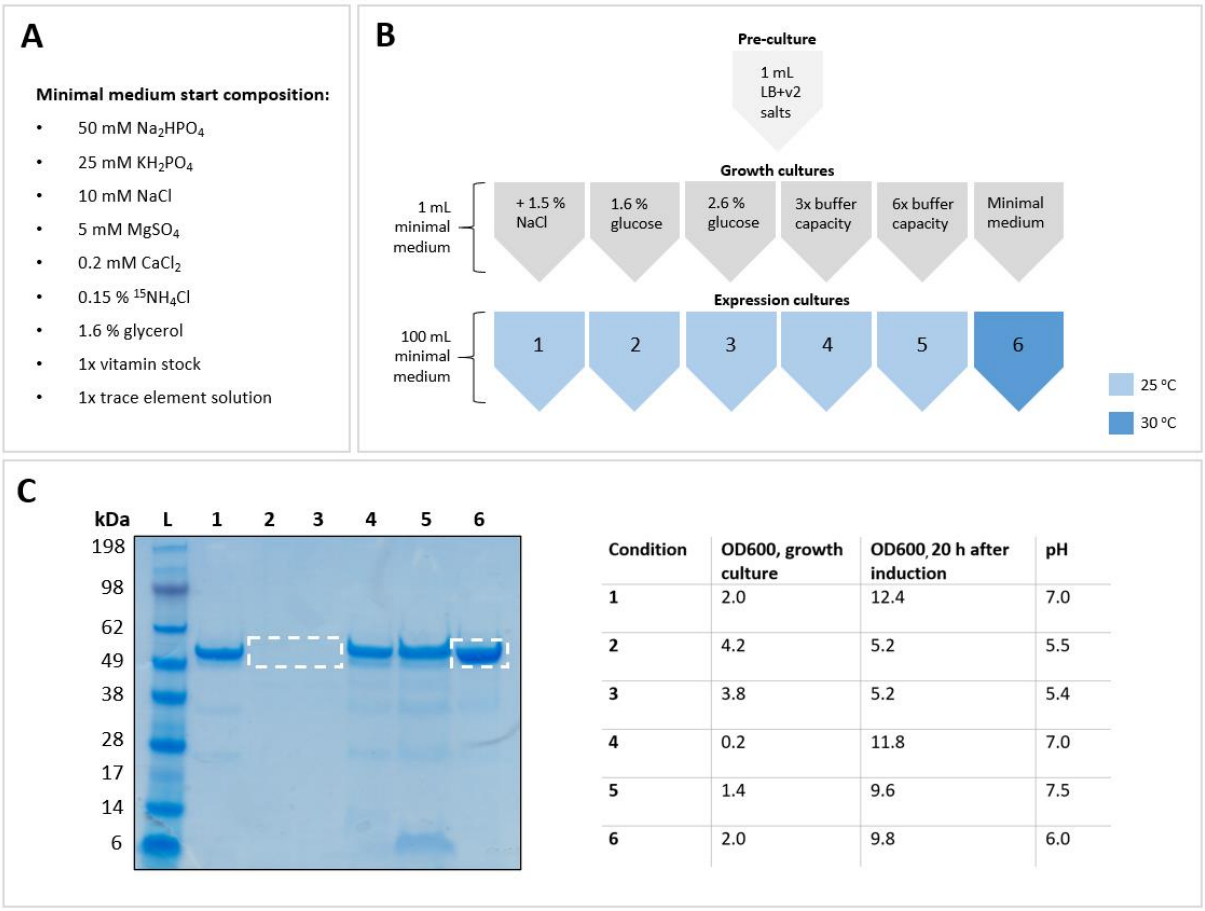

Condition	OD600, growth culture	OD600, 20 h after induction	pH
1	2.0	12.4	7.0
2	4.2	5.2	5.5
3	3.8	5.2	5.4
4	0.2	11.8	7.0
5	1.4	9.6	7.5
6	2.0	9.8	6.0

Figure 10. Optimization trial for expression of ^{15}N-FL-GbpA in Vmax cells. **A:** Minimal medium start composition, used as a starting point for different parameters tested in the optimization trial. **B:** Overview of the optimization workflow. 3x and 6x refers to a 3-fold and 6-fold increase in buffer component concentrations (Na_2HPO_4 and KH_2PO_4). **C:** *Left*: SDS-PAGE analysis of samples taken from the culture supernatant after expression. Condition 6 appeared to result in the highest expression yield. In conditions 2 and 3, glucose was used as a carbon source (instead of glycerol), which likely prevented expression of ^{15}N-FL-GbpA. *Right*: summarized result from the optimization trial, showing OD600 measurements of growth cultures before inoculation of expression cultures as well as the OD600 and pH at harvesting.

Based on the results from the optimization trial, the protocol for Vmax expression of ^{15}N-FL-GbpA was scaled up to 1 L (Figure 5A). SDS-PAGE analysis of SEC fractions revealed high purity (Figure 11B). An efficient, high-yield protocol for production of ^{15}N-FL-GbpA was established (Figure 11A), resulting in an expression yield of 60 mg/L, close to four times as high as that obtained by expression in *E. coli* (Table 5).

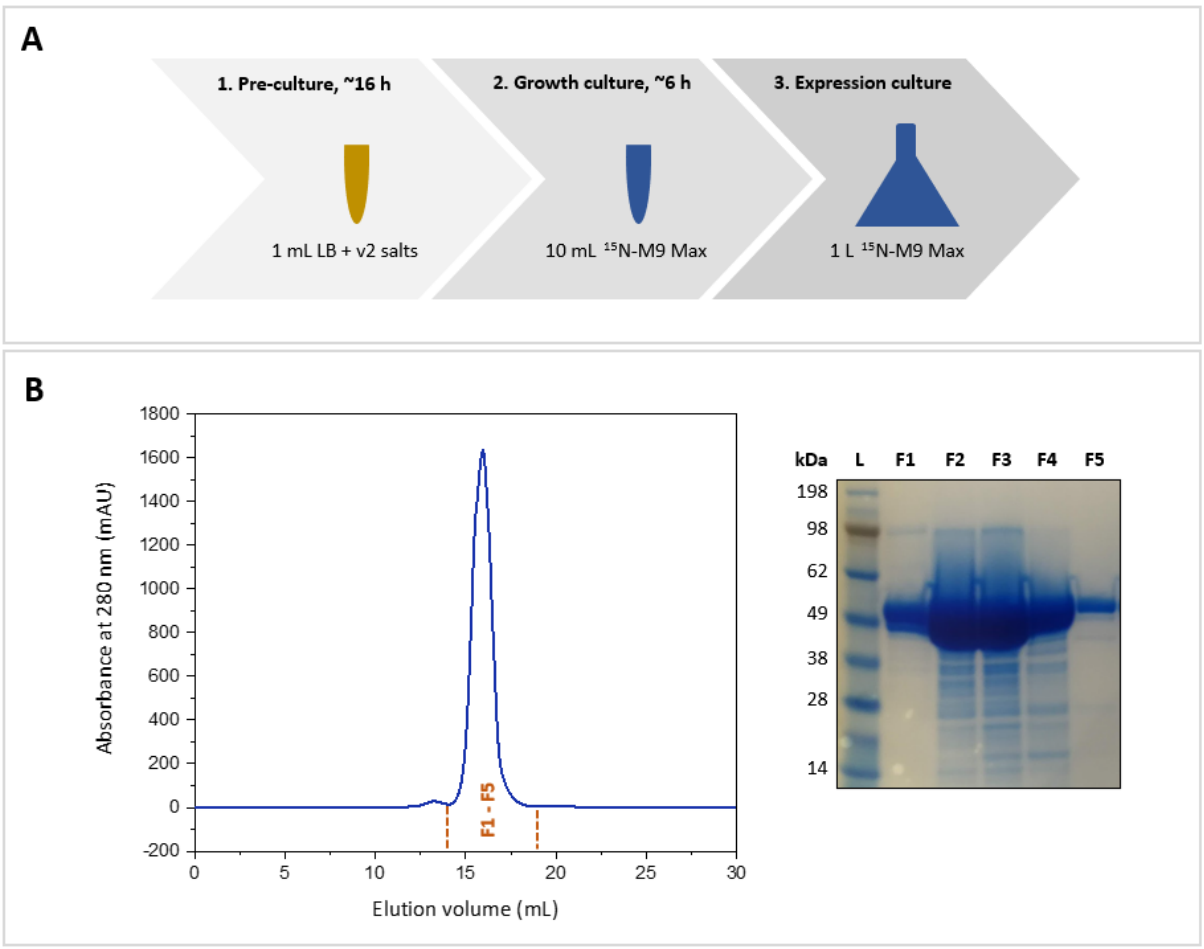

Figure 11. Analysis of ^{15}N-FL-GbpA purification. **A:** Overview of high-yield protocol for Vmax expression of ^{15}N-FL-GbpA. **B:** *Left:* SEC chromatogram of ^{15}N-FL-GbpA expressed in Vmax. 5 fractions of 1 mL were collected and analysed by SDS-PAGE. *Right:* SDS-PAGE analysis of ^{15}N-FL-GbpA SEC fractions, demonstrating a high purity.

3.3 Deuteration of GbpA using Vmax cells

3.3.1 Deuteration of FL-GbpA

Deuteration of proteins is very beneficial for neutron scattering and diffraction techniques, due to the particular sensitivity of neutrons to the isotopes of hydrogen [91]. Moreover, deuteration is an essential tool in protein NMR [102]. In combination with ^{13}C and ^{15}N labelling, deuteration (i.e. the replacement of ^{1}H by ^{2}H) greatly improves the quality of NMR spectra of larger proteins [102]. Deuteration of FL-GbpA (^{2}H-FL-GbpA) in Vmax using shaker flasks was carried out in collaboration with Henrik V. Sørensen, to demonstrate the feasibility of deuteration in Vmax and to enable neutron studies of FL-GbpA for his PhD. Deuteration of proteins by recombinant bacterial expression can be

obtained by growing cells in deuterated media with deuterated glycerol or glucose as a sole carbon source. Expression levels of deuterated proteins are usually lower than for non-deuterated proteins since the growth rate of bacteria in D_2O-based media is slower than in media with H_2O. Conditions for Vmax expression of ^{2}H-FL-GbpA were based on a deuteration protocol for FL-GbpA in *E. coli* (Sørensen et al., unpublished results), and the protocol for Vmax expression of ^{15}N-FL-GbpA (Figure 11A). We named this optimized minimal medium recipe M9 Max (Appendix B). The expression protocol of ^{2}H-FL-GbpA (Figure 12A) followed the same principles as the ^{15}N-labelling protocol, where all hydrogenated compounds where replaced by deuterated material and a few modifications to the expression protocol were made to enable adaptation of Vmax to deuterated medium. This involved a deuterated LB-v2 (D-LB-v2, Appendix B) pre-culture, prepared by a 1:10 dilution of a hydrogenated LB-v2 culture with D-LB-v2 medium. Moreover, the D-M9 Max (Appendix B) growth culture was incubated for 14 hours instead of 6 and after inoculation of the expression culture, induction was performed after 3 hours (OD600 = 1.3). The culture supernatant was collected after 22 hours, followed by dialysis against the AEX binding buffer, and purification by AEX and SEC as described under Section 3.1.1. Samples taken of AEX and SEC purification fractions were analysed by SDS-PAGE, revealing high purity already after the first purification step (Figure 12B). From 100 mL expression cultures, a yield of 45 mg/L culture was obtained, almost four times as high compared to when ^{2}H-FL-GbpA was expressed in *E. coli* BL21 (DE3) (Table 5).

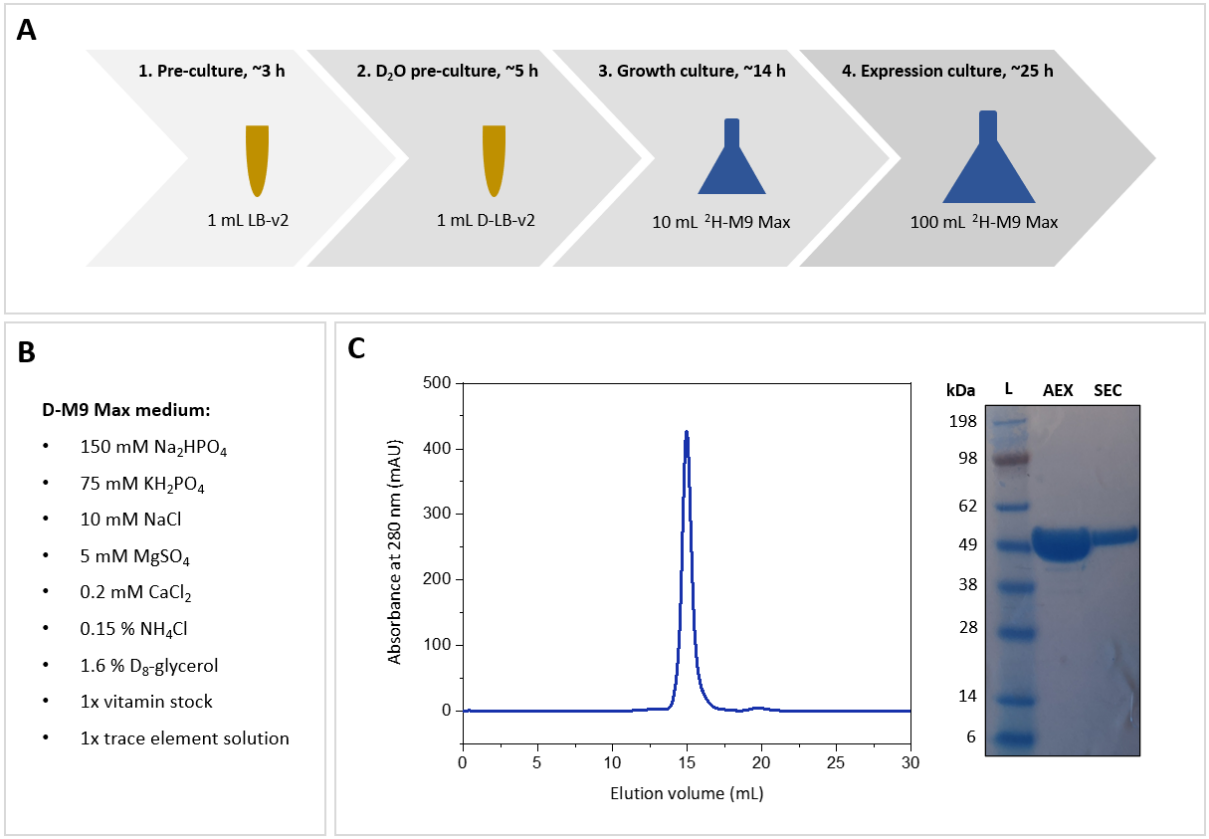

Figure 12. Analysis of Vmax ^{2}H-FL-GbpA production. **A:** Overview of high-yield protocol for Vmax expression of ^{2}H-FL-GbpA. **B:** Composition of D-M9 Max medium. Components were dissolved in D_2O. C: *Left:* SEC chromatogram of ^{2}H-FL-GbpA. SEC fractions were collected and analysed by SDS-PAGE. *Right:* SDS-PAGE analysis of ^{2}H-FL-GbpA AEX and SEC fractions, showing high sample purity after the first purification step.

For expression in deuterated media, this is a very high yield, which enables smaller deuterated cultures to be used, resulting in a fourfold reduction of the overall cost of ^{2}H-FL-GbpA production. For optimal expression of ^{2}H-FL-GbpA in *E. coli*, induction was performed at OD600 = 3, which typically takes 9-12 hours and requires OD600 levels to be closely monitored. With Vmax, early induction greatly simplified the protocol, as high yields were obtained when expression was induced after only 3 hours. The high expenses of D_2O and deuterated carbon sources, as well as slow growth in deuterated media, can be major limitations in the production of deuterated protein, particularly when low expression levels are obtained. In recent years, the Vmax expression system has been recognized due to fast growth rate and high expression yields [2, 8]. However, there is currently no literature regarding deuteration using Vmax. This high-yield deuteration protocol for FL-GbpA dramatically reduces the cost and time for production and demonstrates the amazing potential of deuteration with Vmax.

3.3.2 Deuteration of GbpA-D1

Deuteration of the LPMO domain of GbpA (GbpA-D1) was carried out according to the protocol for Vmax expression of ^{2}H-FL-GbpA (Figure 12A). Unexpectedly, Vmax cells expressing GbpA-D1 had a considerably lower growth rate in M9 Max medium than for Vmax cells expressing FL-GbpA (Section 3.3.1). An OD600 of 3.7 and 2.45 was measured in the deuterated pre-culture and the growth culture, respectively. Due to the low growth rate after inoculation of the expression culture, induction was performed after 7 hours, instead of 3, when the OD600 was 0.62. After incubation for 22 hours, the culture supernatant was dialysed against the AEX binding buffer (Appendix B) and purified as described under Section 3.1.1.

Purification by SEC led to co-elution of several impurities (Figure 13A), the most significant being two proteins at ~30 kDa and ~40 kDa (Figure 13B), which were also observed after purification of H-GbpA-D1 in Vmax (Figure 8C). A yield of 7 mg/L ^{2}H-GbpA-D1 was obtained from a 100 mL expression culture, which is considerably lower than for ^{2}H-FL-GbpA (Table 5). A number of factors may explain the difference in expression yields of ^{2}H-FL-GbpA and ^{2}H-GbpA-D1. It is possible that the differently sized insert in the plasmid affects the expression of the resistance gene. However, the expression test of GbpA-D1 in M9* medium (Section 3.1.2) indicated high expression levels. Therefore, lower yields of ^{2}H-GbpA-D1 might be a result of slow growth of Vmax expressing GbpA-D1 in deuterated medium. A reason for this might be that the colony selected after transformation of the GbpA-D1 plasmid into Vmax cells did not adapt as well to D_2O, thereby resulting in lower expression yields. Better adaptation to deuterated media could perhaps be achieved by plating cells on solid medium and selecting colonies performing best on solid deuterated medium [91]. Alternatively, higher yields might be obtained by incubating the pre-cultures for a longer period, such that the cell density is higher when inoculating the D-M9 Max growth culture. Optimization of expression and purification conditions is necessary to further improve the efficiency and expression yield of this protocol. However, considering that a yield of 0.5-1 mg/L is typically obtained by minimal medium expression of GbpA-D1 in *E. coli* BL21(DE3) shaker cultures (Sørensen et al., unpublished results) (Table 5), a yield of 7 mg/L ^{2}H-GbpA-D1 is already a major improvement.

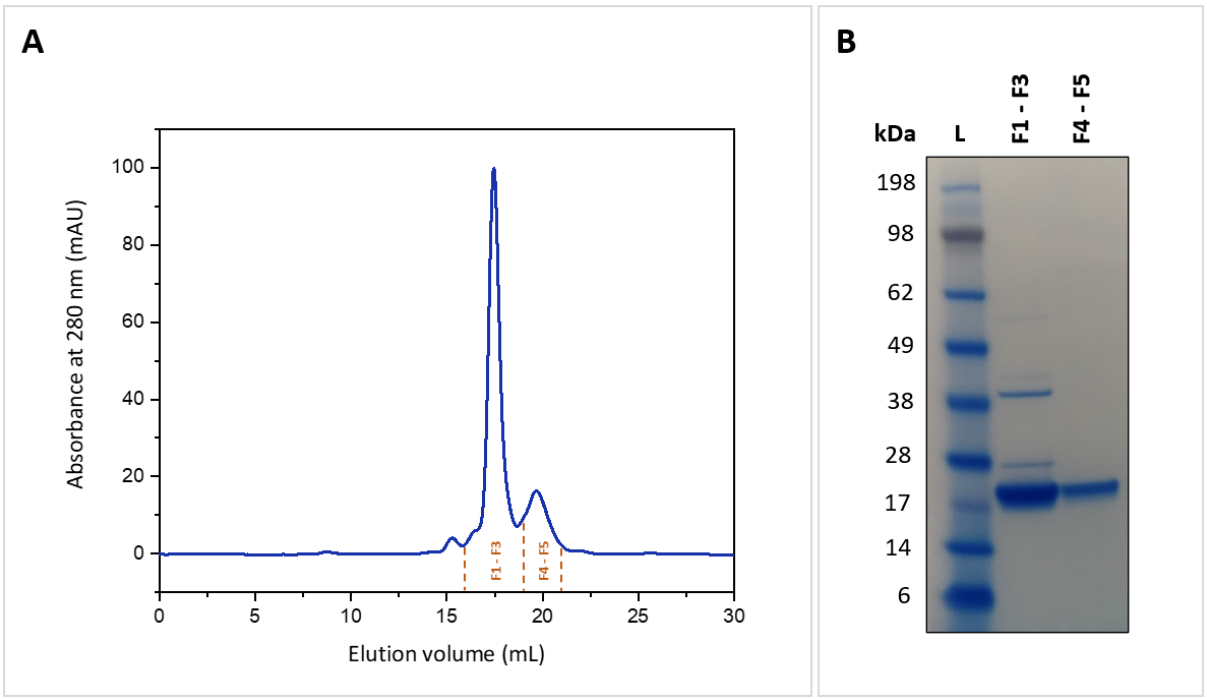

Figure 13. Analysis of ^{2}H-GbpA-D1 purification. **A:** SEC chromatogram of ^{2}H-GbpA-D1 expressed in Vmax. Fractions F1-F3 and F4-F5 were pooled and subsequently analysed by SDS-PAGE. **B:** SDS-PAGE analysis of ^{2}H-GbpA-D1 SEC fractions, revealing that the largest fraction of ^{2}H-GbpA-D1 eluted together with several impurities.

Table 5. Comparison of yields obtained by expression of GbpA in *E. coli* BL21(DE3) and Vmax.

Protein	**BL21(DE3) yield, mg/L**	**Vmax yield, mg/L**
FL-GbpA	TB: 6-7 M9*: 15-16	50
GbpA-D1	TB: 6-7 M9*: 0.5-1	25
^{15}N-FL-GbpA	16	60
^{2}H-FL-GbpA	12	45
^{2}H-GbpA-D1	Not determined	7

Typical yields of *E. coli* expressed FL-GbpA and GbpA-D1 are given for expression in terrific broth (TB) and M9* medium (Appendix B).

3.4 Production of GbpA-D4

The three-dimensional structure of the C-terminal, chitin-binding domain of GbpA (GbpA-D4) is currently unknown. However, circular dichroism (CD) experiments have demonstrated that GbpA-D4 mainly consists of β-secondary structure [72]. In this thesis, the secondary structure of GbpA-D4 was studied by CD spectroscopy to support these results and contribute to the current understanding of this domain. Moreover, preliminary expression trials of GbpA-D4 in minimal medium were conducted to lay the groundwork for future studies by NMR spectroscopy.

3.4.1 Expression in terrific broth (TB) medium

GbpA-D4 was produced based on the Bachelor project report of Caroline Harby (Krengel lab) and previously reported expression and purification conditions [72]. GbpA-D4 was expressed as a glutathione S-transferase (GST)-tagged fusion construct, using a pGEX-6P vector. GST is a 26 kDa protein frequently incorporated as a tag to improve expression levels and solubility, and to facilitate purification [104]. Briefly, an overnight culture was diluted 1:100 with TB medium and expression was performed when OD600 reached 0.8. Cell lysis and purification was performed according to the conditions described under Section 3.4.1. Samples were taken at several steps during expression and purification and were analysed by SDS-PAGE (Figure 14). The GST-tag was removed by incubation with PreScission protease, which cleaves between the Gln and Gly residues of a specific recognition sequence within the GST-tag. GST-GbpA-D4 was incubated with the PreScission protease for 12 hours, resulting in complete cleavage of the GST-tag. Finally, GbpA-D4 was separated from the GST-tag and the PreScission protease by SEC (Figure 15), resulting in a yield of ~1.5 mg/L.

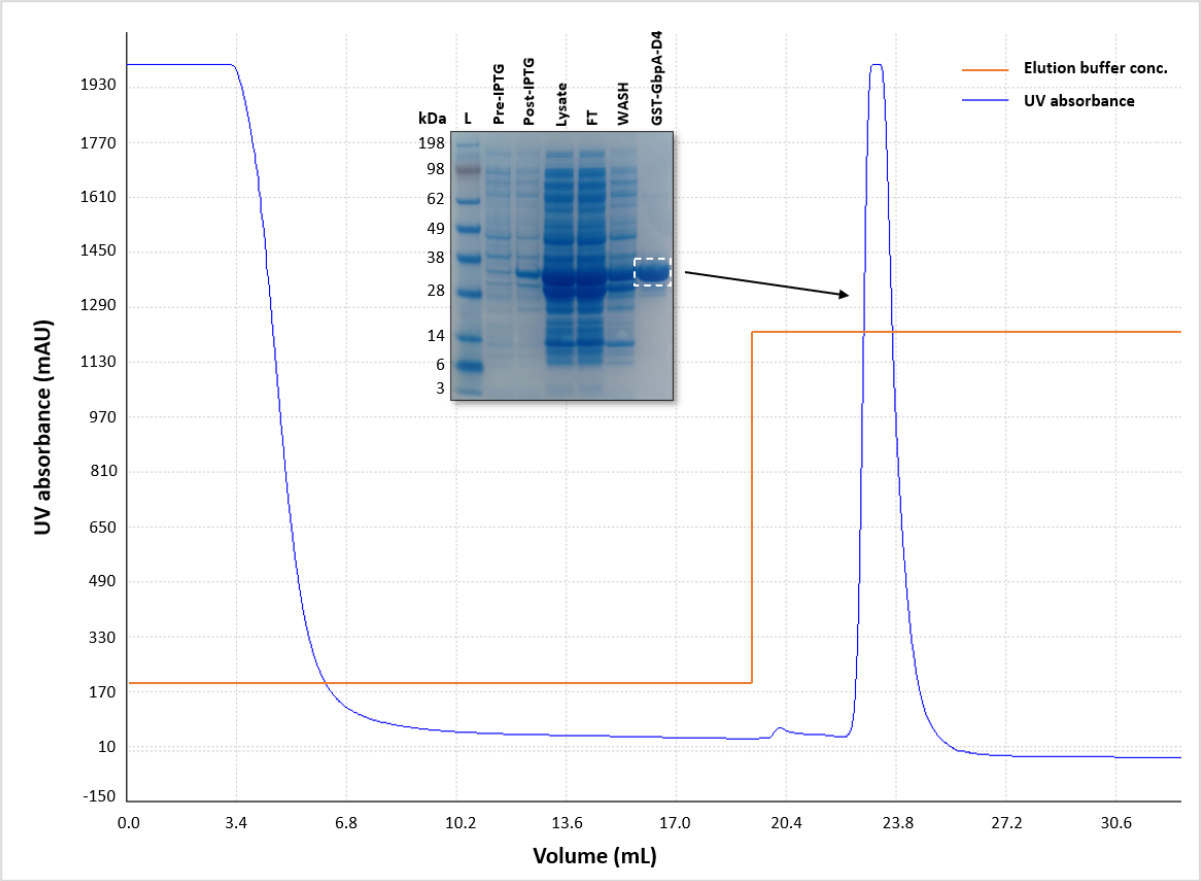

Figure 14. Analysis of GST-GbpA-D4 purification. GST affinity Chromatogram showing the wash step (0 % elution buffer) and elution step (100 % elution buffer) of GST-GbpA-D4 purification. The SDS-PAGE analysis revealed that a major fraction of GST-GbpA-D4 eluted in the flow-through and wash fractions.

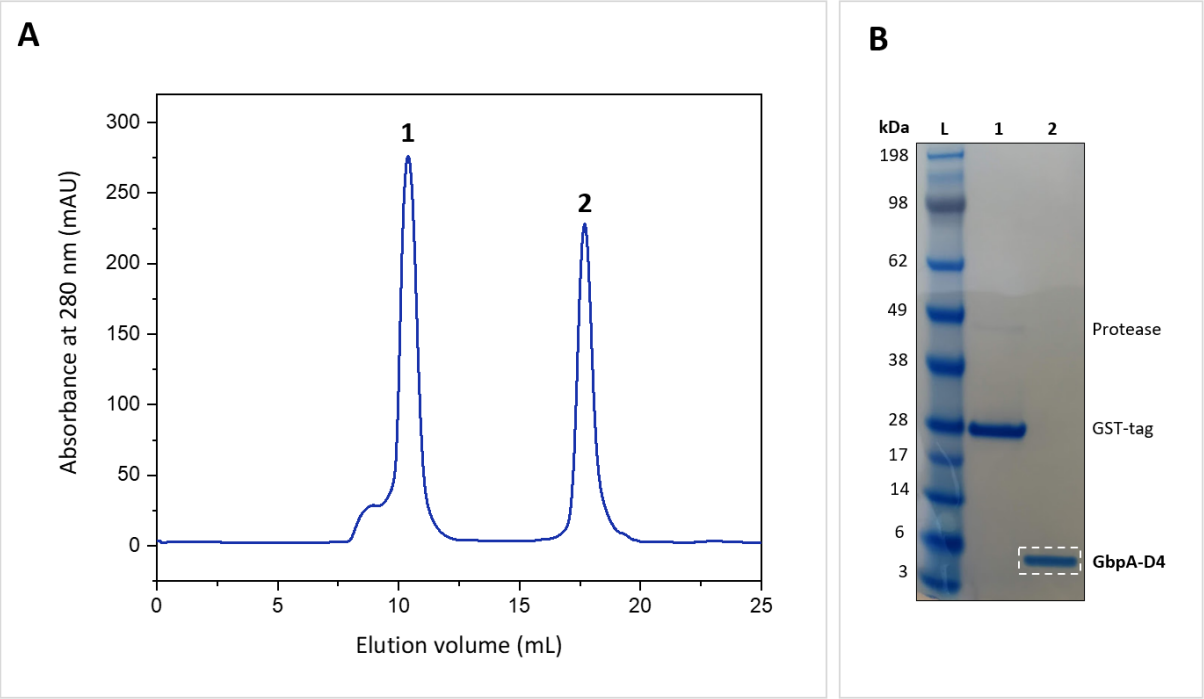

Figure 15. Separation of GbpA-D4 from the cleaved GST-tag and the PreScission protease. **A:** SEC chromatogram showing successful separation of the protease and GST-tag (1) from GbpA-D4 (2). **B:** SDS-PAGE analysis of fractions corresponding to peak 1 and 2 in the SEC chromatogram (A).

SDS-PAGE analysis of purification fractions revealed that a significant amount of GST-GbpA-D4 ended up in the flow-through and wash fractions (Figure 14B), presumably due to inefficient binding to the column material. For maximum binding capacity, it is recommended to keep the flow rate <1 mL/min due to slow binding kinetics between GST and glutathione [105]. However, when the lysate was loaded at a flow rate of 0.5 mL/min, no improvement was observed in the binding capacity, even when a new column was used. It is possible that the lysis conditions partially denatured the GST-tag, preventing it from binding to glutathione. Misfolding of the GST-tag during expression could also affect the binding efficiency. Although sufficient yields were obtained for CD spectroscopy, further optimization of purification conditions is necessary to improve the yields.

3.4.2 Expression in minimal medium

Preliminary expression trials of GST-GbpA-D4 in minimal media using *E. coli* BL21(DE3) were conducted according to the protocol for M9* medium expression of FL-GbpA in *E. coli* (Sørensen et al., unpublished results), resulting in low expression yields. Due to the success of Vmax expression of GbpA in minimal medium, Vmax was also considered as an expression system for GbpA-D4. According to the Vmax Express user guide [98], expression vectors commonly used for *E. coli*

are compatible with Vmax and guidelines for transformation are given for a variety of vectors. However, after several attempts, transformation of the pGEX-6P plasmid encoding GST-GbpA-D4 into Vmax cells was not successful. To improve the yield of GST-GbpA-D4, expression optimization was therefore carried out in *E. coli* BLI21(DE3). An optimization trial was conducted to evaluate how expression is affected by IPTG concentration, expression temperature and OD600 at induction (Figure 16A). Six M9* growth cultures were prepared by a 1:10 dilution of an LB pre-culture. After 15 hours of incubation, the growth cultures were diluted 1:10 with M9* medium and expression was performed according to the conditions summarized in Figure 16A. Samples were taken before and 18 hours after induction and analysed by SDS-PAGE to evaluate the result (Figure 16A). The IPTG concentration (Figure 10A) was the most important parameter affecting expression levels, leading to poor expression of GST-GbpA-D4, while induction at a lower OD600 appeared to be beneficial. Highest expression levels were obtained for conditions 5 and 6, where expression was performed at 16 °C and 20 °C.

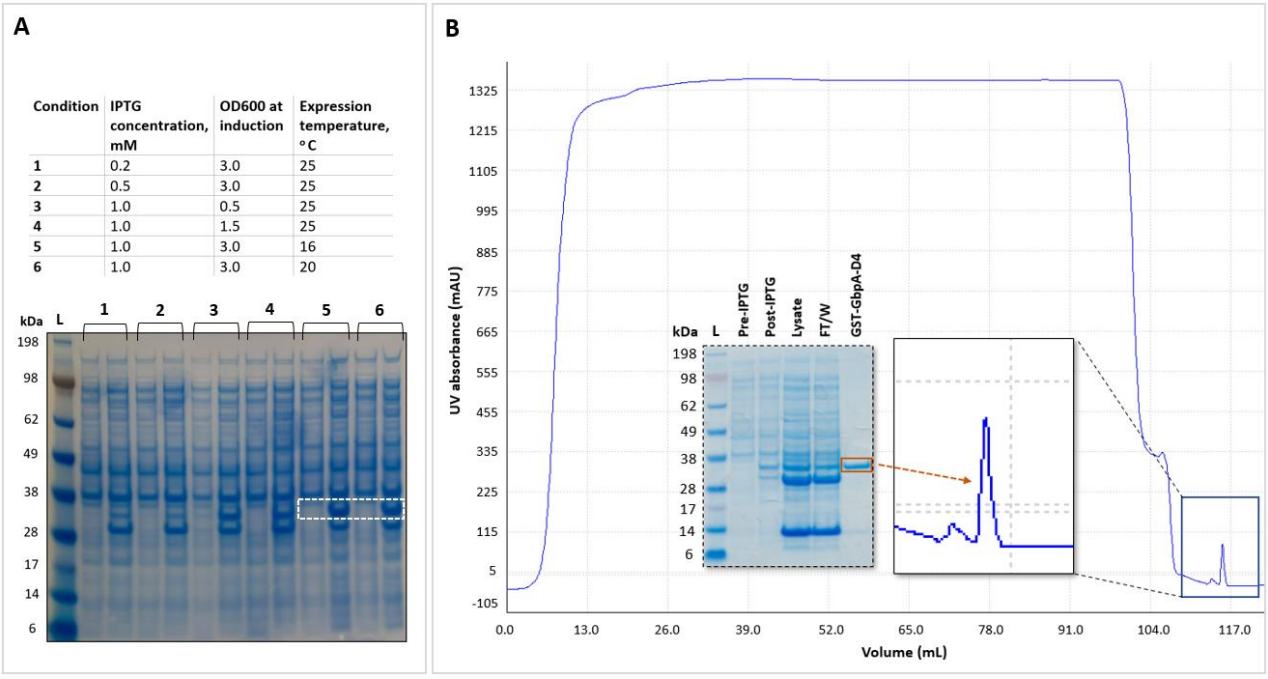

Figure 16. Minimal medium expression optimization of GST-GbpA-D4. **A:** Optimization conditions and the corresponding SDS-PAGE analysis of samples taken before (left) and after (right) induction with IPTG. **B:** GST affinity purification chromatogram of scaled-up GST-GbpA-D4 expression, and SDS-PAGE analysis of samples taken after each expression and purification step.

A lower expression temperature can improve the solubility and folding of recombinantly expressed proteins, by preventing aggregation. Furthermore, for proteins sensitive to proteolytic degradation lower expression temperatures can be beneficial. Since a lower expression temperature appeared to result in highest expression levels, the expression protocol was scaled up to 1 L based on condition 5 (Figure 16A). Cell lysis was carried out by freeze-thaw cycles and incubation with lysozyme. After purification by GST affinity chromatography, a yield of ~0.5 mg was obtained, which is comparable to that obtained for *E. coli* expression of GbpA-D1 in M9* medium, although significantly lower than yields obtained for FL-GbpA (Table 5). A significant amount of GST-GbpA-D4 was observed in the flow-through and wash fractions after purification (Figure 16), which was also the case when GST-GbpA-D4 was produced in TB medium (Section 3.4.1). Compared to the starting conditions, a significant improvement in expression yields was achieved. However, it is necessary to further optimize expression and lysis conditions to obtain sufficient yields for NMR characterisation. As lower IPTG concentrations had a negative impact on expression levels, it would be beneficial to test higher concentrations of IPTG, while varying the time point of induction and expression temperatures.

3.5 Secondary structure estimation by CD spectroscopy

To obtain structural information on GbpA-D4, CD spectra were acquired (Figure 17). Unfortunately, the spectra were drastically affected by noise at wavelengths below 210 nm, despite extensive purification and several rounds of buffer exchange. Similar noise characteristics as well as spectral characteristics were observed for GbpA-D4 by Wong et al [72]. To determine the degree of secondary structure of proteins from the CD spectrum GbpA-D4, we tried the three deconvolution techniques CONTINLL, SELCON3 and CDSSTR in the CDpro package [106]. Spectrum deconvolution was done by varying the frequency regions, to reduce the effect of noise, and basis sets. Deconvolution of the whole frequency region indicated a high content of β-strands and unstructured regions (Figure S1, S2, Appendix D). However, the high level of noise below 210 nm lead to inconsistent results. Likely, the noise was a result of the strong UV absorbance in the sample, which was significantly higher than what is expected for amino acids (Kristiansen, P. E., personal communication). This indicates the presence of a strongly absorbing species, such as a chromophore. One possibility is that GbpA-D4 was non-specifically bound to a chromophore, which is therefore not removed after purification and dialysis. To address this, the sample should be analysed by mass spectrometry (MS).

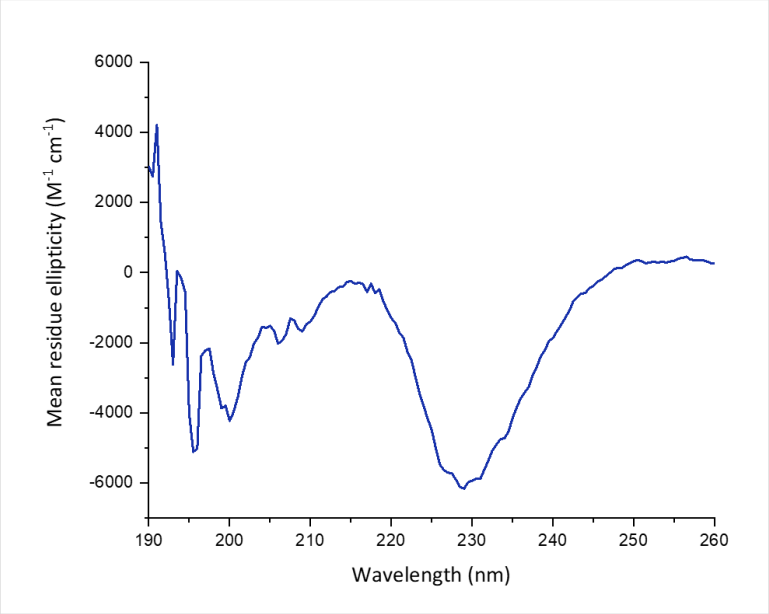

Figure 17. CD spectrum of GbpA-D4 in 10 mM sodium phosphate buffer (pH 7.4) at 20 °C.

3.6 Isolation of *V. cholerae* lipopolysaccharide

Lipopolysaccharide (LPS) was isolated from *V. cholerae* El Tor ΔCTX cells in collaboration with Daniel Hatlem[7], in the lab of Dirk Linke, IBV. The El Tor ΔCTX strain has a deletion of the cholera toxin gene, which was chosen due to safety precautions (see Appendix E for safety statement). LPS was isolated by the phenol-water extraction method described by Westphal et al [107], with a few modifications (see section 2.5.1). *V. cholerae* LPS shows a characteristic pattern on the gel, as reported by [108]. Samples were taken from different steps of the procedure and analysed by silver-stained SDS-PAGE (Figure 12).

After cell lysis and removal of DNA and RNA, LPS was dispensed and solubilised by addition of SDS and sonication. Cell components were then pelleted by centrifugation. Silver-stain SDS-PAGE analysis revealed nevertheless a significant amount of LPS in the pellet (Figure 12). This indicates that the LPS was not sufficiently solubilised before centrifugation. Therefore, the pellet was stored for later LPS purification. During phenol-water extraction, LPS is shown to be extracted into the aqueous phase and proteins into the phenol phase [107]. However, three phases were observed, which made it difficult to estimate which phase contained LPS. Samples from each of the three phases were therefore

[7] Researcher, Department of Biosciences, University of Oslo, Norway

analysed using silver-stain SDS-PAGE (Figure 18), revealing that the "bottom phase" contained LPS. The LPS showed a similar pattern as reported previously for *V. cholerae* LPS [108]. After dialysis and treatment with DNase, RNase and protein kinase A, the LPS fraction appeared to be of high purity (Figure 18). To confirm that the correct SDS-PAGE conditions were used, *S. typhimurium* LPS was used as a control (Figure 18) [109]. *V. cholerae* LPS was successfully isolated and purified, and a yield of 52 mg was obtained from 8 L of bacterial culture.

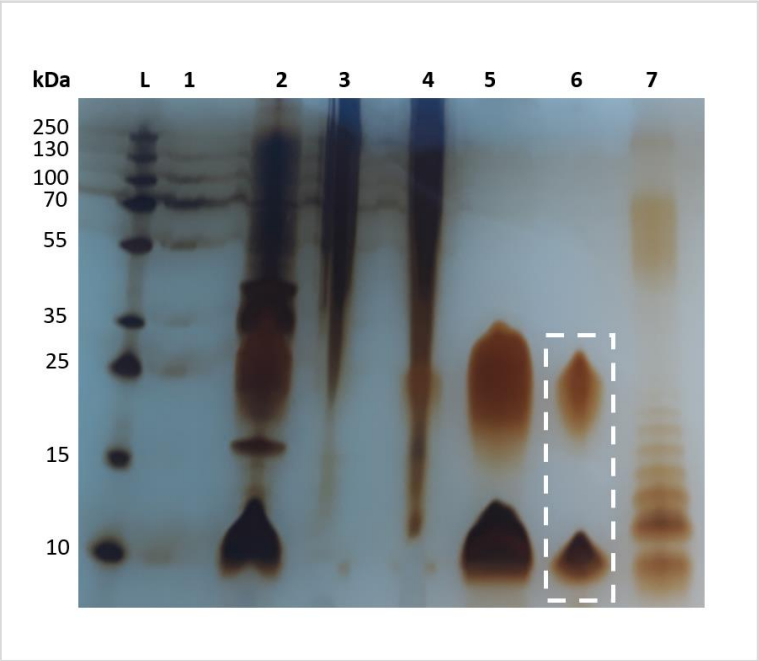

Figure 18. Silver-stained SDS-PAGE analysis of *V. cholerae* LPS isolation and purification. **[L]** Ladder (molecular weight marker). **[1]** Supernatant after ethanol precipitation. **[2]** Pellet after addition of SDS. **[3]** Top phase (phenol extraction). **[4]** Middle "protein" phase (phenol extraction). **[5]** Bottom phase, containing LPS (phenol extraction). **[6]** Bottom phase after dialysis and treatment with DNase, RNase, PK. LPS is highlighted in white. **[7]** *S. typhimurium* smooth LPS, used as a standard.

3.7 NMR titration experiments

Previous experiments indicated that GbpA binds to the surface of *V. cholerae* cells through domains 2 and 3 [72]. Furthermore, GbpA has been shown to bind to various forms of chitin through domains 1 and 4, including β-chitin and chito-oligosaccharides of varying length [69], [72]. In this thesis, interactions of FL-GbpA with various substrates were probed by ^{15}N-TROSY titration experiments, including whole *V. cholerae* cells, *V. cholerae* LPS, β-chitin and pentaacetyl-chitopentaose (GlcNAc-5).

LPS was viewed as a potential interaction partner for GbpA, as it is an abundant molecule on the surface of Gram-negative bacteria. In addition, LPS is involved in numerous processes related to colonization and infection [110]. LPS forms aggregates in solution [111], which complicates interaction studies as most techniques rely on soluble substrates. In titration experiments the NMR signals from the heat-labile enterotoxin (hLTB) of *E. coli* disappeared when LPS was added (Hatlem, D., Master's thesis). When hLTB binds to this LPS aggregates, the hLTBs tumbling will be affected, leading to decreased T1 and increased T2 relaxation and thus peak broadening and loss of signal. Hatlem et al. concluded that it was this effect that lead to the loss of signal. Although residue specific information cannot be derived from such an experiment, we intended to evaluate binding of FL-GbpA to *V. cholerae* LPS. Additionally, this can be used to evaluate binding of GbpA to *V. cholerae* cells.

In a similar study, Madland et al. demonstrated binding of a family 14 carbohydrate-binding module (CBM14) to β-chitin using ^{15}N-HSQC titrations [112]. Although β-chitin is insoluble in aqueous solutions, Madland et al. observed chemical shift perturbation upon addition of β-chitin. This was possible due to fast exchange and high affinity of CBM14 towards β-chitin (Aachmann, F. L., personal communication). Since GbpA has similar chitin-binding properties, we hoped to observe a similar effect for GbpA and β-chitin.

3.7.1 Vibrio cholerae LPS

^{15}N-TROSY titration experiments were conducted to probe the interaction between FL-GbpA and *V. cholerae* LPS. In a series of ^{15}N-TROSY experiments, *V. cholerae* LPS was titrated to a solution of ^{15}N-FL-GbpA. Final concentrations of LPS and GbpA were 327 µM and 221 µM, respectively, giving a molar ratio of 1.48:1 of LPS:GbpA (see Table 1, section 2.6.2). The spectra of ^{15}N-FL-GbpA before and after the titration series were overlayed (Figure 19). No signal reduction was observed, indicating little to no binding between FL-GbpA and LPS.

A strong interaction between FL-GbpA and *V. cholerae* LPS can therefore likely be ruled out. However, it is possible that a weak interaction occurred, that was not detected at these concentrations. Given that the difference in chemical shift needs to be at least 0.1 ppm to detect a binding [113, 114], the estimated dissociation constant (K_d) must be >1.13 mM (see calculations in Appendix D). Consequently, if there is an interaction between FL-GbpA and LPS, it is likely weak. To further evaluate this, titrations with higher concentrations of LPS could be performed. An alternative solution could be to incorporate

LPS in detergent micelles [115], [116], which would allow LPS to be solubilised. The interaction could then be evaluated by monitoring chemical shift perturbations, such that weak interactions could also be detected.

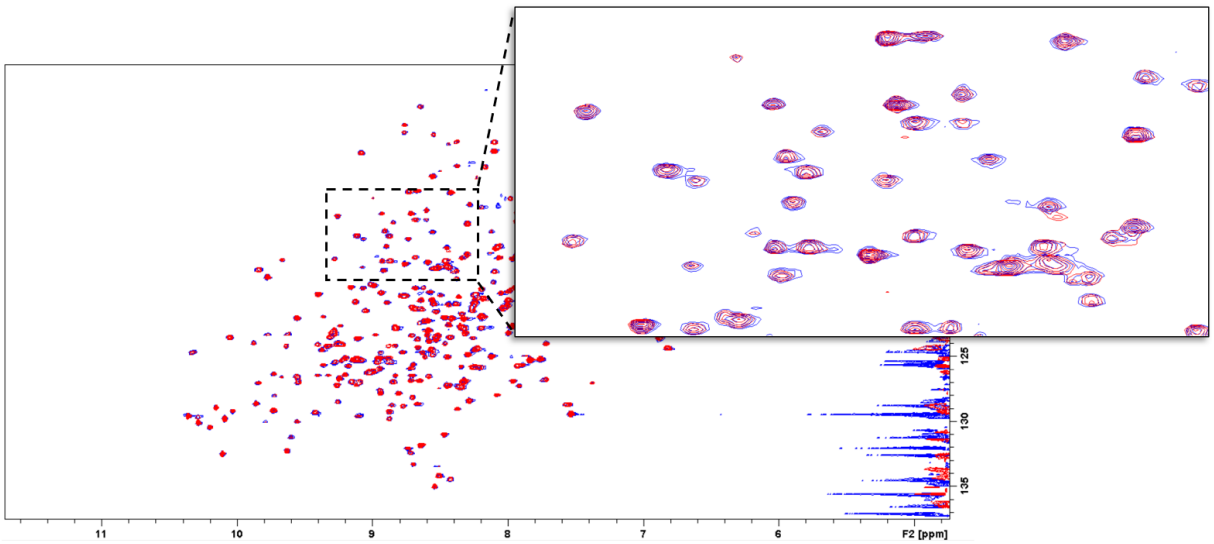

Figure 19. ^{15}N-TROSY spectra of ^{15}N-FL-GbpA. The spectrum of FL-GbpA before addition of LPS (blue) and the final spectrum where the GbpA:LPS molar ratio is 1:1.48 (red)**.** A part of the spectrum is magnified, showing that all peaks are overlapping.

3.7.2 *V. cholerae* cells

Wong et al. demonstrated that GbpA interacts with the surface of *V. cholerae* cells, by a cell-binding assay, where various construct truncation of GbpA were incubated with cells coated in wells, followed by detection using antibodies [72]. To gain further insight into the binding of GbpA to *V. cholerae* cells, ^{15}N-TROSY titrations were performed with washed *V. cholerae* cells, killed with gentamycin. Gentamycin was considered as a suitable antibiotic since the mechanism of action does not rely on membrane lysis. The final concentration of GbpA was 232 µM (9.57×10^{16} molecules) and the amount of cells was approximately 2×10^{8} (see Table 2, section 2.6.2). An overlay of the ^{15}N-FL-GbpA spectra before and after the titration series revealed that no signal reduction had occurred (Figure S3, Appendix D). This indicates that GbpA does not bind to *V. cholerae* cells in a manner that is observable by NMR at NMR-compatible concentrations.

While this is in contrast to finding of Wong et al., the amount of cells relative to the amount of GbpA was approximately 1000 times higher than used here. It is therefore possible that an interaction occurred but was not detected due to the high concentration of GbpA. Wong et al. used N1RB3 cells,

which contains an in-frame deletion of the *gbpA* gene [69]. It is possible that FL-GbpA does not bind to or has a weaker affinity towards *V. cholerae* El Tor ΔCTX. Furthermore, when FL-GbpA was expressed in Vmax (related to *V. cholerae*), the protein was not observed in the soluble fraction of the pellet (Figure 7A, section 3.1.1), demonstrating that GbpA has little to no affinity for the cell surface of Vmax. Small-angle neutron scattering experiments have shown that GbpA undergoes a conformational change when binding to β-chitin (Sørensen et al., unpublished results). Once secreted, it is possible that GbpA binds to chitin surfaces and undergoes a conformational change that enables a stronger interaction to take place between GbpA and the cell surface.

3.7.3 β-Chitin

Preliminary ^{15}N-TROSY titration experiments were performed to evaluate binding of FL-GbpA to β-chitin. In a series of ^{15}N-TROSY experiments, a β-chitin suspension (see section 2.6.1) was added to a solution of ^{15}N-FL-GbpA. The final concentration of FL-GbpA was 164 µM (8.5 mg) and the amount of β-chitin was 1.5 mg (see Table 3, section 2.6.2). The spectra of ^{15}N-FL-GbpA before and after the titration series were overlayed (Figure 20). Significant chemical shift perturbations were observed for several peaks. This suggested that a binding between FL-GbpA and β-chitin was detected.

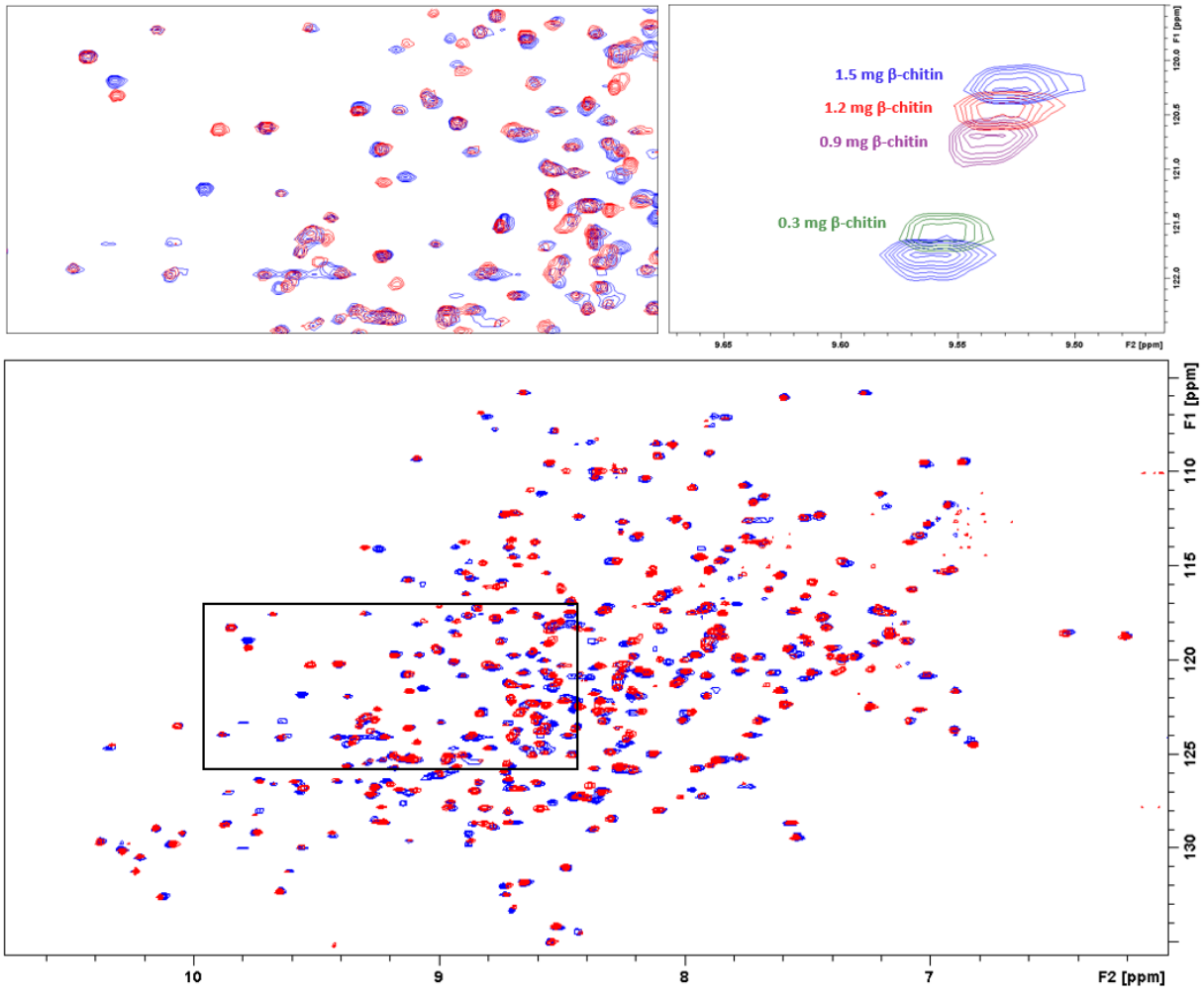

Figure 20. ^{15}N-TROSY spectra of ^{15}N-FL-GbpA. *Top left:* Magnified part of the spectrum, showing several residues are affected. *Top right:* chemical shit perturbations upon addition of β-chitin (pH 5.0). *Bottom:* The spectrum of FL-GbpA before addition of β-chitin (blue) and the final spectrum where the concentration of FL-GbpA is 164 µM and the amount of β-chitin is 1.5 mg (red).

However, the β-chitin suspension had a pH of 5.0, while GbpA was in a buffer at pH 5.5. Changes in pH affect the chemical shift of proteins because the pK_a value for amide protons is dependent on pH [117]. As a control experiment, the titrations were conducted as before, but with both solutions at pH 5.5, which did not lead to chemical shift perturbations. Moreover, an overlay of the ^{15}N-TROSY spectra of FL-GbpA at pH 5.5 and 7.4 revealed that the same residues were affected by pH. It is therefore likely that the chemical shift perturbations seen when β-chitin was titrated to GbpA was a result of pH change. Failed detection could be a result of weaker binding affinity of GbpA towards β-chitin compared to CBM14, which can therefore not be detected using this method. Further insight could be obtained by characterising the interaction using other methods, such as hydrogen-deuterium exchange mass spectrometry (HDX-MS).

3.7.4 GlcNAc-5

Wong et al. quantified binding of GbpA to chito-oligosaccharides using a glycan microarray, where pentaacetyl-chitopentaose (GlcNAc-5) showed highest binding by GbpA [72]. Here, ^{15}N-TROSY titration experiments were conducted to evaluate binding of GbpA to GlcNAc-5. In a series of ^{15}N-TROSY experiments, GlcNAc-5 was titrated to a solution of ^{15}N-FL-GbpA. Final concentrations of GlcNAc-5 and GbpA were 9.65 mM and 0.221 mM, respectively, giving a molar ratio of 45.73:1 of GlcNAc-5:GbpA (see Table 4, section 2.6.2). The spectra of ^{15}N-FL-GbpA before and after the titration series were overlayed (Figure S4, Appendix D). No significant chemical shift changes were observed, indicating that GbpA does not bind to GlcNAc-5, or that the interaction is weak.

Notably, some of the peaks were not observable in the spectrum of FL-GbpA, which could be a result of fast amide proton solvent exchange or increased relaxation rates. It is therefore possible that residues involved in binding are not observable in the spectrum. However, the binding affinity of chitin-binding proteins to chito-oligosaccharides are generally weak, which likely explains why binding was not detected at the concentrations used here. According to these observations, the estimated K_d for the reaction must be 38.4 mM, which corresponds to a weak binding (see calculations in Appendix D). In the glycan microarray by Wong et al., GlcNAc-5 is immobilized to a surface, making GlcNAc-5 resemble the more crystalline substrate of GbpA, which could perhaps result in higher binding affinity of FL-GbpA towards GlcNAc-5. Since binding of GbpA to chito-oligosaccharide is believed to be mediated through domains 1 and 4, further insight might be achieved by titration experiments with ^{15}N-GbpA-D1. As GbpA-D1 is significantly smaller than FL-GbpA, it should be easier to obtain well-resolved peaks and improved sensitivity, which could reveal residues involved in binding. Alternatively, the binding affinity of FL-GbpA to GlcNAc-5 could be determined by e.g. isothermal titration calorimetry (ITC), to evaluate if NMR is a suitable technique to study interactions of GbpA with GlcNAc-5.

4 Summary and future outlook

4.1 High-yield expression of GbpA in Vmax

In this thesis, we developed high-yield, efficient production protocols and isotope labelling protocols for GbpA, using the Vmax expression system. Vmax is derived from *V. natriegens* and has recently been recognized as an expression platform for cost-effective isotope labelling of protein [99]. A high-yield, efficient protocol for expression of ^{15}N-labelled FL-GbpA was developed, resulting in a fourfold increase in expression yields compared to when the protein was produced in *E. coli* BL21(DE3). This enabled sufficient yields for NMR to be obtained from just 200 mL cultures. Preliminary expression trials of GbpA in Vmax revealed that GbpA is secreted into the culture medium during expression, which after buffer exchange, allowed the protein to be purified directly from the supernatant.

In order to enable structural studies of FL-GbpA and GbpA-D1, deuteration protocols were developed. The literature on isotope labelling in Vmax is very limited, and currently no literature on deuteration has been reported. Here, we demonstrated that Vmax is a very suitable expression host for deuteration. We established a protocol for deuteration of FL-GbpA and obtained yields of 45 mg/L culture, which drastically reduces the cost of deuteration. Moreover, this protocol allowed early induction to be performed, which significantly reduced the time of the protocol. Deuteration of GbpA-D1 following the same protocol resulted in a yield of 7 mg/L culture, which was also a significant improvement compared to yields from expression in *E. coli* BL21(DE3).

4.2 Interaction studies by NMR

In this thesis, interaction studies with FL-GbpA were conducted by ^{15}N-TROSY titration experiments. ^{15}N-TROSY spectra of ^{15}N-labelled GbpA expressed in Vmax were well-resolved and suited for interaction studies. Titrations with FL-GbpA and *V. cholerae* LPS indicated that there was no interaction or that the interaction is weak. To verify this, additional experiments should be performed. It would be interesting to probe interactions with surface plasmon resonance (SPR) or isothermal titration calorimetry (ITC) experiments.

To test binding of GbpA to *V. cholerae* cells, ^{15}N-TROSY titrations were performed. In contrast to previously reported results [72], an interaction between GbpA and *V. cholerae* cells could not be

detected. Likely, the concentrations required to detect binding were not NMR-compatible. It would be beneficial to closely replicate the protocol of Wong et al. [72], and perhaps also with GbpA expressed in Vmax to evaluate if a different expression system affects the result. During this project, a binding assay was planned to test for interactions of FL-GbpA with whole *V. cholerae* cells, the outer membrane fraction and LPS. With everything planned, future work on this project should prioritize this experiment as it could provide valuable insight into interactions of GbpA.

GbpA is catalytically active on chitinous surfaces [73]. Studying the detailed molecular interactions of surface-active proteins is challenging. Madland el al demonstrated binding of CBM14 to β-chitin using ^{15}N-HSQC NMR [112]. As GbpA has similar chitin-binding properties to CBM14, we probed the interaction of FL-GbpA and β-chitin by ^{15}N-TROSY titrations. Unfortunately, the interaction could not be detected by, despite several attempts. Although it may not be possible to detect the interaction using this method, it would be interesting to evaluate interaction of GbpA-D1 or GbpA-D4 with β-chitin. Alternatively, chitin-binding could be characterised by SPR using chitin surfaces. It would also be interesting to investigate residues involved in binding of FL-GbpA to β-chitin by hydrogen-deuterium exchange mass spectrometry (HDX-MS).

FL-GbpA has been demonstrated to bind to pentaacetyl-chitopentaose (GlcNAc-5) through domains 1 and 4 [72]. In this project, the interaction was probed by ^{15}N-TROSY titrations. After the titration series, there was no indication of binding. Most likely, the interaction between GbpA and GlcNAc-5 is weak and could therefore not be detected at these concentrations. Consequently, alternative methods should be considered, such as microscale thermophoresis (MST) or ITC.

4.3 Structural studies of GbpA-D4

Currently, a high-resolution three-dimensional structure of GbpA-D4 has not been reported. Being a small domain of 7 kDa, we considered NMR a suitable technique for structure determination. An expression protocol for GbpA-D4 in minimal medium was established, providing a good starting point for an ^{15}N-labelling protocol. Structure analysis of GbpA-D4 by CD spectroscopy showed a high content of β-strands and unstructured region. The spectrum was significantly affected by noise at wavelengths below 210 nm, which resulted in somewhat inconsistent results. However, similar noise and spectral characteristics have been observed for GbpA-D4 by Wong et al. We suspect that the noise in the spectrum is due to the presence of absorbing species in the sample, such as a chromophore. To investigate this, the sample should be analysed by mass spectrometry (MS).

To achieve sufficient yields for NMR, future work should focus on further optimization of the protocol by building on the results from the optimization trial of GbpA-D4. It would be beneficial to test higher IPTG concentrations at induction or to test a different lysis method such as sonication. When sufficient yields are achieved, an ^{15}N-HSQC spectrum should be acquired to evaluate if the protein is suitable for structure determination by NMR. Solving the structure of this domain could increase our knowledge of the function of GbpA and could provide insight into substrate binding.

4.4 Conclusions

In this thesis, a high-yield, efficient ^{15}N-labelling protocol for FL-GbpA was developed, using the Vmax expression system. Furthermore, Vmax proved to be a very suitable expression host for deuteration of FL-GbpA, drastically reducing the time and cost of deuteration. ^{15}N-TROSY titration experiments probed interactions of GbpA with *V. cholerae* cells, LPS and GlcNAc-5, which will hopefully be useful for future interaction studies. The secondary structure of GbpA-D4 was investigated by CD spectroscopy, showing similar spectral characteristics as reported previously for this domain. Moreover, production trials of GbpA-D4 in minimal medium laid the groundwork for future structure determination by NMR.

5 References

[1] E. J. Nelson, J. B. Harris, J. G. Morris Jr, S. B. Calderwood, and A. Camilli, "Cholera transmission: the host, pathogen and bacteriophage dynamic," *Nat. Rev. Microbiol.*, vol. 7, no. 10, pp. 693–702, Oct. 2009, doi: 10.1038/nrmicro2204.

[2] M. Ali, A. R. Nelson, A. L. Lopez, and D. A. Sack, "Updated global burden of cholera in endemic countries," *PLoS Negl. Trop. Dis.*, vol. 9, no. 6, pp. e0003832–e0003832, Jun. 2015, doi: 10.1371/journal.pntd.0003832.

[3] J. N. Zuckerman, L. Rombo, and A. Fisch, "The true burden and risk of cholera: implications for prevention and control.," *Lancet. Infect. Dis.*, vol. 7, no. 8, pp. 521–530, Aug. 2007, doi: 10.1016/S1473-3099(07)70138-X.

[4] Z. Asadgol, H. Mohammadi, M. Kermani, A. Badirzadeh, and M. Gholami, "The effect of climate change on cholera disease: The road ahead using artificial neural network," *PLoS One*, vol. 14, no. 11, pp. e0224813–e0224813, Nov. 2019, doi: 10.1371/journal.pone.0224813.

[5] R. A. Finkelstein, "Cholera, Vibrio cholerae O1 and O139, and Other PathogenicVibrios," *Medical Microbiology*. 1996, [Online]. Available: http://www.ncbi.nlm.nih.gov/pubmed/21413330.

[6] B. Y. Hsueh and C. M. Waters, "Combating Cholera," *F1000Research*, vol. 8, p. F1000 Faculty Rev-589, Apr. 2019, doi: 10.12688/f1000research.18093.1.

[7] A. Jutla, R. Khan, and R. Colwell, "Natural Disasters and Cholera Outbreaks: Current Understanding and Future Outlook," *Curr. Environ. Heal. Reports*, vol. 4, no. 1, pp. 99–107, 2017, doi: 10.1007/s40572-017-0132-5.

[8] "WHO | Cholera in Haiti." [Online]. Available: https://www.who.int/csr/don/2010_10_26/en/.

[9] M. Eppinger *et al.*, "Genomic epidemiology of the Haitian cholera outbreak: a single introduction followed by rapid, extensive, and continued spread characterized the onset of the epidemic.," *MBio*, vol. 5, no. 6, p. e01721, Nov. 2014, doi: 10.1128/mBio.01721-14.

[10] Y. Leibovici-Weissman, A. Neuberger, R. Bitterman, D. Sinclair, M. A. Salam, and M. Paul, "Antimicrobial drugs for treating cholera.," *Cochrane database Syst. Rev.*, vol. 2014, no. 6, p. CD008625, Jun. 2014, doi: 10.1002/14651858.CD008625.pub2.

[11] “WHO | Cholera.” 2015, [Online]. Available: http://www.who.int/mediacentre/factsheets/fs107/en/.

[12] D. Lippi and E. Gotuzzo, “The greatest steps towards the discovery of Vibrio cholerae,” *Clin. Microbiol. Infect.*, vol. 20, no. 3, pp. 191–195, 2014, doi: https://doi.org/10.1111/1469-0691.12390.

[13] B. Bertani and N. Ruiz, “Function and Biogenesis of Lipopolysaccharides,” *EcoSal Plus*, vol. 8, no. 1, pp. 10.1128/ecosalplus.ESP-0001–2018, Aug. 2018, doi: 10.1128/ecosalplus.ESP-0001-2018.

[14] C. Erridge, E. Bennett-Guerrero, and I. R. Poxton, “Structure and function of lipopolysaccharides,” *Microbes Infect.*, vol. 4, no. 8, pp. 837–851, 2002, doi: https://doi.org/10.1016/S1286-4579(02)01604-0.

[15] C. Galanos *et al.*, “Synthetic and natural Escherichia coli free lipid A express identical endotoxic activities.,” *Eur. J. Biochem.*, vol. 148, no. 1, pp. 1–5, Apr. 1985, doi: 10.1111/j.1432-1033.1985.tb08798.x.

[16] V. Sampath, “Bacterial endotoxin-lipopolysaccharide; structure, function and its role in immunity in vertebrates and invertebrates,” *Agric. Nat. Resour.*, vol. 52, no. 2, pp. 115–120, 2018, doi: https://doi.org/10.1016/j.anres.2018.08.002.

[17] M. Lukáčová, I. Barák, and J. Kazár, “Role of structural variations of polysaccharide antigens in the pathogenicity of Gram-negative bacteria,” *Clin. Microbiol. Infect.*, vol. 14, no. 3, pp. 200–206, 2008, doi: https://doi.org/10.1111/j.1469-0691.2007.01876.x.

[18] R. A. Johnson *et al.*, “Comparison of Immune Responses to the O-Specific Polysaccharide and Lipopolysaccharide of Vibrio cholerae O1 in Bangladeshi Adult Patients with Cholera,” *Clin. Vaccine Immunol.*, vol. 19, no. 11, pp. 1712 LP – 1721, Nov. 2012, doi: 10.1128/CVI.00321-12.

[19] S. Kabir and P. Mann, “Immunological properties of the cell envelope components of Vibrio cholerae.,” *J. Gen. Microbiol.*, vol. 119, no. 2, pp. 517–525, Aug. 1980, doi: 10.1099/00221287-119-2-517.

[20] S. Raziuddin, “Toxic and immunological properties of the lipopolysaccharides (O-antigens) from Vibrio el-tor.,” *Immunochemistry*, vol. 15, no. 9, pp. 611–614, Sep. 1978, doi: 10.1016/0161-5890(78)90032-9.

[21] D. S. Chitnis, K. D. Sharma, and R. S. Kamat, “Role of bacterial adhesion in the pathogenesis of cholera.,” *J. Med. Microbiol.*, vol. 15, no. 1, pp. 43–51, Feb. 1982, doi: 10.1099/00222615-15-1-43.

[22] S. L. Chiang and J. J. Mekalanos, “Use of signature-tagged transposon mutagenesis to identify Vibrio cholerae genes critical for colonization.,” *Mol. Microbiol.*, vol. 27, no. 4, pp. 797–805, Feb. 1998, doi: 10.1046/j.1365-2958.1998.00726.x.

[23] M. K. Waldor, R. Colwell, and J. J. Mekalanos, “The Vibrio cholerae O139 serogroup antigen includes an O-antigen capsule and lipopolysaccharide virulence determinants.,” *Proc. Natl. Acad. Sci. U. S. A.*, vol. 91, no. 24, pp. 11388–11392, Nov. 1994, doi: 10.1073/pnas.91.24.11388.

[24] S. N. Chatterjee and J. Das, “Electron microscopic observations on the excretion of cell-wall material by Vibrio cholerae.,” *J. Gen. Microbiol.*, vol. 49, no. 1, pp. 1–11, Oct. 1967, doi: 10.1099/00221287-49-1-1.

[25] J. W. Schertzer and M. Whiteley, “Bacterial outer membrane vesicles in trafficking, communication and the host-pathogen interaction.,” *J. Mol. Microbiol. Biotechnol.*, vol. 23, no. 1–2, pp. 118–130, 2013, doi: 10.1159/000346770.

[26] B. Lindmark *et al.*, “Outer membrane vesicle-mediated release of cytolethal distending toxin (CDT) from Campylobacter jejuni.,” *BMC Microbiol.*, vol. 9, p. 220, Oct. 2009, doi: 10.1186/1471-2180-9-220.

[27] N. C. Kesty, K. M. Mason, M. Reedy, S. E. Miller, and M. J. Kuehn, “Enterotoxigenic Escherichia coli vesicles target toxin delivery into mammalian cells.,” *EMBO J.*, vol. 23, no. 23, pp. 4538–4549, Nov. 2004, doi: 10.1038/sj.emboj.7600471.

[28] S. N. Wai, A. Takade, and K. Amako, “The release of outer membrane vesicles from the strains of enterotoxigenic Escherichia coli.,” *Microbiol. Immunol.*, vol. 39, no. 7, pp. 451–456, 1995, doi: 10.1111/j.1348-0421.1995.tb02228.x.

[29] S. M. Faruque, M. J. Albert, and J. J. Mekalanos, “Epidemiology, genetics, and ecology of toxigenic Vibrio cholerae,” *Microbiol. Mol. Biol. Rev.*, vol. 62, no. 4, pp. 1301–1314, Dec. 1998, [Online]. Available: https://pubmed.ncbi.nlm.nih.gov/9841673.

[30] C. Matz, D. McDougald, A. M. Moreno, P. Y. Yung, F. H. Yildiz, and S. Kjelleberg, “Biofilm formation and phenotypic variation enhance predation-driven persistence of Vibrio cholerae.,” *Proc. Natl. Acad. Sci. U. S. A.*, vol. 102, no. 46, pp. 16819–16824, Nov. 2005, doi:

10.1073/pnas.0505350102.

[31] M. L. Tamplin, A. L. Gauzens, A. Huq, D. A. Sack, and R. R. Colwell, “Attachment of Vibrio cholerae serogroup O1 to zooplankton and phytoplankton of Bangladesh waters.,” *Appl. Environ. Microbiol.*, vol. 56, no. 6, pp. 1977–1980, Jun. 1990, doi: 10.1128/AEM.56.6.1977-1980.1990.

[32] K. L. Meibom, X. B. Li, A. T. Nielsen, C.-Y. Wu, S. Roseman, and G. K. Schoolnik, “The Vibrio cholerae chitin utilization program.,” *Proc. Natl. Acad. Sci. U. S. A.*, vol. 101, no. 8, pp. 2524–2529, Feb. 2004, doi: 10.1073/pnas.0308707101.

[33] J. G. Conner, J. K. Teschler, C. J. Jones, and F. H. Yildiz, “Staying Alive: Vibrio cholerae’s Cycle of Environmental Survival, Transmission, and Dissemination,” *Microbiol. Spectr.*, vol. 4, no. 2, pp. 10.1128/microbiolspec.VMBF-0015–2015, Apr. 2016, doi: 10.1128/microbiolspec.VMBF-0015-2015.

[34] S. M. Faruque *et al.*, “Transmissibility of cholera: in vivo-formed biofilms and their relationship to infectivity and persistence in the environment,” *Proc. Natl. Acad. Sci. U. S. A.*, vol. 103, no. 16, pp. 6350–6355, Apr. 2006, doi: 10.1073/pnas.0601277103.

[35] D. M. Moncada, S. J. Kammanadiminti, and K. Chadee, “Mucin and Toll-like receptors in host defense against intestinal parasites,” *Trends Parasitol.*, vol. 19, no. 7, pp. 305–311, Jul. 2003, doi: 10.1016/S1471-4922(03)00122-3.

[36] H. FLOREY, “Mucin and the protection of the body.,” *Proc. R. Soc. London. Ser. B, Biol. Sci.*, vol. 143, no. 911, pp. 147–158, Jan. 1955, doi: 10.1098/rspb.1955.0001.

[37] M. A. McGuckin, S. K. Lindén, P. Sutton, and T. H. Florin, “Mucin dynamics and enteric pathogens.,” *Nat. Rev. Microbiol.*, vol. 9, no. 4, pp. 265–278, Apr. 2011, doi: 10.1038/nrmicro2538.

[38] J. H. Leitão, “Microbial Virulence Factors,” *Int. J. Mol. Sci.*, vol. 21, no. 15, p. 5320, Jul. 2020, doi: 10.3390/ijms21155320.

[39] A. Casadevall and L.-A. Pirofski, “Virulence factors and their mechanisms of action: the view from a damage-response framework.,” *J. Water Health*, vol. 7 Suppl 1, pp. S2–S18, 2009, doi: 10.2166/wh.2009.036.

[40] P. Klemm and M. A. Schembri, “Bacterial adhesins: function and structure,” *Int. J. Med. Microbiol.*, vol. 290, no. 1, pp. 27–35, 2000, doi: https://doi.org/10.1016/S1438-

4221(00)80102-2.

[41] R. Bhowmick *et al.*, “Intestinal adherence of Vibrio cholerae involves a coordinated interaction between colonization factor GbpA and mucin.,” *Infect. Immun.*, vol. 76, no. 11, pp. 4968–4977, Nov. 2008, doi: 10.1128/IAI.01615-07.

[42] S. M. Faruque *et al.*, “Pathogenic potential of environmental Vibrio cholerae strains carrying genetic variants of the toxin-coregulated pilus pathogenicity island,” *Infect. Immun.*, vol. 71, no. 2, pp. 1020–1025, Feb. 2003, doi: 10.1128/iai.71.2.1020-1025.2003.

[43] W. H. O. S. W. Group, “Cholera and other vibrio-associated diarrhoeas,” *Bull. World Health Organ.*, vol. 58, no. 3, pp. 353–374, 1980, [Online]. Available: https://pubmed.ncbi.nlm.nih.gov/6968251.

[44] D. A. Herrington, R. H. Hall, G. Losonsky, J. J. Mekalanos, R. K. Taylor, and M. M. Levine, “Toxin, toxin-coregulated pili, and the toxR regulon are essential for Vibrio cholerae pathogenesis in humans.,” *J. Exp. Med.*, vol. 168, no. 4, pp. 1487–1492, Oct. 1988, doi: 10.1084/jem.168.4.1487.

[45] T. Beddoe, A. W. Paton, J. Le Nours, J. Rossjohn, and J. C. Paton, “Structure, biological functions and applications of the AB5 toxins,” *Trends Biochem. Sci.*, vol. 35, no. 7, pp. 411–418, Jul. 2010, doi: 10.1016/j.tibs.2010.02.003.

[46] C. J. O’Neal, E. I. Amaya, M. G. Jobling, R. K. Holmes, and W. G. J. Hol, “Crystal structures of an intrinsically active cholera toxin mutant yield insight into the toxin activation mechanism.,” *Biochemistry*, vol. 43, no. 13, pp. 3772–3782, Apr. 2004, doi: 10.1021/bi0360152.

[47] W. S. Dallas and S. Falkow, “Amino acid sequence homology between cholera toxin and Escherichia coli heat-labile toxin.,” *Nature*, vol. 288, no. 5790, pp. 499–501, Dec. 1980, doi: 10.1038/288499a0.

[48] T. K. Sixma *et al.*, “Crystal structure of a cholera toxin-related heat-labile enterotoxin from E. coli.,” *Nature*, vol. 351, no. 6325, pp. 371–377, May 1991, doi: 10.1038/351371a0.

[49] E. A. Merritt, F. van den Akker, and W. G. J. Hol, “E. Coli Heat Labile Enterotoxin and Cholera Toxin B-Pentamer—Crystallographic Studies of Biological Activity BT - Protein Toxin Structure,” M. W. Parker, Ed. Berlin, Heidelberg: Springer Berlin Heidelberg, 1996, pp. 147–172.

[50] A. L. Horstman and M. J. Kuehn, “Bacterial surface association of heat-labile enterotoxin through lipopolysaccharide after secretion via the general secretory pathway,” *J. Biol. Chem.*, vol. 277, no. 36, pp. 32538–32545, Sep. 2002, doi: 10.1074/jbc.M203740200.

[51] A. L. Horstman, S. J. Bauman, and M. J. Kuehn, “Lipopolysaccharide 3-deoxy-D-manno-octulosonic acid (Kdo) core determines bacterial association of secreted toxins,” *J. Biol. Chem.*, vol. 279, no. 9, pp. 8070–8075, Feb. 2004, doi: 10.1074/jbc.M308633200.

[52] B. Moussian, “Chitin: Structure, Chemistry and Biology BT - Targeting Chitin-containing Organisms,” Q. Yang and T. Fukamizo, Eds. Singapore: Springer Singapore, 2019, pp. 5–18.

[53] R. Hamid *et al.*, “Chitinases: An update,” *J. Pharm. Bioallied Sci.*, vol. 5, no. 1, pp. 21–29, Jan. 2013, doi: 10.4103/0975-7406.106559.

[54] “CAZy - GH.” 2020, [Online]. Available: http://www.cazy.org/Glycoside-Hydrolases.html.

[55] G. Vaaje-Kolstad *et al.*, “An oxidative enzyme boosting the enzymatic conversion of recalcitrant polysaccharides.,” *Science*, vol. 330, no. 6001, pp. 219–222, Oct. 2010, doi: 10.1126/science.1192231.

[56] E. T. REESE, R. G. H. SIU, and H. S. LEVINSON, “The biological degradation of soluble cellulose derivatives and its relationship to the mechanism of cellulose hydrolysis,” *J. Bacteriol.*, vol. 59, no. 4, pp. 485–497, Apr. 1950, doi: 10.1128/JB.59.4.485-497.1950.

[57] Z. Forsberg *et al.*, “Polysaccharide degradation by lytic polysaccharide monooxygenases,” *Curr. Opin. Struct. Biol.*, vol. 59, pp. 54–64, 2019, doi: https://doi.org/10.1016/j.sbi.2019.02.015.

[58] J. V Vermaas, M. F. Crowley, G. T. Beckham, and C. M. Payne, “Effects of lytic polysaccharide monooxygenase oxidation on cellulose structure and binding of oxidized cellulose oligomers to cellulases.,” *J. Phys. Chem. B*, vol. 119, no. 20, pp. 6129–6143, May 2015, doi: 10.1021/acs.jpcb.5b00778.

[59] Z. Forsberg, B. Bissaro, J. Gullesen, B. Dalhus, G. Vaaje-Kolstad, and V. G. H. Eijsink, “Structural determinants of bacterial lytic polysaccharide monooxygenase functionality,” *J. Biol. Chem.*, vol. 293, no. 4, pp. 1397–1412, Jan. 2018, doi: 10.1074/jbc.M117.817130.

[60] A. Levasseur, E. Drula, V. Lombard, P. M. Coutinho, and B. Henrissat, “Expansion of the enzymatic repertoire of the CAZy database to integrate auxiliary redox enzymes.,” *Biotechnol. Biofuels*, vol. 6, no. 1, p. 41, Mar. 2013, doi: 10.1186/1754-6834-6-41.

[61] V. Lombard, H. Golaconda Ramulu, E. Drula, P. M. Coutinho, and B. Henrissat, “The carbohydrate-active enzymes database (CAZy) in 2013.,” *Nucleic Acids Res.*, vol. 42, no. Database issue, pp. D490-5, Jan. 2014, doi: 10.1093/nar/gkt1178.

[62] V. G. H. Eijsink *et al.*, "On the functional characterization of lytic polysaccharide monooxygenases (LPMOs)," *Biotechnol. Biofuels*, vol. 12, no. 1, p. 58, 2019, doi: 10.1186/s13068-019-1392-0.

[63] S. J. Horn, G. Vaaje-Kolstad, B. Westereng, and V. Eijsink, "Novel enzymes for the degradation of cellulose," *Biotechnol. Biofuels*, vol. 5, no. 1, p. 45, 2012, doi: 10.1186/1754-6834-5-45.

[64] V. Eijsink and G. Vaaje-Kolstad, "Auxiliary Activity Family 10 - CAZypedia." 2018, [Online]. Available: https://www.cazypedia.org/index.php/Auxiliary_Activity_Family_10.

[65] G. Vaaje-Kolstad, D. R. Houston, A. H. K. Riemen, V. G. H. Eijsink, and D. M. F. van Aalten, "Crystal Structure and Binding Properties of the Serratia marcescens Chitin-binding Protein CBP21 *," *J. Biol. Chem.*, vol. 280, no. 12, pp. 11313–11319, Mar. 2005, doi: 10.1074/jbc.M407175200.

[66] M. Agostoni, J. A. Hangasky, and M. A. Marletta, "Physiological and Molecular Understanding of Bacterial Polysaccharide Monooxygenases.," *Microbiol. Mol. Biol. Rev.*, vol. 81, no. 3, Sep. 2017, doi: 10.1128/MMBR.00015-17.

[67] R. F. Frederiksen *et al.*, "Bacterial chitinases and chitin-binding proteins as virulence factors.," *Microbiology*, vol. 159, no. Pt 5, pp. 833–847, May 2013, doi: 10.1099/mic.0.051839-0.

[68] D. K. Paspaliari, J. S. M. Loose, M. H. Larsen, and G. Vaaje-Kolstad, "Listeria monocytogenes has a functional chitinolytic system and an active lytic polysaccharide monooxygenase.," *FEBS J.*, vol. 282, no. 5, pp. 921–936, Mar. 2015, doi: 10.1111/febs.13191.

[69] T. J. Kirn, B. A. Jude, and R. K. Taylor, "A colonization factor links Vibrio cholerae environmental survival and human infection.," *Nature*, vol. 438, no. 7069, pp. 863–866, Dec. 2005, doi: 10.1038/nature04249.

[70] F. Askarian *et al.*, "The lytic polysaccharide monooxygenase CbpD promotes Pseudomonas aeruginosa virulence in systemic infection," *Nat. Commun.*, vol. 12, no. 1, p. 1230, 2021, doi: 10.1038/s41467-021-21473-0.

[71] A. J. Book, R. M. Yennamalli, T. E. Takasuka, C. R. Currie, G. N. Phillips, and B. G. Fox, "Evolution of substrate specificity in bacterial AA10 lytic polysaccharide monooxygenases," *Biotechnol. Biofuels*, vol. 7, no. 1, p. 109, 2014, doi: 10.1186/1754-6834-7-109.

[72] E. Wong *et al.*, "The Vibrio cholerae colonization factor GbpA possesses a modular structure that governs binding to different host surfaces.," *PLoS Pathog.*, vol. 8, no. 1, p. e1002373, Jan.

2012, doi: 10.1371/journal.ppat.1002373.

[73] J. S. M. Loose, Z. Forsberg, M. W. Fraaije, V. G. H. Eijsink, and G. Vaaje-Kolstad, “A rapid quantitative activity assay shows that the Vibrio cholerae colonization factor GbpA is an active lytic polysaccharide monooxygenase.,” *FEBS Lett.*, vol. 588, no. 18, pp. 3435–3440, Sep. 2014, doi: 10.1016/j.febslet.2014.07.036.

[74] Z. Mutahir *et al.*, “Characterization and synergistic action of a tetra-modular lytic polysaccharide monooxygenase from Bacillus cereus.,” *FEBS Lett.*, vol. 592, no. 15, pp. 2562–2571, Aug. 2018, doi: 10.1002/1873-3468.13189.

[75] S. Chaudhuri, B. N. Gantner, R. D. Ye, N. P. Cianciotto, and N. E. Freitag, “The Listeria monocytogenes ChiA chitinase enhances virulence through suppression of host innate immunity.,” *MBio*, vol. 4, no. 2, pp. e00617-12, Mar. 2013, doi: 10.1128/mBio.00617-12.

[76] G. Vaaje-Kolstad, Z. Forsberg, J. S. M. Loose, B. Bissaro, and V. G. H. Eijsink, “Structural diversity of lytic polysaccharide monooxygenases,” *Curr. Opin. Struct. Biol.*, vol. 44, pp. 67–76, 2017, doi: https://doi.org/10.1016/j.sbi.2016.12.012.

[77] S. D. Knight, D. Choudhury, S. Hultgren, J. Pinkner, V. Stojanoff, and A. Thompson, “Structure of the S pilus periplasmic chaperone SfaE at 2.2 A resolution.,” *Acta Crystallogr. D. Biol. Crystallogr.*, vol. 58, no. Pt 6 Pt 2, pp. 1016–1022, Jun. 2002, doi: 10.1107/s0907444902005954.

[78] I. Le Trong *et al.*, “Structural basis for mechanical force regulation of the adhesin FimH via finger trap-like beta sheet twisting,” *Cell*, vol. 141, no. 4, pp. 645–655, May 2010, doi: 10.1016/j.cell.2010.03.038.

[79] M. J. Howard, “Protein NMR spectroscopy,” *Curr. Biol.*, vol. 8, no. 10, pp. R331–R333, May 1998, doi: 10.1016/S0960-9822(98)70214-3.

[80] T. D. W. Claridge, “Chapter 1 - Introduction,” T. D. W. B. T.-H.-R. N. M. R. T. in O. C. (Third E. Claridge, Ed. Boston: Elsevier, 2016, pp. 1–10.

[81] P. R. L. Markwick, T. Malliavin, and M. Nilges, “Structural biology by NMR: structure, dynamics, and interactions,” *PLoS Comput. Biol.*, vol. 4, no. 9, pp. e1000168–e1000168, Sep. 2008, doi: 10.1371/journal.pcbi.1000168.

[82] G. Wang, Z.-T. Zhang, B. Jiang, X. Zhang, C. Li, and M. Liu, “Recent advances in protein NMR spectroscopy and their implications in protein therapeutics research,” *Anal. Bioanal. Chem.*, vol. 406, no. 9, pp. 2279–2288, 2014, doi: 10.1007/s00216-013-7518-5.

[83] A. K. Mittermaier and L. E. Kay, “Observing biological dynamics at atomic resolution using NMR.,” *Trends Biochem. Sci.*, vol. 34, no. 12, pp. 601–611, Dec. 2009, doi: 10.1016/j.tibs.2009.07.004.

[84] W. Becker, K. C. Bhattiprolu, N. Gubensäk, and K. Zangger, “Investigating protein-ligand interactions by solution nuclear magnetic resonance spectroscopy,” *Chemphyschem*, vol. 19, no. 8, pp. 895–906, Apr. 2018, doi: 10.1002/cphc.201701253.

[85] G. Klebe, “Protein–Ligand Interactions as the basis for drug Action BT - drug design: methodology, concepts, and mode-of-action,” G. Klebe, Ed. Berlin, Heidelberg: Springer Berlin Heidelberg, 2013, pp. 61–88.

[86] M. P. Williamson, “Using chemical shift perturbation to characterise ligand binding.,” *Prog. Nucl. Magn. Reson. Spectrosc.*, vol. 73, pp. 1–16, Aug. 2013, doi: 10.1016/j.pnmrs.2013.02.001.

[87] G. Bodenhausen and D. J. Ruben, “Natural abundance nitrogen-15 NMR by enhanced heteronuclear spectroscopy,” *Chem. Phys. Lett.*, vol. 69, no. 1, pp. 185–189, 1980, doi: https://doi.org/10.1016/0009-2614(80)80041-8.

[88] K. Pervushin, R. Riek, G. Wider, and K. Wüthrich, “Attenuated T2 relaxation by mutual cancellation of dipole-dipole coupling and chemical shift anisotropy indicates an avenue to NMR structures of very large biological macromolecules in solution.,” *Proc. Natl. Acad. Sci. U. S. A.*, vol. 94, no. 23, pp. 12366–12371, Nov. 1997, doi: 10.1073/pnas.94.23.12366.

[89] R. Sprangers, A. Velyvis, and L. E. Kay, “Solution NMR of supramolecular complexes: providing new insights into function.,” *Nat. Methods*, vol. 4, no. 9, pp. 697–703, Sep. 2007, doi: 10.1038/nmeth1080.

[90] S. Ohki and M. Kainosho, “Stable isotope labeling methods for protein NMR spectroscopy,” *Prog. Nucl. Magn. Reson. Spectrosc.*, vol. 53, no. 4, pp. 208–226, 2008, doi: https://doi.org/10.1016/j.pnmrs.2008.01.003.

[91] F. Meilleur, K. L. Weiss, and D. A. A. Myles, “Deuterium labeling for neutron structure-function-dynamics analysis.,” *Methods Mol. Biol.*, vol. 544, pp. 281–292, 2009, doi: 10.1007/978-1-59745-483-4_18.

[92] N. J. Greenfield, “Using circular dichroism spectra to estimate protein secondary structure,” *Nat. Protoc.*, vol. 1, no. 6, pp. 2876–2890, 2006, doi: 10.1038/nprot.2006.202.

[93] S. Beychok, “Circular Dichroism of Biological Macromolecules,” *Science (80-.).*, vol. 154, no.

3754, pp. 1288 LP – 1299, Dec. 1966, doi: 10.1126/science.154.3754.1288.

[94] N. J. Greenfield, “Methods to Estimate the Conformation of Proteins and Polypeptides from Circular Dichroism Data,” *Anal. Biochem.*, vol. 235, no. 1, pp. 1–10, 1996, doi: https://doi.org/10.1006/abio.1996.0084.

[95] S. R. Martin and M. J. B. T.-M. in C. B. Schilstra, “Circular dichroism and its application to the study of biomolecules,” in *Biophysical Tools for Biologists, Volume One: In Vitro Techniques*, vol. 84, Academic Press, 2008, pp. 263–293.

[96] “VMAX X2 CHEMICALLY COMPETENT CELLS Instructions,” 2020.

[97] M. T. Weinstock, E. D. Hesek, C. M. Wilson, and D. G. Gibson, “Vibrio natriegens as a fast-growing host for molecular biology.,” *Nat. Methods*, vol. 13, no. 10, pp. 849–851, Oct. 2016, doi: 10.1038/nmeth.3970.

[98] Synthetic Genomics, “Vmax™ Express Electrocompetent Cells User Guide,” no. 10.04.17, pp. 1–20, 2017, [Online]. Available: https://www.biocat.com/bc/pdf/Vmax_Express_40026_100517-Rev1.6.pdf.

[99] W. Becker, F. Wimberger, and K. Zangger, “Vibrio natriegens: an alternative expression system for the high-yield production of isotopically labeled proteins.,” *Biochemistry*, vol. 58, no. 25, pp. 2799–2803, Jun. 2019, doi: 10.1021/acs.biochem.9b00403.

[100] J. T. Sockolosky and F. C. Szoka, “Periplasmic production via the pET expression system of soluble, bioactive human growth hormone,” *Protein Expr. Purif.*, vol. 87, no. 2, pp. 129–135, Feb. 2013, doi: 10.1016/j.pep.2012.11.002.

[101] C. P. Long, J. E. Gonzalez, R. M. Cipolla, and M. R. Antoniewicz, “Metabolism of the fast-growing bacterium Vibrio natriegens elucidated by (13)C metabolic flux analysis,” *Metab. Eng.*, vol. 44, pp. 191–197, Nov. 2017, doi: 10.1016/j.ymben.2017.10.008.

[102] M. Sattler and S. W. Fesik, “Use of deuterium labeling in NMR: overcoming a sizeable problem.,” *Structure*, vol. 4, no. 11, pp. 1245–1249, Nov. 1996, doi: 10.1016/s0969-2126(96)00133-5.

[103] J. Hoff, B. Daniel, D. Stukenberg, B. W. Thuronyi, T. Waldminghaus, and G. Fritz, “Vibrio natriegens: an ultrafast-growing marine bacterium as emerging synthetic biology chassis.,” *Environ. Microbiol.*, vol. 22, no. 10, pp. 4394–4408, Oct. 2020, doi: 10.1111/1462-2920.15128.

[104] S. Harper and D. W. Speicher, “Purification of proteins fused to glutathione S-transferase,”

Methods Mol. Biol., vol. 681, pp. 259–280, 2011, doi: 10.1007/978-1-60761-913-0_14.

[105] G. Hp, G. Hp, G. Sepharose, and H. Performance, "GSTrap™ HP, 1," pp. 1–24.

[106] N. Sreerama and R. W. Woody, "Estimation of protein secondary structure from circular dichroism spectra: comparison of CONTIN, SELCON, and CDSSTR methods with an expanded reference set," *Anal. Biochem.*, vol. 287, no. 2, pp. 252–260, 2000, doi: https://doi.org/10.1006/abio.2000.4880.

[107] O. Westphal, O. Lüderitz, and F. Bister, "Über die extraktion von Bakterien mit Phenol/Wasser," *Zeitschrift für Naturforsch. B*, vol. 7, no. 3, pp. 148–155, 1952, doi: doi:10.1515/znb-1952-0303.

[108] K. D. Seed, S. M. Faruque, J. J. Mekalanos, S. B. Calderwood, F. Qadri, and A. Camilli, "Phase variable O antigen biosynthetic genes control expression of the major protective antigen and bacteriophage receptor in Vibrio cholerae O1," *PLoS Pathog.*, vol. 8, no. 9, pp. e1002917–e1002917, Sep. 2012, doi: 10.1371/journal.ppat.1002917.

[109] R. P. Darveau and R. E. Hancock, "Procedure for isolation of bacterial lipopolysaccharides from both smooth and rough Pseudomonas aeruginosa and Salmonella typhimurium strains," *J. Bacteriol.*, vol. 155, no. 2, pp. 831–838, Aug. 1983, doi: 10.1128/JB.155.2.831-838.1983.

[110] S. N. Chatterjee and K. Chaudhuri, "Lipopolysaccharides of Vibrio cholerae: III. Biological functions," *Biochim. Biophys. Acta - Mol. Basis Dis.*, vol. 1762, no. 1, pp. 1–16, 2006, doi: https://doi.org/10.1016/j.bbadis.2005.08.005.

[111] N. C. Santos, A. C. Silva, M. A. R. B. Castanho, J. Martins-Silva, and C. Saldanha, "Evaluation of lipopolysaccharide aggregation by light scattering spectroscopy.," *Chembiochem*, vol. 4, no. 1, pp. 96–100, Jan. 2003, doi: 10.1002/cbic.200390020.

[112] E. Madland, O. Crasson, M. Vandevenne, M. Sørlie, and F. L. Aachmann, "NMR and fluorescence spectroscopies reveal the preorganized binding site in family 14 carbohydrate-binding module from human chitotriosidase," *ACS omega*, vol. 4, no. 26, pp. 21975–21984, Dec. 2019, doi: 10.1021/acsomega.9b03043.

[113] D. Hatlem, J. E. Heggelund, D. Burschowsky, U. Krengel, and P. E. Kristiansen, "1H, 13C, 15N backbone assignment of the human heat-labile enterotoxin B-pentamer and chemical shift mapping of neolactotetraose binding," *Biomol. NMR Assign.*, vol. 11, no. 1, pp. 99–104, 2017, doi: 10.1007/s12104-017-9728-9.

[114] M. A. Rahman *et al.*, "The Arabidopsis histone methyltransferase SUVR4 binds ubiquitin via a

domain with a four-helix bundle structure," *Biochemistry*, vol. 53, no. 13, pp. 2091–2100, Apr. 2014, doi: 10.1021/bi401436h.

[115] U. Zähringer *et al.*, "NMR-based structural analysis of the complete rough-type lipopolysaccharide isolated from Capnocytophaga canimorsus," *J. Biol. Chem.*, vol. 289, no. 34, pp. 23963–23976, Aug. 2014, doi: 10.1074/jbc.M114.571489.

[116] I. Kucharska, B. Liang, N. Ursini, and L. K. Tamm, "Molecular interactions of lipopolysaccharide with an outer membrane protein from Pseudomonas aeruginosa probed by solution NMR," *Biochemistry*, vol. 55, no. 36, pp. 5061–5072, Sep. 2016, doi: 10.1021/acs.biochem.6b00630.

[117] A. Bundi and K. Wüthrich, "1H NMR titration shifts of amide proton resonances in polypeptide chains," *FEBS Lett.*, vol. 77, no. 1, pp. 11–14, 1977, doi: https://doi.org/10.1016/0014-5793(77)80182-8.

6 Appendix

Appendix A – chemicals, materials and software

Table S1. Chemicals and suppliers.

Chemicals	**Supplier**
β-chitin nanofibers from squid pen	Scientific gift, Prof. Vaaje-Kolstand, NMBU
2-mercaptoethanol	Sigma
Acetic acid (glacial) 100 %	Merck
Agar-agar	Merck
Ammonium chloride	VWR
Ammonium N-15 chloride	Cortecnet
Ampicillin sodium salt	Applichem
Bolt LDS sample buffer (4X)	Thermo Scientific
Bolt MES SDS running buffer (20X)	Thermo Scientific
BugBuster protein extraction reagent	Merck
Calcium chloride anhydrous	Baker
Coomassie Brilliant Blue G-250	Fluka
D_8-glycerol	Chemsupport
Deuterium oxide	Chemsupport
Di-potassium hydrogen phosphate	Merck
Di-potassium sulphate	VWR
Di-sodium hydrogen phosphate anhydrous	VWR
DNase I	Thermo Scientific
DTT	Applichem
EDTA disodium dihydrate	Sigma
Gentamycin sulphate	Sigma

Glutathione reduced form	Sigma
Glycerol bidistilled	VWR
Hydrochloric acid fuming	Merck
Isopropyl beta-D-1-thiogalactopyranoside	Sigma
Kanamycin sulphate	Sigma
Lysozyme from chicken egg white	Sigma
Magnesium chloride anhydrous	Fluka
Magnesium sulphate	VWR
MEM vitamins solution 100x	Sigma
Pentaacetyl-chitopentaose	Megazyme
Peptone	Sigma
Phenol 99+ %, detached crystals	VWR
Potassium chloride	Fluka
Potassium dihydrogen phosphate	VWR
PreScission protease	Merck
Protein kinase A	Sigma
RNase A	Sigma
SeeBlue Plus2 Pre-stained protein standard	Thermo Scientific
Sodium acetate anhydrous	Fluka
Sodium chloride	VWR
Sodium hydroxide	VWR
Tris(hydroxymethyl)aminomethane	Sigma
Tryptone (peptone from casein)	VWR
Urea	VWR
Yeast extract, power, Ultrapure	VWR

Table S2. Disposables and suppliers.

Disposables	**Supplier**
1.5 mL Eppendorf tube	Eppendorf
2 mL Eppendorf tube	Eppendorf
15 mL Falcon tube	Thermo Scientific
50 mL Falcon tube	Thermo Scientific
Amicon Ultra – 0.5 Ultracel membrane 10 000 MWCO	Merck
Amicon Ultra Centrifugal Units 5 000 MWCO	Merck
Centrifugal filter modified nylon 0.2 µm	VMR
Bolt 4-12 % Bis-Tris Plus polyacrylamide gel	Thermo Scientific
Disposable cuvettes polystyrene 1.5 mL	VWR
L-shaped cell spreader	VWR
Filter upper cup 500 mL bottle top filter 0.2 µm filter PES membrane	VWR
Filter upper cup 500 mL bottle top filter 0.45 µm filter PES membrane	VWR
Millex-GS MCE membrane 0.22 µm syringe filter	Millex
NMR tube 5 mm diameter precision	Sigma-Aldrich
PCR tubes	VWR
Petri dish, polystyrene	VWR
Pur-A-Lyzer Midi 3 500 MWCO, 50-800 µL	Sigma-Aldrich
SnakeSkin Dialysis tubing 3 500 MWCO 22 mm diameter	Thermo Scientific
SpectraPor Dialysis membrane, 3 500 MWCO	SpectraPor
VIVASPIN 20 PES membrane 3 000 MWCO	VWR
VIVASPIN 20 PES membrane 5 000 MWCO	VWR
VIVASPIN 20 PES membrane 10 000 MWCO	VWR

Table S3. Kits and suppliers.

Kit	**Supplier**
NucleoBond® Xtra Midi kit	Macherey-Nagel
NucleoSpin® Plasmid	Macherey-Nagel

Table S4. Chromatography columns and suppliers

Column	**Supplier**
GSTrap HP 1 mL	Cyitiva
HiTrap Q XL 5 mL	Cytiva
Superdex 75 increase 10/300 GL	Cytiva
Superdex 200 Increase 10/300 GL	Cytiva

Table S5. Cells and plasmids and suppliers.

Cells/plasmids	**Supplier**
E. coli BL21 (DE3) Chemically Competent Cells transformed with pGEX-6P cloning vector	Scientific gift, Prof. Vaaje-Kolstad, NMBU
pET26b(+) cloning vector	GenScript
Vmax™ X2 Chemically Competent Cells	SGI-DNA

Table S6. Instruments and suppliers.

Instrument	**Supplier**
3510 pH meter	Jenway
5810R bench-top refrigerated centrifuge	Eppendorf
ÄKTA Pure 25 M1	GE healthcare
ÄKTA Start	GE healthcare

Avance Ascend AVIII HD 800	Bruker
Avanti JXN-26 centrifuge	Beckman-Coulter
CO800 OD600 spectrophotometer	BioChrom-WPA
CP224S scale	Sartorius
Direct-Q 5	Millipore
Dri-Block DB 2A heating block	Techne
EcoTron benchtop incubator-shaker	InforsHT
EPS601 electrophoreses powersupply	GE healthcare
F-34-6-38 Fixed-Angle Rotor	Eppendorf
Heraeus Biofuge Fresco 21 centrifuge	Thermo Scientific
HiLoad PUMP P-50 peristaltic pump	GE-Pharmacia
JA-10 Fixed-Angle Rotor	Beckman-Coulter
JA-25.50 Fixed-Angle Rotor	Beckman-Coulter
Kelvitron T incubator	Heraeus
LP-2102i precision scale	VWR
Mini Gel Tank Electrophoreses System	Invitrogen
Miniorbital Shaker SSM1	Stuart
Multitron Standard incubator-shaker	InforsHT
NanoPhotometer nanodrop	Implen
Rocking platform	VWR
Thermomixer Comfort	Eppendorf
UltroSpec 2100 Pro spectrophotometer	Amersham Biosciences
Vapour Line Steam Sterilizer 80-M + FA	VWR
VP 100 vacuum pump	VWR

Table S7. Software and suppliers.

Software	Supplier
CONTINLL, SELCON3, CDSSTR	CDpro
ChemDraw® 19.1	PerkinElmer
Excel	Microsoft
Origin 2020	OriginLab
PowerPoint	Microsoft
ProtParam tool	ExPasy
SnapGene® 5.2	GSL Biotech LLC
Topspin 3.6	Bruker
UNICORN™ 5.31	GE healthcare

Appendix B – buffers and solutions

Cell cultures

Table S8. Composition of LB medium (1 L).

Component	Amount
NaCl	10 g
Peptone	10 g
Yeast extract	5 g

pH 7.1. Components were mixed with 1 L MQ-H_2O and autoclaved.

Table S9. Composition of LB-v2 and D-LB-v2 medium (1 L).

Component	**Amount**
KCl	313 mg
$MgCl_2$	2.2 g
NaCl	21.9 g
Peptone	10 g
Yeast extract	5 g

pH 7.1. Components were mixed with MQ-H_2O or D_2O and the solution was autoclaved.

Table S10. Composition of TB medium (1 L).

Component	**Amount**
Yeast extract	24 g
Peptone	12 g
K_2HPO_4	9.4 g
KH_2PO_4	2.2 g
Glycerol	4 mL

pH 7.1. Components were mixed with MQ-H_2O and the solution was autoclaved. K_2HPO_4 and KH_2PO_4 were autoclaved separately.

Table S11. Composition of LB-v2 agar (250 mL).

Component	**Amount**
LB-v2 medium	250 mL
Agar-agar	3.5 g

pH 7.1. Components were mixed with MQ-H_2O and autoclaved.

Table S12. Composition of M9* minimal medium.

Component	Amount
K_2HPO_4	19.0 g
KH_2PO_4	5.0 g
Na_2HPO_4	9.0 g
K_2SO_4	2.4 g
$MgCl_2$	0.95 g
NH_4Cl	5.0 g
Glycerol	1.6 %
MEM vitamins 100X	1X
Trace element solution 1000X	1X

pH 7.4. Components were mixed with MQ-H_2O and the solution was autoclaved. Glycerol was autoclaved separately. MEM vitamins, trace element solution (Table S14) and $MgCl_2$ (sterile filtered) was added after autoclavation.

Table S13. Composition of M9 Max and D-M9 Max minimal medium.

Component	Concentration
Na_2HPO_4	150 mM
KH_2PO_4	75 mM
NaCl	10 mM
$CaCl_2$	0.2 mM
$MgSO_4$	5 mM
NH_4Cl[1]	0.15 %
Glycerol[2]	1.6 %
MEM vitamins 100X	1X
Trace element solution 1000X	1X

pH 8.1. Components were mixed with MQ-H_2O or D_2O and the solution was autoclaved. Glycerol was autoclaved separately. MEM vitamins, trace element solution (Table S14) and $CaCl_2$ (sterile filtered) was added after autoclavation.

[1] $^{15}NH_4Cl$ was used for ^{15}N-labelling

[2] d_8-glycerol was used for deuteration

Table S14. Composition of 1000X trace element solution for minimal medium.

Component	Amount
$FeSO_4(7H_2O)$	0.6 g
$CaCl_2(2H_2O)$	0.6 g
$MnCl_2(4H_2O)$	0.12 g
$CoCl_2(6H_2O)$	0.08 g
$ZnSO_4(7H_2O)$	0.07 g
$CuCl_2(2H_2O)$	0.03 g
H_3BO_4	0.002 g
$(NH_4)_6Mo_7O_{24}(4H_2O)$	0.025 g
EDTA	0.5 g

The solution was stirred for 2 hours and sterile filtered.

Table S15. Composition of lysis buffer for GST-GbpA-D4.

Component	Amount
NaCl	150 mM
Tris-HCl pH 7.5	50 mM
EDTA	1 mM

The components were mixed with MQ-H_2O and the solution was filtered.

Table S16. Composition of cleavage buffer for GST-GbpA-D4.

Component	Amount
NaCl	150 mM
Tris-HCl pH 7	50 mM
DTT	1 mM
EDTA	1 mM

The components were mixed with MQ-H_2O and the solution was filtered.

Protein purification

Table S17. Composition of AEX buffers for GbpA-D1.

Binding buffer	**Elution buffer**
50 mM NaCl 20 mM Tris-HCl pH 8	400 mM NaCl 20 mM Tris-HCl pH 8

The components were diluted in MQ-H_2O and the solution was filtered.

Table S18. Composition of AEX buffers for FL-GbpA.

Binding buffer	**Elution buffer**
100 mM NaCl 20 mM Tris-HCl pH 8	400 mM NaCl 20 mM Tris-HCl pH 8

The components were diluted in MQ-H_2O and the solution was filtered.

Table S19. Composition of GST buffers for GST-GbpA-D4.

Binding buffer	**Elution buffer**
50 mM Tris-HCl pH 7.5 150 mM NaCl 1 mM EDTA 10 mM DTT	50 mM Tris-HCl pH 8 10 mM reduced glutathione 1 mM EDTA 10 mM DTT

The components were diluted in MQ-H_2O and the solution was filtered.

SDS-PAGE

Table S20. Coomassie staining solution (1 L).

Component	Amount
Coomassie Brilliant Blue G-250	80 mg
HCl, concentrated	3 mL

The components were diluted in MQ-H_2O and the solution was stirred for 20 minutes.

NMR

Table S21. Composition of potassium phosphate buffer for NMR.

Component	Concentration
K_2HPO_4	93.5 mM
KH_2PO_4	6.5 mM

pH 7.4. Components were mixed with 800 mL MQ-H_2O and the pH was adjusted with NaOH. MQ-H_2O was then added to a final volume of 1 L.

Table S22. Composition of sodium acetate buffer for NMR (1 L).

Component	Concentration
Acetate	0.0052 M
Sodium acetate	0.0448 M

pH 5.5. Components were mixed with 800 mL MQ-H_2O and the pH was adjusted with NaOH. MQ-H_2O was then added to a final volume of 1 L.

CD spectroscopy

Table S23. Composition of sodium phosphate buffer for CD spectroscopy.

Component	Concentration
Na_2HPO_4	7.5 mM
NaH_2PO_4	2.5 mM

pH 7.4. Components were mixed with 800 mL MQ-H_2O and the pH was adjusted with NaOH. MQ-H_2O was then added to a final volume of 1 L.

Appendix C – amino acid sequences and vectors

Genes encoding GbpA-D1 and FL-GbpA were cloned into the pET26b(+) vector by GenScript®, using restriction sites Nco I and Xho I. The gene encoding GST-GbpA-D4, cloned into the pGEX-6P-1 vector was provided by Prof. Gustav Vaaje-Kolstad, NMBU. Biophysical properties (molecular weight, theoretical pI and molar extinction coefficient) of each construct are listed below.

FL-GbpA amino acid sequence:

```
  10         20         30         40         50
MKKQPKMTAI ALILSGISGL AYGHGYVSAV ENGVAEGRVT LCKFAANGTG
        60         70         80         90        100
EKNTHCGAIQ YEPQSVEGPD GFPVTGPRDG KIASAESALA AALDEQTADR
       110        120        130        140        150
WVKRPIQAGP QTFEWTFTAN HVTKDWKYYI TKPNWNPNQP LSRDAFDLNP
       160        170        180        190        200
FCVVEGNMVQ PPKRVSHECI VPEREGYQVI LAVWDVGDTA ASFYNVIDVK
       210        220        230        240        250
FDGNGPVLPD WNPAGQIIPS MDLSIGDTVY TRVFDNDGEN PAYRTELKID
       260        270        280        290        300
SETLTKANQW SYALATKINQ TQKQQRAGQL NGDQFVPVYG TNPIYLKEGS
       310        320        330        340        350
GLKSVEIGYQ IEAPQPEYSL TVSGLAKEYE IGEQPIQLDL TLEAQGEMSA
       360        370        380        390        400
ELTVYNHHQK PLASWSQAMT DGELKSITLE LSEAKAGHHM LVSRIKDRDG
       410        420        430        440        450
NLQDQQTLDF MLVEPQTPPT PGDYDFVFPN GLKEYVAGTK VLASDGAIYQ
```

```
        460         470         480
CKPWPYSGYC QQWTSNATQY QPGTGSHWEM AWDKR
```

FL-GbpA:

Signal sequence Domain 1 (LPMO AA10 module) Flexible linker Domain 2 (unknown function) Rigid linker Domain 3 (unknown function) Flexible linker Domain 4 (CMB74 module)

GbpA-D1:

Molecular weight: 19 801.06 Da

Theoretical pI: 5.05

Extinction coefficient (ε): 36 440 M^{-1} cm^{-1}; assuming all cysteine residues are reduced

FL-GbpA:

Molecular weight: 51 254.08 Da

Theoretical pI: 4.81

Extinction coefficient (ε): 97 290 M^{-1} cm^{-1}; assuming all cysteine residues are reduced

GST-GbpA-D4:

Molecular weight: 33 809.88 Da

Theoretical pI: 5.71

Extinction coefficient (ε): 73 800 M^{-1} cm^{-1}; assuming all cysteine residues are reduced

GbpA-D4:

Molecular weight: 7 243.00 Da

Theoretical pI: 5.55

Extinction coefficient (ε): 30 940 M^{-1} cm^{-1}; assuming all cysteine residues are reduced

Appendix D - supplementary results

Expression optimization of ^{15}N-FL-GbpA

Table S24. Minimal medium compositions for conditions 1-6 used in the optimization trial of ^{15}N-FL-GbpA.

Component	**1**	**2**	**3**	**4**	**5**	**6**
Na_2HPO_4	50 mM	50 mM	50 mM	150 mM	300 mM	50 mM
KH_2PO_4	25 mM	25 mM	25 mM	75 mM	150 mM	25 mM
NaCl	267 mM	10 mM	10 mM	10 mM	10 mM	10 mM
$MgSO_4$	5 mM	5 mM	5 mM	5 mM	5 mM	5 mM
$CaCl_2$	0.2 mM	0.2 mM	0.2 mM	0.2 mM	0.2 mM	0.2 mM
$^{15}NH_4Cl$	0.15 %	0.15 %	0.15 %	0.15 %	0.15 %	0.15 %
Glycerol	1.6 %			1.6 %	1.6 %	1.6 %
Glucose		1.6 %	2.6 %			
MEM vitamins 100X	1X	1X	1X	1X	1X	1X
Trace element solution 1000X	1X	1X	1X	1X	1X	1X

CD spectroscopy

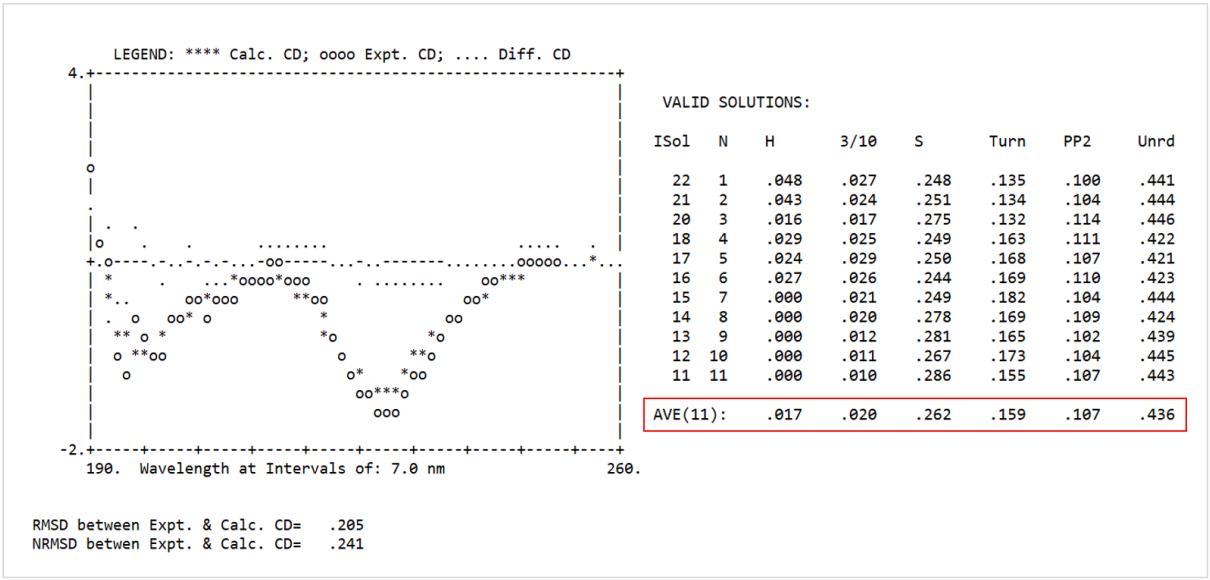

Figure S1. Deconvolution of the CD spectrum of GbpA-D4, using the CONTINLL program and dataset 2 in the CDpro package. The degree of secondary structure is highlighted in red.

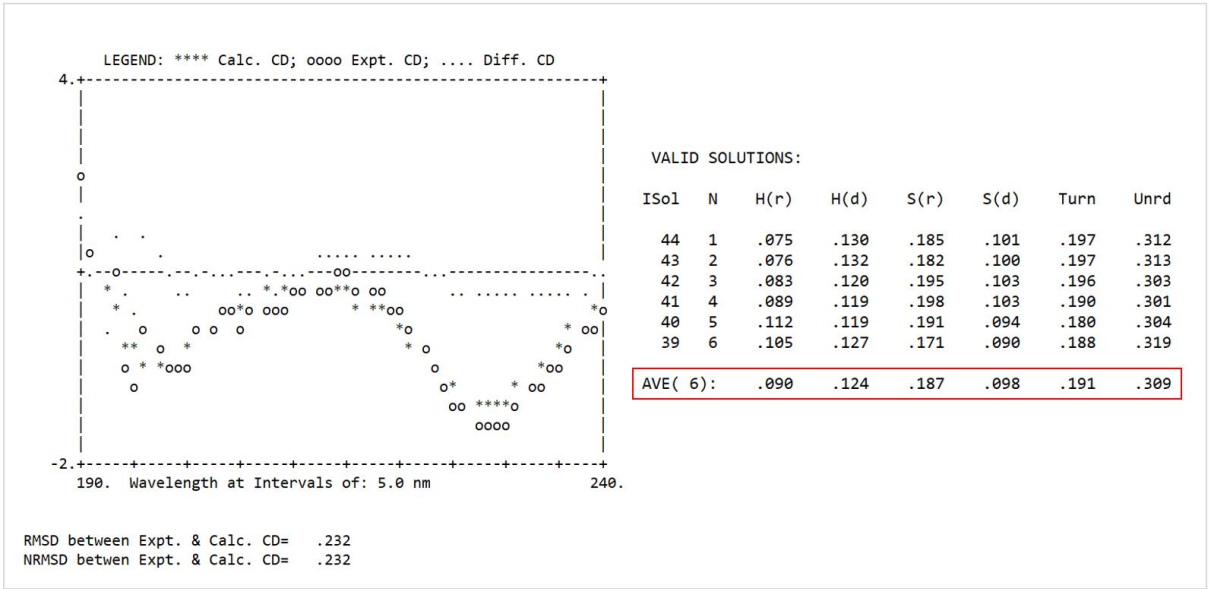

Figure S2. Deconvolution of the CD spectrum of GbpA-D4, using the CONTINLL program and dataset 4 in the CDpro package. The degree of secondary structure is highlighted in red.

^{15}N-TROSY titrations

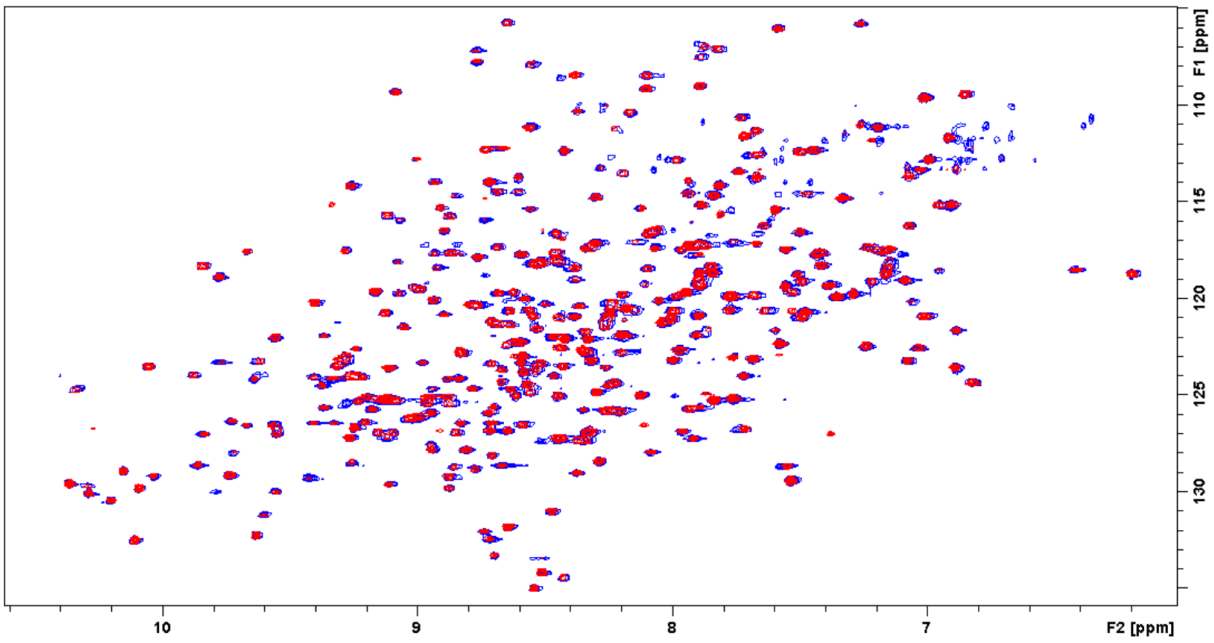

Figure S3. ^{15}N-TROSY spectra of ^{15}N-FL-GbpA. The spectrum of FL-GbpA before addition of *V. cholerae* cells (blue) and the final spectrum where the concentration of FL-GbpA was 232 µM and the amount of cells was approximately 2×10^8 (red).

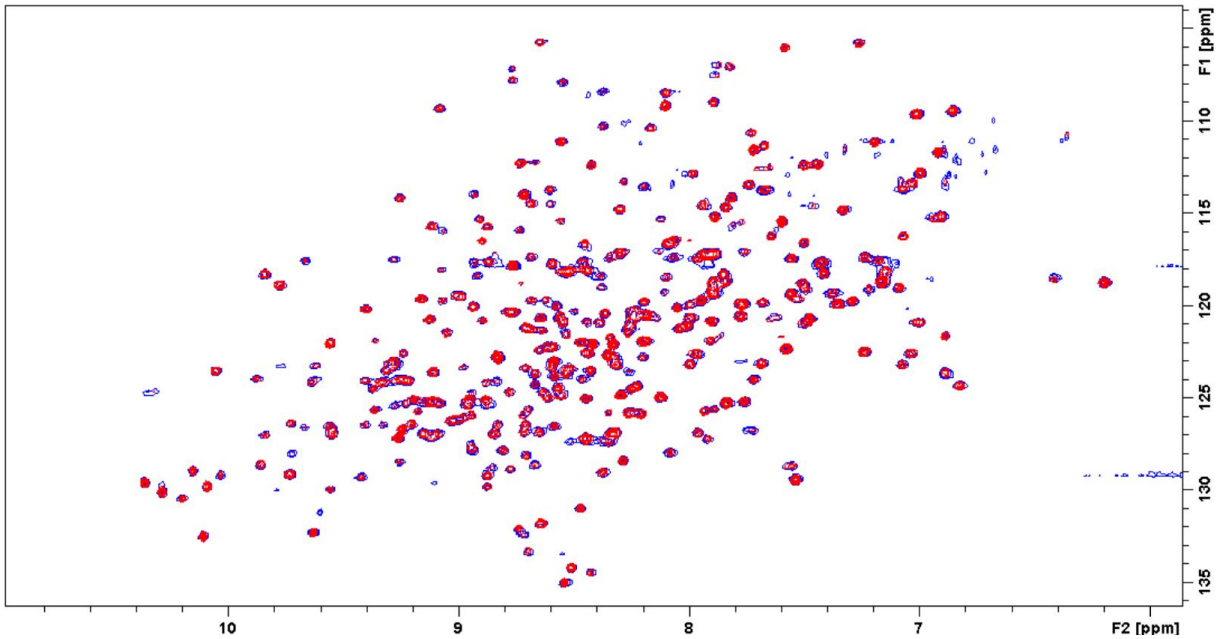

Figure S4. ^{15}N-TROSY spectra of ^{15}N-FL-GbpA. The spectrum of FL-GbpA before addition of GlcNAc-5 (blue) and the final spectrum where the GbpA:LPS molar ratio is 1:1.48 (red).

Estimation of lower K_d from ^{15}N-TROSY titrations

δ_A and shift δ_{AB} are the chemical shifts of unbound and bound form of GbpA, respectively.

Shifts in fast exchange have the following dependence on the fractions:

$\delta_{Obs} = f_A\delta_A + f_B\delta_B$
$f_A + f_b = 1$

, where $f_A = \frac{[A]}{[A]+[AB]}$ and $F_B = \frac{[B]}{[A]+[AB]}$

$\Delta\delta = (f_A \times \delta_A) + (f_{AB} \times \delta_{AB} - \delta_A)$
$f_A = 1 - f_{AB}$

$\Delta\delta = [(1 - f_{AB}) \times \delta_A] + (f_{AB} \times \delta_{AB} - \delta_A)$

$f_{AB} = \frac{\Delta\delta}{\delta AB - \delta A}$

K_d is then given by:

$K_d = \frac{[A][B]}{[AB]} = \frac{conc.A0\ (1-f_{AB}) \times (\text{conc.B0} - \text{conc.A0} \times f_{AB})}{conc.A0 \times f_{AB}} = \frac{(1-f_{AB}) \times (conc.B - conc.A * f_{AB})}{f_{AB}}$

, where A0 is the concentration of GbpA and B0 is the ligand concentration

To detect binding of GbpA and LPS, $\Delta\delta$ is > 0.02 ppm and $\delta_{AB} - \delta_A > 0.1$

$f_{AB} = \frac{0.02}{0.1} = 0.2$

$K_d = \frac{(1-0.2) \times (327\ \mu M - 221\ \mu M \times 0.2)}{0.2} = 1.13$ mM

Appendix E – safety statement

This project involves laboratory experiments with *V. cholerae* El Tor ΔCTX cells. *V. cholerae* is a biosafety level 2 (BSL-2) pathogen. To reduce the risk of infection and contamination, safety precautions according to BSL-2 were taken, which included appropriate personal protection equipment, biohazard warning signs and decontamination for proper disposal of bacteria. This lab was approved by Sosial- og Helsedirektoratet for work with BLS-2 pathogens, and safety procedures are accessible in our lab. In addition, I was vaccinated with Dukoral® as an extra safety measure.